

**ASSESSMENT OF STRESS-STRAIN BEHAVIOUR
OF CORRODED STEEL REBARS USING
DIGITAL IMAGE CORRELATION TECHNIQUE**

A THESIS

submitted by

RANJITHA RAJAGOPAL

for the award of the degree

of

MASTER OF SCIENCE



BUILDING TECHNOLOGY AND CONSTRUCTION MANAGEMENT DIVISION

**DEPARTMENT OF CIVIL ENGINEERING
INDIAN INSTITUTE OF TECHNOLOGY MADRAS,
CHENNAI, INDIA -600036**

JULY 2016

THESIS CERTIFICATE

This is to certify that the thesis titled '**ASSESSMENT OF STRESS-STRAIN BEHAVIOUR OF CORRODED STEEL REBARS USING DIGITAL IMAGE CORRELATION TECHNIQUE**', submitted by **Ranjitha Rajagopal**, to the Indian Institute of Technology Madras, for the award of the degree of Master of Science, is a bonafide record of the research work carried out by her under my supervision. The contents of this thesis, in full or in parts, have not been submitted to any other Institute or University for the award of any degree or diploma.

Chennai, India
July 14, 2016

Dr. Radhakrishna G. Pillai
(Research Guide)
Assistant Professor
Department of Civil Engineering
Indian Institute of Technology Madras
Chennai - 600 036

ACKNOWLEDGEMENT

I would like to take this opportunity to express my sincere gratitude to my research supervisor, Dr. Radhakrishna G. Pillai, for his technical guidance and immense motivation during the course of this research. The very first meeting with became a turning point in my life. It paved the way from joining M.S. program in IITM and the completion of this research project satisfactorily. He has been a true mentor in all respects, professionally and personally, and moreover, an inspiring human being.

I thank Prof. Sankara J. Subramanian for his willingness to collaborate, and for the excellent technical guidance offered throughout this project. I am grateful for the technical guidance offered by Prof. Ravindra Gettu, who has played a very important role in channelizing the research objectives and shaping up this project. I thank my General Test Committee (GTC) members, Prof. Amlan Kumar Sengupta and Prof. M. S. Sivakumar for their guidance and support. I thank Prof. Meher Prasad, Head of the Department of Civil Engineering, for providing all necessary facilities and excellent technical support. The technical guidance offered at various phases of this project by Prof. Manu Santhanam, Prof. Mark Alexander, Prof. Surendra Shah, and Prof. Vellore Gopalaratnam is highly appreciated. The three year period in Civil Engineering Department of IITM gave me opportunity to interact with these highly reputed and world renowned professors. I am also grateful to Prof. Ravishankar Kottada, Prof. G. Saravana Kumar, Prof. Krishnan Balasubramanian and Prof. Koshy Varghese for the technical assistance extended by providing access to various laboratories in IITM.

One of the persons I remain indebted to is Sameer Sharma who has been a vital part of this research project. He has offered immense technical help for getting trained in DIC technique and Matlab programming. He was an inspiring person with a strong passion for research and excellent attitude towards life. Sameer, thanks for all the technical help and the moral support extended to me as a friend during the course of this work.

I extend my gratitude towards my fellow researchers, Ranjith, Jayachandran, Prabha, Sooraj, Sanoop, Saarthak, and Sripriya for the frequent technical discussions. I also thank the summer interns, especially Meera, Namitha and Shyam, for the assistance in lab work during May-June 2014. I also thank Eshwar, Iniyan, Venketachalam and Chetana for helping me resolve the hurdles faced with the DIC technique.

I extend my sincere gratitude to the staff of the Central Workshop in IITM and Central Fabrication Facility (CFF) to all the help offered in this project and the

excellent quality of the work which deserves appreciation. I am also grateful to the assistance from the technical staff from the laboratories, Ms. Malavizhi, Mr. Soundrapandian, Mr. Krishnan, Mr. Subramani, Mr. Govindasamy, Mr. Rajkumar, Mr. Vincent, Mr. Chellapandiyar, Mr. Shiva and Mr. Dominic in conducting my experiments. My special thanks to Mr. Ramamoorthy, supervisor of Rapid Prototyping Laboratory, for his kind heartedness and the sincerity towards his job, which inspired me a lot. I also thank the hostel and security staff of IITM for their special lab-hostel transport services during late night hours.

This journey of M. S. at IITM would not have been this memorable if it were not for my friends. I say a big thanks to Anna, who had been with me through the ups and downs of the research life and who was always there by my side to say at the end of a tough day, “*Hey, let’s eat out!!*” and “*It’s gonna be alright*”. Anna, thanks for being there. Sahila (Kaaluu) is another beautiful soul I met in IITM, who has left me awestruck with her always-happy face and her amazing attitude towards life. Kaalu, thank you for spending time on several nights discussing and figuring out ways to overcome the hurdles with this project. I also thank my friends, Nithya, Saimy, Abul, Sai, Amritha, Shyam, Madhu, Zareena and Mandhakini, for the time spent together. I thank Shyam for accompanying me to Parrys and Guindy on various occasions for the purchases needed for this project. My special thanks to Praveen for his advice to join for M.S. program in IITM which indeed turned out to be a life changing experience.

Above all, my dad has been the greatest support and the best of friends for every endeavour of my life including this. A huge thanks to him for enduring all my fretting and fuming when things were not going right and for making me strong and independent in the process. Thanks to Amma, for being the inspiring strong lady she is and my little brother, Roopu, for springing up to solve my problems in his own little ways. I also thank my in-law family, Amma, Achan and Achu, for supporting me fulfil my dreams. I also thank my brother, Athu, for all the help with the photoshop and moreover for the special bond we share which helped me at several moments. I thank Priyanka for the moral support and practical advices offered.

Finally, and most importantly, my special thanks to my husband, Ram, for being by my side to help me at my difficult times, for the countless number of times he boosted my spirits, for all the technical advices and for being the strong pillar of support during this endeavour.

-Ranjitha

ABSTRACT

Several Reinforced Concrete (RC) structures are experiencing corrosion of the embedded reinforcing bars (rebars). The loss of steel from the surface of the rebars due to corrosion may affect the load carrying capacity and performance of RC structures. To understand the behaviour of RC structures experiencing corrosion, it is essential to understand the effect of corrosion on the stress-strain behaviour of steel rebars and the mechanical properties (namely, the elastic modulus, yield strength, ultimate strength and ductility). Several researchers have attempted to study the stress-strain behaviour of corroded rebars. The literature exhibit considerable differences in opinion among researchers regarding the effect of corrosion on the mechanical properties of rebars. Some of the researchers have pointed out that the reason for the differences in opinion is the differences in the adopted experimental techniques. This is due to the challenges associated with the tension testing and stress/strain computations for corroded rebars with uneven cross-sectional area along the length. Also, there are limited standardized procedures/guidelines on the tension testing of corroded rebars and evaluating their mechanical properties.

This study consists of mainly two phases. The first phase of the study deals with the development of the testing and evaluation method using DIC technique and 3D laser scanning technique. In the second phase, the stress-strain behaviour of a set of corroded steel rebars were assessed using the method developed in the first phase.

In the first phase, after multiple trials of various testing and evaluation methods, a refined testing and evaluation method was developed to assess the stress-strain behaviour of corroded rebars using Digital Image Correlation (DIC) technique. This method is intended to achieve certain improvements in the determination of the mechanical properties of the rebars. The DIC techniques estimate the full-field deformation of a predefined region of the specimen. This helps to capture the strain heterogeneity, due to the uneven cross-sectional area, along the length of the rebars. Thus, the developed method can provide a better understanding of the effect of corrosion on the ductility of the rebars. This method also incorporates 3D laser scanning technique to estimate the residual cross-sectional area profile of the rebars, which facilitates an accurate identification of the probable fracture locations (based on the least cross-sectional area) prior to the tension test. The feasibility of the proposed method to meet the intended purpose is assessed using a Plain Mild (PM) steel rebar

and three corroded Cold-Twisted Deformed (CTD) steel rebars (with uneven cross-sectional area) with three different degrees of corrosion (i.e., 3, 24 and 33% area loss).

In the second phase, a set of thirteen CTD steel rebar specimens (including the three specimens in the first phase) are tested. The effect of natural corrosion on the stress-strain behaviour and the mechanical properties of these specimens are evaluated using the testing and evaluation method developed in the first phase of this study. The assessment of the feasibility of the proposed testing and evaluation method showed that this method could capture the stress-strain behaviour close to the fracture location with sufficient accuracy. Using the proposed method, strain could be captured at approximately every 1 mm along 60 mm length of the rebar. This provided a very good estimate of the strain distribution in the corroded rebars. The evaluation of the effect of corrosion on the stress-strain behaviour of CTD steel rebars showed that the strength properties of the residual steel are not significantly affected by corrosion. However, ductility (in terms of ultimate strain) exhibited by the rebar specimens varied considerably due to corrosion. This variation was studied in detail and the study showed that the pattern of corrosion has a significant effect on the ultimate strain at fracture location of the rebars. This study suggests that the local mechanical properties at the fracture location (instead of over a typical gauge length) give a better estimate of the mechanical properties of the corroded rebars. This study also emphasizes the need for full-field deformation techniques like DIC to assess the stress-strain behaviour of corroded rebars with uneven cross-sectional area.

KEYWORDS: Reinforcing bars, corrosion, tension testing, stress-strain behaviour, Digital Image Correlation (DIC), cross-sectional area profile, strain localization, pattern of corrosion

CONTENTS

ACKNOWLEDGEMENT	iii
ABSTRACT.....	v
LIST OF FIGURES	xi
LIST OF TABLES	xv
ABBREVIATIONS	xvii
NOTATIONS.....	xix
CHAPTER 1 INTRODUCTION	1
1.1 PROBLEM STATEMENT.....	1
1.2 DEFINITIONS	2
1.3 RESEARCH OBJECTIVES AND SCOPE.....	4
1.4 RESEARCH ASSUMPTIONS.....	5
1.5 RESEARCH HYPOTHESES.....	5
1.6 RESEARCH SIGNIFICANCE.....	5
1.7 THESIS ORGANIZATION	7
CHAPTER 2 LITERATURE REVIEW.....	9
2.1 INTRODUCTION	9
2.2 CORROSION OF EMBEDDED REINFORCEMENT.....	9
2.3 PATTERN OF CORROSION ON REBARS IN STRUCTURES	10
2.4 ASSESSMENT OF STRESS-STRAIN BEHAVIOUR OF CORRODED REBARS – CONVENTIONAL METHOD.....	11
2.5 METHODS OF INDUCING CORROSION IN LABORATORY TESTING	12
2.5.1 Impressed Current Technique (Galvanostatic Method)	12
2.5.2 Artificial Corrosive Climate.....	13
2.5.3 Other methods	14
2.6 ISSUES ASSOCIATED WITH STRESS COMPUTATION.....	14
2.6.1 Mass or weight loss technique	15
2.6.2 Liquid displacement technique.....	15
2.6.3 Using Vernier calipers.....	16
2.6.4 Quantification of degree of corrosion	16
2.7 ISSUES ASSOCIATED WITH MEASUREMENT OF STRAIN IN CORRODED REBARS.....	17
2.8 EFFECT OF CORROSION ON STRENGTH PROPERTIES OF CORRODED REBARS.....	19
2.8.1 Effect of corrosion on yield strength of unstressed rebar specimens	19
2.8.2 Effect of corrosion on ultimate strength of unstressed rebar specimens	20

2.8.3	Effect of corrosion on strength properties of stressed rebars	21
2.8.4	Possible reasons for differences in opinion	22
2.9	EFFECT OF CORROSION ON DUCTILITY OF REBARS	23
2.9.1	Effect of pattern of corrosion on ductility of rebars	27
2.10	EFFECT OF CORROSION ON ELASTIC MODULUS OF REBARS	28
2.11	CURRENT RESEARCH NEEDS	28
2.12	DIGITAL IMAGE CORRELATION (DIC) TECHNIQUE.....	32
2.12.1	Applications of DIC in civil engineering	33
2.12.2	Vic-2D™ software program	34
2.13	SUMMARY	35
CHAPTER 3 EXPERIMENTAL PROGRAM		37
3.1	INTRODUCTION	37
3.2	SPECIMEN DETAILS	38
3.3	DEVELOPMENT OF TESTING AND EVALUATION METHOD.....	42
3.3.1	Specimen preparation	42
3.3.2	Determination of residual cross-sectional area and identification of probable fracture location	44
3.3.3	Selection of Area of Interest (AOI)	48
3.3.4	Speckling.....	49
3.3.5	Tensile testing and image capture	50
3.3.6	Quantification of degree of corrosion	53
3.3.7	Computation of full-field displacement using DIC technique.....	55
3.3.8	Challenges associated with strain computation in Vic-2D™	57
3.3.9	Strain computation using Principal Component Analysis (PCA).....	57
3.3.10	Strain computation using ‘Virtual extensometer method (VEM)’	59
3.3.11	Computation of effective strain over the gauge length	59
3.3.12	Computation of stress.....	59
3.3.13	Assessment of the feasibility of the proposed technique	61
3.4	EVALUATION OF THE MECHANICAL PROPERTIES OF CORRODED REBARS USING THE DEVELOPED METHOD	62
3.5	SUMMARY	63
CHAPTER 4 RESULTS AND DISCUSSION.....		65
4.1	INTRODUCTION	65
4.2	DEVELOPMENT OF TESTING AND EVALUATION METHOD.....	65
4.2.1	Estimation of residual cross-sectional area	65
4.2.2	Selection of strain computation method.....	67
4.2.3	True and engineering stress-strain curve plotted using the proposed method	70

4.2.4	Study of the strain distribution along the AOI	72
4.3	STRESS-STRAIN BEHAVIOUR OF CORRODED CTD REBARS	75
4.3.1	Stress-strain curves obtained using the developed method	76
4.3.2	Strain distribution along the length of rebars	76
4.3.3	Effect of corrosion on proof stress	82
4.3.4	Effect of corrosion on ultimate strength.....	84
4.3.5	Effect of corrosion on ultimate strain.....	85
4.3.6	Effect of pattern of corrosion on the ultimate strain measured at fracture location.....	85
4.3.7	Effect of corrosion on elastic modulus.....	88
4.4	SUMMARY.....	89
CHAPTER 5 CONCLUSIONS AND RECOMMENDATIONS		91
5.1	INTRODUCTION.....	91
5.2	LIMITATIONS AND ASSUMPTIONS	91
5.3	USE OF DIC TECHNIQUE TO ASSESS THE STRESS-STRAIN BEHAVIOUR OF CORRODED REBARS.....	92
5.4	EFFECT OF CORROSION ON MECHANICAL PROPERTIES OF CORRODED CTD REBARS EVALUATED USING THE DEVELOPED METHOD	93
5.5	FUTURE RECOMMENDATIONS	94
REFERENCES		95
APPENDIX.....		101
LIST OF PUBLICATIONS		111
CURRICULUM VITAE		113
GENERAL TEST COMMITTEE		115

LIST OF FIGURES

Figure 2.1 Illustration of fracture line and fracture location on a corroded rebar specimen	3
Figure 2.1 Localized (pitting) corrosion topography of the rebar (Source: Francois et al. 2012)	11
Figure 2.2 Uneven corrosion topography along the length of the rebar	11
Figure 2.3 A typical setup for inducing galvanic corrosion in rebars using impressed current (Source: Yuan et al. 2007)	13
Figure 2.4 Schematic diagram depicting the possible selection of gauge lengths for corroded rebar with uneven cross-sectional area	18
Figure 2.5 Plot showing no significant effect on yield strength with increasing degree of corrosion [reproduced from Cairns et al. (2005)]	20
Figure 2.6 Reduction in yield strength due to corrosion [reproduced from Du et al. (2005)]	20
Figure 2.7 Increase in ultimate strength [reproduced from Francois et al. (2012)]	22
Figure 2.8 Ultimate strain measured using nested extensometers -- 25 mm within 75 mm gauge length -- [reproduced from Palsson and Mirza (2002)]	24
Figure 2.9 29% reduction in ductility (ultimate strain) due to 10% corrosion measured in [reproduced from Du et al. (2005)]	25
Figure 2.10 Decrease in ultimate strain with the reduction in the cross sectional area [reproduced from Cairns et al. (2005)]	26
Figure 2.11 Exponential reduction in ductility with increasing degree of corrosion [reproduced from Apostolopoulos and Papadakis (2008)]	26
Figure 2.12 Reduction in ductility [reproduced from Francois et al. (2012)]	27
Figure 2.13 The influence of the variation in cross-sectional area on the ultimate strain [reproduced from Palsson and Mirza (2002)]	28
Figure 2.14 Schematic diagram illustrating the principles of DIC	32
Figure 3.1 Flowchart providing an outline of the experimental program	37
Figure 3.2 Two types of steel used in this study – (a) Plain Mild steel (PM) and (b) Cold-Twisted Deformed (CTD) steel rebars	39

Figure 3.3	Plain mild (PM) steel and corroded CTD rebar specimens with degree of corrosion varying from 3 to 40%.	40
Figure 3.4	The extender rebars (corroded CTD steel rebars) used in the dummy columns on top of the roof slab of the building	41
Figure 3.5	Milled surface on the PM steel and CTD steel rebars	44
Figure 3.6	Wax imprinting technique to estimate the residual cross-sectional area at the fracture location of the corroded rebar specimen	45
Figure 3.7.	Virtual 3D model of the PM steel and CTD steel rebars obtained using laser scanning	47
Figure 3.8	Illustration of the selection of AOI	49
Figure 3.9	Speckling using black and white coloured spray paints and the speckles formed on the surface of the specimen	50
Figure 3.10.	Experimental set up used for testing the plain mild steel specimens [Arrangement of camera, lights etc. and Zwick Roell (Model Z100) tension testing machine]	51
Figure 3.11.	Experimental set up used for testing all the CTD steel specimens [Arrangement of camera, lights, etc. and the MTS (Model 311.11) tension testing machine]	51
Figure 3.12	The placing of the camera with its focal plane parallel to the AOI	52
Figure 3.13	Initial and the final images of the AOI taken during the tension test of CTD rebar specimen	53
Figure 3.14	Schematic representation of the computation of degree of corrosion – (a) The original cross-sectional area of the pristine rebar, (b) The nominal cross-sectional area of the milled specimen (without considering the corrosion), and (c) The residual cross-sectional area at the fracture location of the specimen	54
Figure 3.15	Pixels occupied by the AOI in the image	56
Figure 3.16.	Schematic representation of the computation of instantaneous area	60
Figure 4.1	Cut surface of a wax imprint of corroded specimen revealing imperfections in the imprint	66
Figure 4.2	Comparison of the ultimate strain computed using PCA based algorithm and in-built function in Vic-2D TM software	68

Figure 4.3	Comparison of the stress-strain curves plotted using all three methods of strain computation – Vic-2D TM , VEM, and PCA based algorithm: (a) S0 (0% corrosion), (b) S1 (3% corrosion), (c) S7 (24% corrosion) and (d) S12 (33% corrosion).....	69
Figure 4.4	Comparison of the engineering and true stress-strain curves corresponding to the fracture location and engineering stress-strain curve obtained using the conventional method – (a) S0 (0% corrosion), (b) S1 (3% corrosion), (c) S7 (24% corrosion) and (d) S12 (33% corrosion)....	71
Figure 4.5	Stress-strain curves at different points along the control specimen indicating the strain distribution	73
Figure 4.6	Strain distribution along the length of CTD rebars with 3, 24 and 33% corrosion.....	74
Figure 4.7	Engineering and true stress-strain curves of the thirteen corroded CTD specimens- (a) S1 to S7 (3 – 24% corrosion) and (b) S8 to S13 (25 – 40% corrosion)	77
Figure 4.8	Effect of corrosion on the strain distribution along the length of the CTD rebar specimens – (a) S2 (4% corrosion) and (b) S3 (4% corrosion).....	78
Figure 4.9	Effect of corrosion on the strain distribution along the length of the CTD rebar specimens – (a) S4 (18% corrosion) and (b) S5 (18% corrosion)..	79
Figure 4.10	Effect of corrosion on the strain distribution along the length of the CTD rebar specimens – (a) S6 (23% corrosion) and (b) S8 (28% corrosion)..	80
Figure 4.11	Effect of corrosion on the strain distribution along the length of the CTD rebar specimens – (a) S9 (30% corrosion) and (b) S10 (31% corrosion)	81
Figure 4.12	Effect of corrosion on the strain distribution along the length of the CTD rebar specimens – (a) S11 (32% corrosion) and (b) S13 (40% corrosion)	82
Figure 4.13	Variation in the proof stress of CTD rebar specimens with increasing degree of corrosion	83
Figure 4.14	Variation in ultimate strength of rebars with increasing degree of corrosion	84
Figure 4.15	Variation in (a) effective ultimate strain measured over 60 mm gauge length and (b) ultimate strain measured at the fracture location, with increasing degree of corrosion.....	86
Figure 4.16	Rate of change of cross-sectional area at the fracture location (over 1 mm) for specimens S2, S6 and S12.....	87

Figure 4.17	Variation in ultimate strain at fracture location with the rate of change of cross-sectional area at the fracture location.....	88
Figure 4.18	Variation in elastic modulus with increasing degree of corrosion	89
Figure A.1	Flowchart of the testing and evaluation procedure using the developed method	101
Figure A.2	The nominal cross-sectional area of a pristine rebar showing the radius (R) and chord length (l_c)	107

LIST OF TABLES

Table 2.1	Comparison of the experimental technique adopted in some of the previous studies.....	30
Table 2.2	A comparison of the effect of corrosion on the mechanical properties of rebars reported in the literature	31
Table 3.1	Typical chemical composition of PM steel and CTD steel	39
Table 3.2	Details of the specimens used in this study	39
Table 3.3.	Details of Computation of the degree of corrosion for the three CTD rebars.....	55
Table 3.4.	Computed degree of corrosion for the thirteen CTD specimens evaluated using the developed method.....	63
Table 4.1	Computed mechanical properties at the fracture location of corroded unstressed CTD steel rebars.....	75
Table 4.2	The rate of change of cross-sectional area (dA/dy) at the fracture location quantifying the localization of corrosion	87

ABBREVIATIONS

AOI	Area of Interest
CSA	Cross-sectional area
CTD	Cold-Twisted Deformed (steel)
DIC	Digital Image Correlation
FL	Fracture Location
PM	Plain Mild (steel)
RC	Reinforced Concrete

NOTATIONS

A_0	Nominal cross-sectional area of the pristine rebar
A_i	Nominal cross-sectional area of the as-received milled specimen
A_{FL}	Residual cross-sectional area at the fracture location
$[H]$	Displacement gradient matrix
ε	Strain tensor
σ_{engg}	Engineering stress (MPa)
σ_{true}	True Stress (MPa)
ε_{gauge}	Strain measured over a gauge length
ε_{FL}	Strain measured at the fracture location
$\sigma_{engg} - \varepsilon_{FL}$	Engineering stress-strain curve corresponding to the fracture location
$\sigma_{true} - \varepsilon_{FL}$	True stress-strain curve corresponding to the fracture location
σ_p	Proof stress (MPa)
σ_u	Ultimate strength (MPa)
$\varepsilon_{gauge,ult}$	Ultimate strain measured over a gauge length
$\varepsilon_{FL,ult}$	Ultimate strain measured at the fracture location
dA/dy	Rate of change of cross-sectional area at over 1 mm at fracture location

CHAPTER 1

INTRODUCTION

1.1 PROBLEM STATEMENT

Corrosion of embedded reinforcing bars (rebars) is one of the predominant cause of premature deterioration of the reinforced concrete structures when exposed to aggressive environments. Corrosion leads to a reduction in the effective cross-sectional area of the steel rebars, which can lead to the reduction in the load carrying capacity and changes in the structural behaviour of the RC structures. Nations all over the world are spending a huge amount of money in tackling problems due to corrosion in the infrastructure segments. The NACE Report (2016) estimated a global cost of about 3.4% of the global Gross Domestic Product. Business Standard (2012) reported that the annual cost of corrosion in the infrastructure and industry segments alone in India is about 2.7 Lakh Crores approximately (say, about 40 billion USD). Singh et al. (2010) have predicted the corrosion cost in India to reach 120billion USD by the year 2020, out of which 16.24% would be due to corrosion in infrastructure segments.

To effectively tackle the problems due to corrosion in infrastructure and to minimize the expenditure on maintenance and repair, it is essential to formulate effective maintenance and repair strategies for reinforced concrete systems experiencing corrosion. Also, to ensure the safety of the public, it is essential to re-estimate the service life of the corroding structures. Hence, there is a need to understand the structural capacity and behaviour of RC structures experiencing corrosion. This, in turn, necessitates the need to assess the stress-strain behaviour and mechanical properties (namely elastic modulus, yield strength, ultimate strength, and ductility or the strain at fracture) of corroded reinforcement bars (rebars).

The conventional tension testing method is primarily formulated for pristine rebars with the uniform cross-sectional area along the length of the rebars. The tension testing and the corresponding computation of stress and strains of corroded rebars is a challenging task due to the uneven cross-sectional area profile along the length of

rebars. Also, there are limited guidelines to evaluate the stress-strain behaviour of corroded rebars. These limitations in testing and evaluating corroded rebars has led to considerable difference in opinion among researchers regarding the effect of corrosion on the variations in the mechanical properties of rebars (Du et al. 2005b, Taha and Morsy 2013). Hence, there is a need for a refined method to assess the stress-strain behaviour of corroded rebars.

1.2 DEFINITIONS

In this document, the following terms related to the testing and evaluation of corroded rebars are defined as follows.

- Actual strength – the strength of a corroded rebar computed (in units of stress) using the measured residual cross-sectional area of the rebar (after corrosion, if any).
- Area of Interest (AOI) – the predefined region of the surface of the specimen which is captured in the images during the tension test. The displacements are computed for the defined points in the AOI using DIC technique.
- Cross-sectional area profile – the variation in cross-sectional area quantified in terms of the residual cross-sectional area at every 1 mm interval of length along the specimen.
- Deformed specimen – the elongated specimen during the tension test (Note that this is different from the meaning of the term ‘deformed’ in ‘Cold-Twisted Deformed rebars’).
- Degree of corrosion – the amount of corrosion in the specimen quantified in terms of percentage reduction in cross-sectional area at the fractured location compared to the nominal cross-sectional area of the as-received milled specimen (discussed in detail in Section 3.3.6).
- Effective strain – strain computed as displacement per unit length, conventionally measured over a gauge length.
- Fracture line (or line of fracture) – the projection of the fracture surface on the milled surface of the rebar (as shown in Figure 2.1).
- Fracture location (FL) – a region of 1 mm length along the rebar around the fracture line, as shown in Figure 2.1 (This location may or may not coincide with the point of rebar where the fracture initiated).

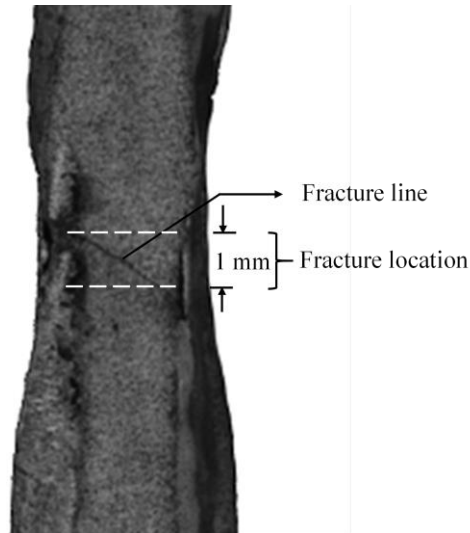


Figure 2.1 Illustration of fracture line and fracture location on a corroded rebar specimen

- Full-field displacement – the displacement of the defined points on the surface of the specimen due to deformation of the specimen under tension along the x - and y -axis of the specimen.
- Image Analysis – the computation of the full-field displacement of defined points on the predefined region of the specimen using images captured during the deformation of the specimen under tension using Digital Image Correlation (DIC) technique.
- Instantaneous area – cross-sectional area at a particular location of the specimen (deforming under tension) at a particular instant of time.
- Milled Segment – the portion of the rebar removed to obtain a plane surface on the rebar.
- Nominal strength – the strength computed (in units of stress) using the nominal diameter of the rebar (without considering the reduction due to corrosion, if any).
- Pattern of corrosion – A qualitative term which indicates the spread of corrosion on the rebar based on the topography of the surface of the rebar specimen or the residual cross-sectional area profile along the length of the specimen. The pattern of corrosion could be uniform, localized, or uneven (as explained in Section 2.3). In this study, the pattern of corrosion is also quantified in terms of the rate of change in cross-sectional area over 1 mm length close to fracture location (denoted as dA/dy).

- Probable fracture location(s) – the location(s) or 1 mm slice thick slices on the corroded rebar specimen with the least residual cross-sectional area.
- Proof stress (σ_p) – the stress corresponding to offset yield point set at 0.2% plastic strain
- Residual cross-sectional area – the cross-sectional area (CSA) of the corroded rebars at a specified location, measured after removing the corrosion products from the surface of the rebar.
- Ultimate strain – strain exhibited by the specimen at fracture.
- Ultimate strength (σ_u) – stress corresponding to maximum load carried by the specimen (or the peak load point in the stress-strain curve).
- Undeformed – the original state of the specimen before it is tested under tension (Also, referred to as the reference state).
- Yield strength – stress at which the steel in the rebar begins to deform plastically.

1.3 RESEARCH OBJECTIVES AND SCOPE

The two objectives of this study are as follows.

Objective 1 – To develop an improved testing and evaluation method to assess the stress-strain behaviour of corroded steel rebars using Two-dimensional Digital Image Correlation (2D DIC) technique. The scope of this objective includes:

- One pristine mild steel (with 0% degree of corrosion) and three corroded CTD steel specimens (with 3, 24, and 33% degrees of corrosion).
- Feasibility assessment of 2D DIC technique for assessing the stress-strain behaviour of corroded rebars
- The selection of input parameters for the computation of full-field displacement and strain using 2D DIC techniques. [Note that the development and modification of the DIC algorithm is out of the scope.]

Objective 2 – To obtain the stress-strain curve and evaluate the mechanical properties of corroded rebars using the testing and evaluation method developed in Objective 1.

The scope of this objective includes:

- The assessment of the stress-strain behaviour and evaluation of the effect of corrosion on the yield strength, ultimate strength, and ultimate strain (or strain at fracture) of corroded rebars.

- Thirteen naturally corroded, unstressed CTD rebar specimens (with degree of corrosion ranging from 3 to 40%).

1.4 RESEARCH ASSUMPTIONS

This study is carried out based on the following assumptions:

- The residual cross-sectional area of the corroded rebars varies considerably along the length. In this study, the residual cross-sectional area is assumed to be uniform over 1 mm long sections along the specimens.
- The unstressed corroded rebars used in this study are assumed to fracture or fail at the location with the least cross-sectional area. The influence of microcracks or flaws in the bulk material is ignored.
- The strain measured at a point on the surface of the rebar is equal to the average strain across the transverse cross-section through that point on that specimen; Plane transverse section of the specimen remains plane till its fracture under tension.
- The geometrical modification due to milling is not significant to affect the estimated mechanical properties.

1.5 RESEARCH HYPOTHESES

This research is conducted based on the following hypothesis:

- Full-field deformation obtained using 2D DIC technique can help to improve the assessment of the stress-strain behaviour of the unstressed naturally corroded Cold-Twisted Deformed (CTD) steel rebars with uneven cross-sectional area along the length.
- The pattern of corrosion can influence the measured or exhibited ductility (in terms of ultimate strain) of the corroded rebars.
- Corrosion do not significantly affect the mechanical properties (yield strength, ultimate strength, and ultimate strain) of naturally corroded, unstressed rebars.

1.6 RESEARCH SIGNIFICANCE

Several existing RC structures are experiencing severe corrosion. Generally, the residual structural capacity and performance of corroding RC systems are estimated based on certain underlying assumptions on the material properties of steel and

concrete. The repair or maintenance strategies are also formulated based on technical know-how, experience and engineering judgement. A realistic estimate of the mechanical properties of corroded rebars using laboratory studies can facilitate a better understanding of the structural performance of RC systems experiencing corrosion.

The conventional method of evaluating the mechanical properties of corroded rebars involves:

- The measurement of the average residual cross-sectional area of the rebar specimen,
- The measurement of strain using extensometers over a pre-defined gauge length.

These techniques have several drawbacks, which are discussed later in Sections 2.6 and 2.7. This study proposes a refined method of testing and evaluating the mechanical properties of corroded rebars. This refined method uses the 2D DIC technique to estimate full-field strain over a predefined region of the specimen. This technique can assess the local strain on the corroded rebars with uneven cross-sectional area better than the conventional method of measuring the effective strain over a predefined gauge length. This method also incorporates the 3D laser scanning technique, which can provide an accurate estimate of the residual cross-sectional area profile, which helps in the reliable prediction of the probable fracture location before the test.

Thus, this method can overcome most of the limitations of the conventional method of evaluation and can also facilitate a better understanding of the stress-strain behaviour of corroded rebars. This method involves the assessment of full-field deformation and can thus, facilitate the estimation of local mechanical properties close to the fracture location. This method can also capture the strain distribution along the predefined region on the specimen that helps in a better understanding of the ductility of the specimen. Also, this method would help to assess the influence of the pattern of corrosion on the strain distribution along the length of the specimen. This method also facilitates a virtual backup of the test specimens using the 3D laser scanning technique, which helps in the posterior assessment of rebars. The strain data of the rebars are also stored as images, which can be used any future analysis if needed.

1.7 THESIS ORGANIZATION

This thesis is organized in a Chapter-section format. The first level headings are referred to as chapters and the second, third and fourth level headings as sections. The contents of this thesis are divided into five chapters and various sections within each chapter. A brief overview of the chapters in this thesis is presented as follows.

- Chapter 1 (current chapter) started with a brief discussion on the problem of corrosion of embedded rebars faced by the RC structures. This is followed by the key definitions of certain terms used in this thesis. Then, the objectives and the scope of this research project are discussed. After this, a brief discussion of the assumptions in this study, the research hypothesis and the significance of this work.
- Chapter 2 provides a comprehensive review of the relevant literature on the stress-strain behaviour of corroded rebars. This chapter starts with an introduction to the process of corrosion in the embedded reinforcement and the topography of naturally corroded rebars. The conventional techniques adopted and the major findings from the previous studies on the assessment of the stress-strain behaviour of corroded rebars are reviewed. Then, a section on the current research need is presented based on this review. A brief review of the Digital Image Correlation (DIC) technique and Vic-2DTM software is also presented towards the end of this chapter.
- Chapter3 presents the experimental program formulated to meet the objectives of this study. The experimental details are presented as two major sections – one, the development of the testing and evaluation method and two, determination of the mechanical properties of Cold –Twisted Deformed (CTD) rebars using the developed method. The various trials included in this study are also discussed in this chapter.
- Chapter4 presents the results obtained from the two major sections of this study. The first section includes the comparison of the multiple trials and alternative methods attempted for the method development and the results from the feasibility study of the proposed method. The next section provides the results from the evaluation of the stress-strain behaviour of naturally corroded unstressed CTD rebars.
- Chapter5 presented the conclusions drawn from this study. The limitations of the proposed testing and evaluation method and future recommendations are also

provided. Later, an appendix on the detailed procedure to be followed to test the corroded rebars and evaluate the mechanical properties using the developed method is included in this thesis.

CHAPTER 2

LITERATURE REVIEW

2.1 INTRODUCTION

Researchers have conducted several studies to understand the effect of corrosion on the stress-strain behaviour of rebars. This chapter presents a comprehensive review of the previous studies on the stress-strain behaviour of corroded rebars. First, a brief outline of the process of corrosion of the embedded rebars in RC structures and the conventional method of evaluating the mechanical properties of corroded rebars is provided. Then, the various experimental techniques involved in the assessment of stress-strain behaviour of corroded rebars are reviewed. Following this, the reported effects of corrosion on the mechanical properties, (namely yield strength, ultimate strength, ultimate strain and elastic modulus) are reviewed. Then, the research needs identified from this review are discussed. Then, a review of the fundamentals of the DIC technique and the details of the DIC software, Vic-2D™, are provided.

2.2 CORROSION OF EMBEDDED REINFORCEMENT

Corrosion of embedded rebars is one of the major durability issues in RC structures. Ideally, the alkalinity (high pH) of the pore solution and the physical barrier provided by the cover concrete provides protection for the embedded rebars from the external environment. Since the pore solution has a high pH and is rich in oxygen, the Fe^{2+} on the surface of the rebar oxidizes into Ferrous Hydroxide ($\text{Fe}(\text{OH})_2$) or Ferric Hydroxide ($\text{Fe}(\text{OH})_3$). They form a passive layer over the steel rebar, which protects the rebar from further corrosion.

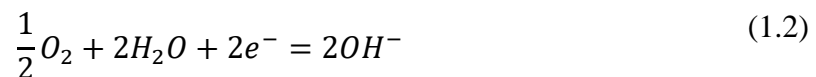
However, when the structures are exposed to corrosive environments, the detrimental elements, especially chlorides, gain access into the structures through the pores or the cracks in the cover concrete. These detrimental agents attack the passive layer and lead to its breakdown. Another factor causing breakage of the passive layer is the carbonation of the concrete surrounding the rebars. Carbonation leads to the reduction of the pH of the pore solution. When the pH of the pore solution drops below 9, the

passive layer gets neutralized. Thus, the detrimental reagents, like chloride ions, reach the surface of the rebar and lead to the corrosion of the steel.

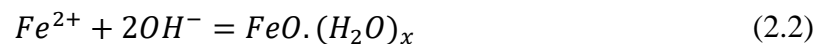
Corrosion is an electrochemical reaction in which the metal gets converted to metal oxides. The anode and cathode are formed on the rebar surface and the pore solution of the concrete acts as the electrolyte through which ion transfer occurs. At the anode, the iron changes to its lower energy state by liberating electrons, as given in Equation (2.1).



At the cathode, the reduction process occurs by accepting the liberated electrons from the anode as per Equation (2.2).



The Fe^{2+} ions released into the electrolyte from the anode reacts with the hydroxyl ions formed at the cathode forming hydrated ferric oxide (rust). This reaction is given in Equation (2.3).



Corrosion of reinforcement leads to loss of steel from the surface of the rebar, thus reducing their effective cross-sectional area. This leads to a reduction in load carrying capacity of rebars, which affects the structural performance and durability of the RC systems. Also, steel expands 6 to 8 times once it corrodes, causing the cracking of the surrounding concrete. Thus, corrosion leads to premature deterioration of RC structures (Broomfield 1997, Song and Shayan 1998).

2.3 PATTERN OF CORROSION ON REBARS IN STRUCTURES

Depending on the type of corrosion, the rebar surface may have different pattern or topographies. One of the common patterns observed in the corroded rebars is the localized reduction in cross-sectional area, as shown in Figure 2.1. This occurs due to pitting (or localized) corrosion. The chloride induced corrosion usually leads to pitting. Pitting corrosion is initiated mainly due to the following reasons – (a) localized chemical or mechanical damage to the passive layer of the rebar due to exposure to a high concentration to chlorides; (b) Localized damage in the protective coating; and/or (c) presence of non-uniformities along the metal structure. When multiple pits accumulate on the specimen, the topography of the rebar surface

becomes highly uneven as shown in Figure 2.2. Another topography of corroded rebars observed is the uniform reduction in cross-sectional area along the length of the rebars. This type of topography is a result of the uniform (or general) corrosion, which mostly occurs in the case of carbonation-induced corrosion.



Figure 2.1 Localized (pitting) corrosion topography of the rebar (Source: Francois et al. 2012)



Figure 2.2 Uneven corrosion topography along the length of the rebar

2.4 ASSESSMENT OF STRESS-STRAIN BEHAVIOUR OF CORRODED REBARS – CONVENTIONAL METHOD

This section presents a general outline of the conventional method of evaluating the effect of corrosion on the stress-strain behaviour of the rebars. Because the natural corrosion occurs with the low corrosion rate, the rebars specimens are artificially corroded in a corrosive environment set up inside the laboratories. Once the rebars are corroded, the corrosion products (rust) are removed from the surface of the rebars. The residual cross-sectional area profile of the rebars is estimated using various techniques (discussed later in Sections 2.6.1 to 2.6.3). The possible locations where the fracture might occur on the specimens can be identified either visually or based on the measured residual cross-sectional area along the length of the rebar. The extensometers are placed over a fixed gauge length (decided based on codes or based on the corrosion in the specimen) covering the predicted fracture location(s). Then, the specimens (with varying levels of corrosion) are tested under tension till the fracture. The load and strain data at regular intervals are recorded during the test. The stress-strain curves of the corroded rebars are plotted using the recorded load and

strain (or displacement) data. From the stress-strain curves, the variation in the mechanical properties (namely, the elastic modulus, yield strength, ultimate strength, and ultimate strain) with increasing degree of corrosion is evaluated.

The following sections provide a review of the conventionally adopted techniques for assessing the stress-strain behaviour of corroded rebars.

2.5 METHODS OF INDUCING CORROSION IN LABORATORY TESTING

The time taken for the rebars embedded in RC structures to corrode under the natural conditions might vary from a few months to many years depending upon the environment of exposure and the quality of surrounding concrete. Since the natural corrosion might take a long time, the laboratory studies to assess the effect of corrosion on the stress-strain behaviour are conducted on artificially corroded specimens. The following sections provide a review of the methods adopted in the previous study to induce corrosion in the specimens. Table 2.1 (page number 30) provides the method of inducing corrosion adopted in the previous studies. The most commonly adopted techniques for inducing artificial corrosion are (1) impressed current technique (also called the galvanostatic method), and (2) artificial corrosive climate.

2.5.1 Impressed Current Technique (Galvanostatic Method)

The impressed current technique (also called the galvanostatic method or anodic polarization) is one of most commonly adopted methods by researchers (Almusallam 2001, Du et al. 2005a, Cairns et al. 2005, Kashani et al. 2013, Taha and Morsy 2014). This technique involves inducing corrosion in the test specimens by supplying an external current. An electrochemical cell is set up consisting of the material to be corroded as the anode, a metal higher up in the electrochemical series as the cathode, an electrolyte and a DC power source to supply the current.

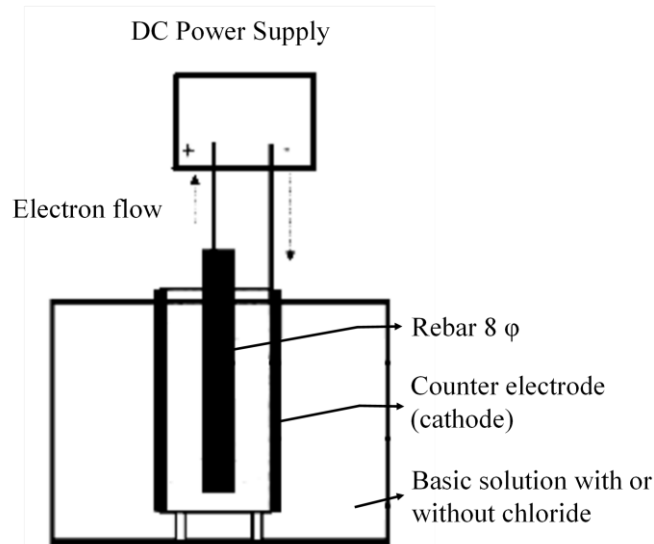


Figure 2.3 A typical setup for inducing galvanic corrosion in rebars using impressed current (Source: Yuan et al. 2007)

Figure 2.3 shows a typical set-up for inducing corrosion in rebars using the impressed current technique (Ahmad 2009). The rebar embedded in concrete is placed as the anode, and stainless steel is the commonly used cathode. Faraday's law gives the relationship between the applied current and the amount of material lost. One of the advantages of this technique is that a desired degree of corrosion can be obtained by supplying an equivalent current. However, studies have reported that the corrosion process by the Galvanostatic method is different from the natural corrosion process and hence does not fully simulate the same (Yuan et al. 2007). Zhang et al. (2012) have reported a greater impact on mechanical properties of rebars due to natural corrosion compared to artificial corrosion using impressed current.

2.5.2 Artificial Corrosive Climate

The chloride-induced corrosion in rebars is simulated in the laboratory by creating an artificial chloride laden environment (Apostolopoulos and Papadakis 2008). ASTM B117-94 has laid down the guidelines for setting up the salt-spray apparatus and the procedure for accelerated chloride corrosion tests. The salt-spray chamber consists of a salt solution reservoir, compressed air supply, nozzles, specimen supports and provision for heating the chamber. The conditions such as temperature, humidity, and exposure cycles are set to accelerate the corrosion rate. ASTM B117-94 recommends a salt solution made of 5 ± 1 parts of NaCl dissolved in 95 parts of distilled water having a pH ranging from 6.5 to 7.2 when atomized at 35°C and a temperature of $35^\circ \pm 2^\circ\text{C}$ at the exposure zone of the chamber. Some researchers have simulated

chloride-induced corrosion by embedding the rebars in concrete mixed with chlorides. Francois et al. (2012) designed a long-term experimental program where the reinforced concrete beams were stored in the chloride environment under different loading conditions for 27 years, subjecting it to alternate wetting and drying cycles to accelerate the corrosion process.

2.5.3 Other methods

Other than impressed current technique and artificial corrosive climate, few researchers have adopted certain other techniques as well to simulate the effects of corrosion in the rebar specimens. Cairns et al. (2005) have created notches by machining the test specimens to simulate the corrosion pits. However, this technique essentially assumes that corrosion causes only loss of material, but no changes in the chemical composition or material structure. Lee and Cho (2009) simulated the uniform corrosion occurring due to carbonation using the *electrical method* and pitting corrosion by accelerated curing of reinforced concrete specimen containing chloride and exposing them to cyclic wetting and drying cycles at a high temperature. Palsson and Mirza (2002) have conducted their study on naturally corroded rebar specimen extracted from a demolished bridge.

2.6 ISSUES ASSOCIATED WITH STRESS COMPUTATION

One of the challenges associated with the testing and evaluating the corroded rebars is the measurement of their residual cross-sectional area. The strength properties of the corroded rebars are computed as $\sigma = \frac{P}{A_0}$, where P is the force applied, and A_0 is the cross-sectional area of the test specimen at the beginning of the test. The computed strength properties of the rebars depends upon the measured residual cross-sectional area. There are two different approaches towards computing the strength of corroded rebars in the previous studies – (a) ‘Nominal’ strength, which is computed using the nominal diameter of the rebar (without considering the reduction in cross-sectional area due to corrosion); and (b) ‘Actual’ strength, which is computed using the residual cross-sectional area of the rebar. ‘Nominal’ strength of corroded rebars gives the reduction in the load carrying capacity of the rebar from the expected design value, whereas the ‘actual’ strength gives the strength of the residual intact steel rebar after corrosion. An accurate estimation of the actual strength of the rebar depends upon the accuracy of the measurement of the residual cross-sectional area at the fracture

location. The commonly used techniques to determine the residual cross-sectional area are the mass loss method, liquid displacement method and using Vernier calipers. The following sections provide a review of the different methods used to estimate the residual cross-sectional area of the corroded rebars in the previous studies.

2.6.1 Mass or weight loss technique

A majority of the previous studies have measured the residual cross-sectional area of the specimens using mass or weight loss method (Almusallam 2001, Ciarns et al. 2005, Apostolopoulos and Papadakis 2008, Zhang et al. 2012, Francois et al. 2012 and Kashani et al. 2013). In this method, the rebar specimens are weighed before and after corrosion, and the loss of weight or mass after corrosion is computed. The residual cross-sectional area is computed from the mass loss as $A = \frac{(M-\Delta M)}{\rho \times L}$, where, M is the original mass of the specimen (before corrosion), ΔM is the measured mass loss due to corrosion, ρ is the density of the steel (which is assumed to be not affected due to corrosion), and L is the length of the specimen. However, this method gives only an average cross-sectional area over the length of the specimen. In the case of uniformly corroded specimen the mass loss method can give a relatively good estimate of the reduction in cross-sectional area. However, in the case of specimens with uneven or localized corrosion, the measured average residual cross-sectional area using mass loss may significantly vary from the residual cross-sectional area at the fracture location of the specimen. Zhu and Francois (2013) have measured the reduction in cross-sectional area from loss of mass of the specimen by cutting the specimen into smaller pieces after the tension test on the specimen, assuming that the specimen did not undergo significant plastic deformation, as a brittle fracture was observed. Du et al. (2005a) have reported that the measurement of the residual cross-sectional area from weight loss method can lead to unreasonable and unsafe evaluation of the residual capacity of the rebars.

2.6.2 Liquid displacement technique

Another commonly used method of measuring the uneven residual cross-sectional area profile along the length of the corroded specimen is the liquid displacement method. In this method, the specimen is immersed in a graduated glass cylinder containing some liquid, normally water. The volume of the liquid displaced with the immersion of certain length of a specimen is measured. The average cross-sectional

area over the immersed length is computed from the displaced volume of the liquid as $A = \frac{V_{liq}}{l}$, where V_{liq} is the displaced volume of the liquid and ' l ' is the immersed length of the specimen and ' A ' is the average cross-sectional area along ' l '. The closeness of the measured cross-sectional area to that at the fracture location would depend upon the unevenness of the cross-sectional area. Also, an accurate estimation of the cross-sectional area profile would be obtained using this technique only if the volume of the rebars is measured over sufficiently short lengths of the specimen. If the length ' l ' is large, the measured average cross-sectional area could be significantly different from the residual cross-sectional area at fracture location, for specimens with uneven or localized corrosion.

2.6.3 Using Vernier calipers

Palsson and Mirza (2002) and Francois et al. (2012) have attempted to use Vernier calipers to measure the cross-sectional area along the length of the corroded rebars. Measurement using Vernier calipers can give a better estimation of the cross-sectional area at specific locations, rather than an average cross-sectional area over a certain length. However, this method measures the diameter assuming that the cross-sectional area is circular while the residual cross-sectional area of corroded rebars can be quite irregular.

2.6.4 Quantification of degree of corrosion

In most of the previous studies, the degree of corrosion in the rebar specimens is expressed in terms of the loss in the cross-sectional area compared to the pristine rebar. It is essential to quantify the degree of corrosion in a specimen to study the trend of variation in the mechanical properties. However, a few studies have expressed the variation in the mechanical properties with respect to the duration of exposure to the chloride environment (Apostolopoulos and Papadakis 2007, Apostolopoulos and Kappatos 2015). This quantification makes it difficult to relate the variation in the computed mechanical properties of the corroded rebars to that in the existing structures.

2.7 ISSUES ASSOCIATED WITH MEASUREMENT OF STRAIN IN CORRODED REBARS

The axial strain in the corroded rebar specimen during the tension test is measured using extensometers as $\varepsilon = \frac{\Delta L}{L_0}$, where ' L_0 ' is the gauge length over which the displacements are measured and ' ΔL ' is the elongation of the gauge length at a particular instant of time. For tension testing of rebar specimens, gauge length is selected as per the recommendations in standard guidelines. IS 1608 (2005) and ASTM E8M (2013) recommends a gauge length of five times the diameter for rounded test specimens. In the case of corroded rebars, the difficulty in visually predicting the fracture location on the corroded rebars compels the researchers to use a 'suitable' gauge length. The selected 'suitable' gauge length depends upon the number and distribution of probable fracture locations.

Figure 2.4 presents a schematic diagram showing the selection of 'suitable' gauge length for corroded rebar test specimen prior to the tension test. The probable fracture locations identified on the specimen is marked by a '×' mark, labeled 'a' and 'b' and the different possible gauge lengths are marked as '1', '2' and '3'. If 'a' is the location with the least cross-sectional area, i.e. the probable fracture location, then extensometer is placed as indicated by '1', while it is placed as indicated by '2' if 'b' is the identified probable fracture location. If there is difficulty in identifying which of these locations would be the fracture location, researchers tend to choose a gauge length as indicated by '3', covering both the probable fracture locations.

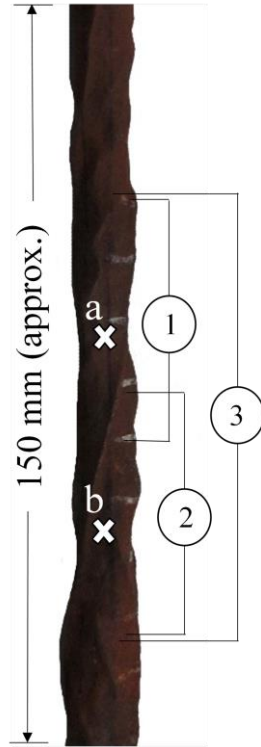


Figure 2.4 Schematic diagram depicting the possible selection of gauge lengths for corroded rebar with uneven cross-sectional area

The different ‘suitable’ gauge lengths selected in the previous studies are presented in the fifth column in Table 2.1. Palsson and Mirza (2002) have measured strain using two a nested extensometer with 25 mm(0.98 in.) gauge length within 75 mm(2.95 in.) gauge length for 16 mm (0.63 in.) diameter rebars. Du et al. (2005) have used 50 mm (1.97 in.) gauge length for testing corroded rebars specimens of nominal diameter 8, 16 and 32 mm (0.32, 0.63, and 1.26 in.). Apostolopoulos and Papadakis (2007) have used 150 mm (5.9 in.) gauge length to measure strain over specimens of 10 mm (0.39 in.) nominal diameter. Francois et al. (2013) have used 200 mm (7.87 in.) as the gauge length for testing rebar specimens of 16 mm (0.63 in.) nominal diameter.

The use of ‘suitable’ gauge length leads to ambiguous strain measurement. Moreover, the measurement of strain in corroded rebars over a gauge length assumes a uniform strain distribution along the length and neglects the strain heterogeneity associated with the uneven cross-sectional area profile of the corroded rebars. Researchers have also reported fracture of the specimens outside the selected gauge length (Palsson and Mirza 2002, Du et al. 2005b, Kashani et al. 2013). This is due to the inability to accurately predict the fracture location before the tension test. The following sections provide a review of the reported effects of corrosion on the mechanical properties of the rebars, from the previous studies.

2.8 EFFECT OF CORROSION ON STRENGTH PROPERTIES OF CORRODED REBARS

The strength properties of the rebars are an important design parameter for RC structures. Therefore, the effect of corrosion on the strength properties of rebars is vital information to understand the response of corroding structures to the load acting on them. In literature, the term ‘strength’ is defined in terms of force (in kN) as well as stress (in MPa). Throughout this study, strength refers to the capacity of the rebars in units of stress (in MPa). The following sections present a review of the effect of corrosion on the yield and ultimate strength of the rebars. The effect of corrosion on the strength properties of unstressed and stressed rebars are reviewed separately.

2.8.1 Effect of corrosion on yield strength of unstressed rebar specimens

The yield strength of the material is the stress at which the material begins to deform plastically. If the material does not show a definite yield point, 0.2% offset stress is taken as the yield strength of the material. Researchers have reported that nominal yield strength of the rebars reduces significantly with the increase in the degree of corrosion (Almusallam 2001, Du et al. 2005, Apostolopoulos and Papadakis 2007). This is due to the use of nominal cross-sectional area instead of the actual cross-sectional area. Du et al. (2005a) and Apostolopoulos and Papadakis (2008) reported that the reduction in ‘nominal’ strength is not proportional to the reduction in cross-sectional area, suggesting that the corrosion may induce more effects in the bulk material than just a reduction in cross-sectional area. However, the researchers differ in their opinion regarding the actual yield strength of corroded rebars. A few of the researchers have stated that corrosion has no significant effect on the actual yield strength of the rebars. Figure 2.5 shows the variation of yield strength with increasing degree of corrosion reported by Cairns et al. (2005). They have reported that corrosion does not significantly affect the yield strength of the rebars. On the other hand, Du et al. (2005a) reported a reduction of 5% in the actual yield strength due to 10% reduction in cross-sectional area (measured using weight loss method). Figure 2.6 shows the reduction in yield strength observed for plain and ribbed 8 mm diameter rebars by Du et al. (2005a).

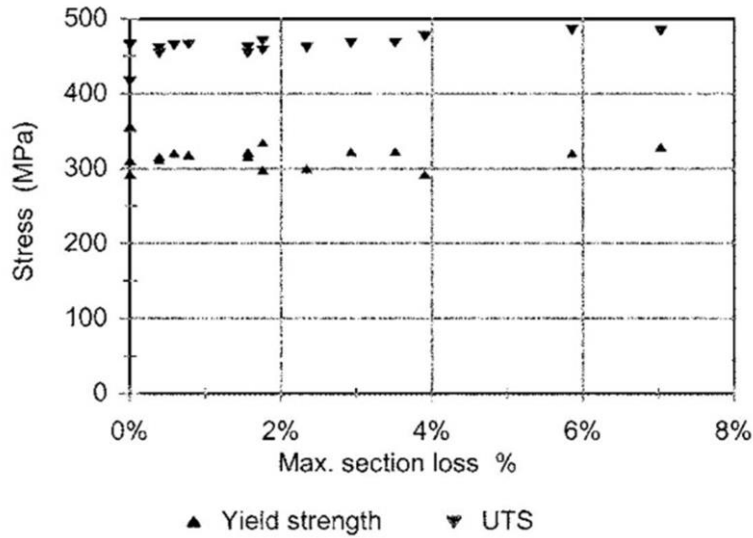


Figure 2.5 Plot showing no significant effect on yield strength with increasing degree of corrosion [reproduced from Cairns et al. (2005)]

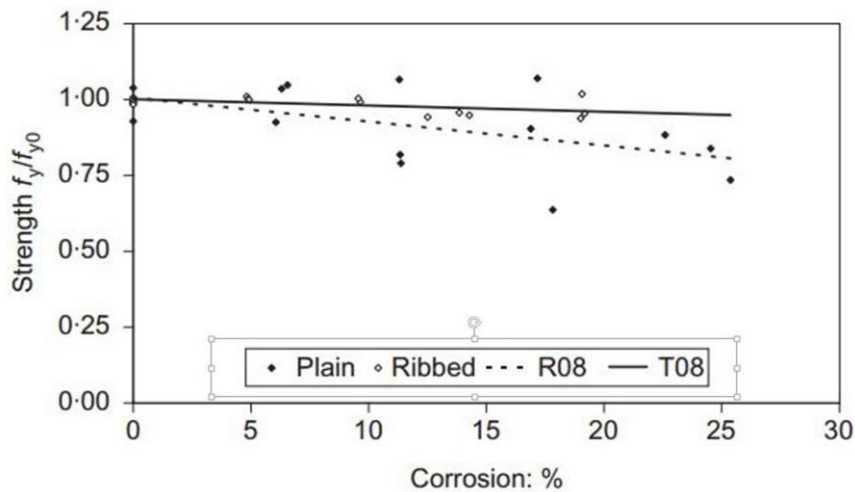


Figure 2.6 Reduction in yield strength due to corrosion [reproduced from Du et al. (2005)]

2.8.2 Effect of corrosion on ultimate strength of unstressed rebar specimens

Similar differences in opinion were observed in the reported effect of corrosion on the ultimate strength of unstressed rebar specimens. Almusallam (2001), Apostolopoulos and Papadakis (2008) and Francois et al. (2012) concluded that nominal ultimate strength reduces, while actual yield strength remains unaffected due to corrosion. This is also because of the computation using the nominal cross-sectional area, which is more than the actual cross-sectional area. However, Du et al. (2005a) reported a marginal reduction of 6% in actual ultimate strength due to 10% corrosion. Apostolopoulos and Papadakis (2008) reported a *moderate* loss in tensile strength of

rebars due to corrosion. On the other hand, Cairns et al. (2005) reported an increase in the measured ultimate strength with increasing degree of corrosion. This is shown in Figure 2.5. Cairns et al. (2005) explained this observation to be due to “...*If a bar does not have a completely uniform cross section and material composition throughout its length, then it would clearly be expected to fracture at the point where the material is weakest. If the position of the pit does not coincide with the location where the steel is weakest, an apparent increase in strength (where this is based on the minimum cross-sectional area) will be measured...*”. The observed increase in ultimate strength with increasing degree of corrosion could be due to underestimation of the residual cross-sectional area of the rebars.

2.8.3 Effect of corrosion on strength properties of stressed rebars

Most of the previous studies are conducted on unstressed corroded rebars. Only a very few researchers have looked into the effect of corrosion on the stress-strain behaviour of stressed specimens (Palsson and Mirza 2002, Francois et al. 2012, Zhu and Francois 2013). Palsson and Mirza (2002) reported, “... a slight increase in the yield strength was noted in the case of the the pitted specimens...”. This could be due to an underestimated residual cross-sectional area of corroded rebars at the location of pit, due to the difficulty in measuring the irregular cross-sectional area. Francois et al. (2012) concluded that corrosion hardly alters the yield behaviour of the rebars collected from loaded concrete beams. However, they reported an increase in ultimate strength in corroded rebars. This is shown in Figure 2.7. This observation was explained as “...*Almost all the corroded bars failed at a pit location and the increase in true ultimate strength at the pit can be explained by the fact that the failure path is imposed by the pit and does not correspond to the weakest point of the steel bar as is the case for non-corroded bar...*”. However, it seems that an in-depth statistical analysis of a larger set of similar specimens might have led to a different conclusion. Zhu and Francois (2014) also reported an increase in the ultimate strength. However, the combined effect of stress and corrosion on the strength properties of the corroded rebars are not very well explored in the previous studies.

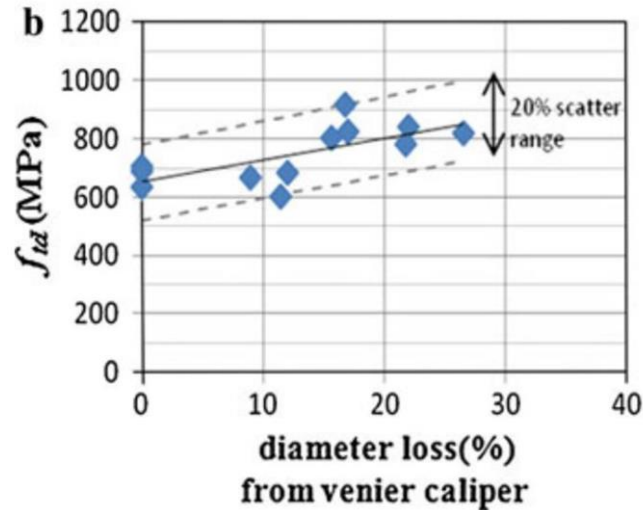


Figure 2.7 Increase in ultimate strength [reproduced from Francois et al. (2012)]

2.8.4 Possible reasons for differences in opinion

Previous studies reveal considerable differences in opinion among researchers regarding the effect of corrosion on the strength properties of rebars. Du et al. (2005b) and Taha and Morsy (2013) have pointed out the differences in opinion among researchers. Du et al. (2005b) have reported that the differences in opinion in the previous studies are mainly due to differences in the experimental techniques adopted in the previous studies and the type of rebars tested. The possible reason for these differences in opinion could be the following:

- The fracture of the specimen may at a location away from the pit or the location with least cross-sectional area due to internal defect in the material. However, the strength could be computed with the measured least cross-sectional area, leading to a measured increase in the strength properties.
- The residual cross-sectional area estimated using the mass loss or liquid displacement method gives only an average reduction in the cross-sectional area over a certain length of the specimen. This value may significantly be different from actual residual cross-sectional area at fracture location, especially if the cross-sectional area profile is highly uneven. This may lead to underestimation of the actual reduction in the cross-sectional area at the fracture location, which might lead to measurement of a decrease in the strength properties.

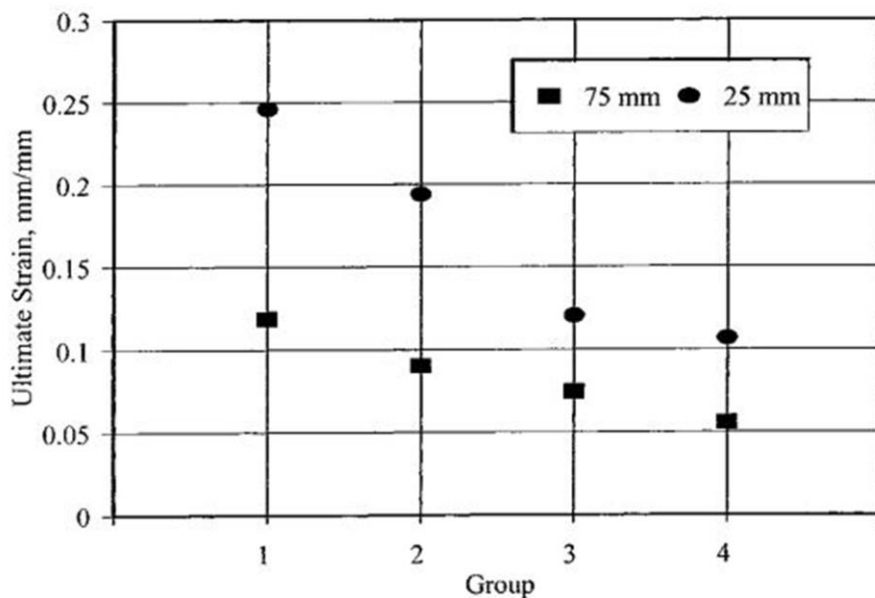
2.9 EFFECT OF CORROSION ON DUCTILITY OF REBARS

Ductility of reinforcement bars indicates the amount of deformation the rebars can undergo before fracture. Ductility of the rebars is one of the important parameter for the structural design, which gives a measure of the deflection of the reinforced concrete elements. The performance of the structure under dynamic/seismic loads and the warning in the form of deflection provided by specimens before failure depends on the ductility of the rebars. The ductility is measured in terms of the strain in by the rebar specimens at fracture. It should be noted that the strain in the rebars is measured using extensometers over a selected gauge length.

Although differences in opinion exist regarding the effect of corrosion on the strength properties of rebars, researchers have similar opinion that the ductility (expressed in terms of strain at fracture or the ultimate strain) reduces due to corrosion. Most of the previous studies have concluded that the effect of corrosion is more prominent on the ductility than the strength of rebars (Du et al. 2005(sept), Apostolopoulos and Papadakis 2008, Zhu and Francois 2013). Researchers have also quantified the reduction in the ultimate strain with the degree of corrosion. The reported variation in ductility in the previous studies is discussed in the following paragraphs.

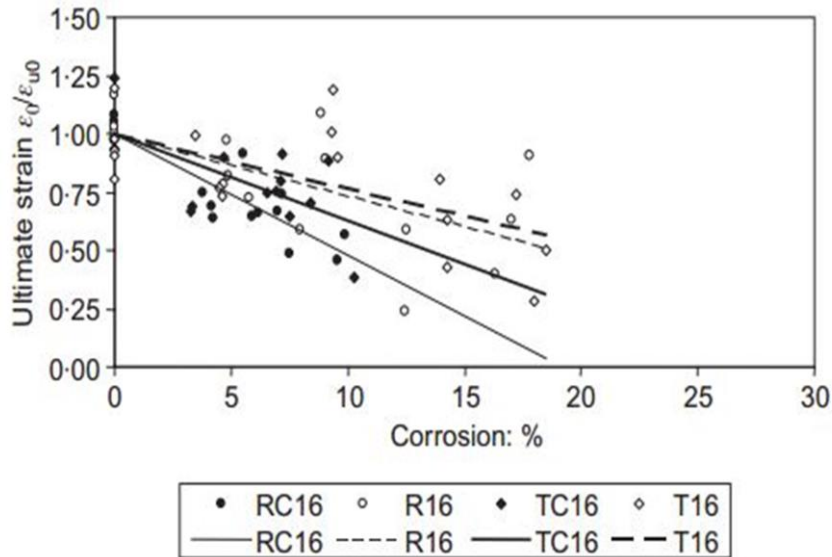
Almusallam (2001) reported a systematic decrease in the yield strain of the rebars with increasing degree of corrosion. They reported that beyond 12% corrosion in 6 mm (0.236 in) diameter rebars, the elongation was less than the minimum requirement of 9% specified for Grade 60 rebars as per ASTM A 615. The measured reduction in the ductility is reported to be due to the stress concentration at the *locally thinned* (or corroded) section, thus leading to a lower strain (measured over the entire gauge length) at the time of fracture. Palsson and Mirza (2002) measured the strain in 16 mm (0.63 in) diameter rebar specimens using two nested extensometer of 25 mm (0.98 in) gauge length within a 75 mm (2.95 in) gauge length. Figure 2.8 shows the strain measured over 25 mm and 75 mm gauge length for specimens classified into four groups based on the degree of corrosion on the specimens. They reported that specimens of group 1 exhibited similar levels of ultimate strain as that of the pristine rebars, while the heavily pitted specimens (group 4) exhibited much less ultimate strain. A higher ultimate strain was measured over 25 mm gauge length compared to 75 mm gauge length, as most of the plastic deformation took place closer to the fracture location.

Figure 2.9 shows the reduction in ultimate strain with increasing degree of corrosion reported by Du et al. (2005b). They observed a decrease of 29% in the ultimate strain with 10% reduction in the cross-sectional area due to corrosion. They have also concluded that the reduction in ductility is primarily a function of degree of corrosion. Figure 2.10 shows the decrease in elongation at fracture reported by Cairns et al. (2005). They reported a reduction of 20% in the ultimate strain with 8% reduction in cross-sectional area. Figure 2.11 shows the exponential decrease in ultimate strain with increase in mass loss (which is a measure of the degree of corrosion in the specimen) reported by Apostolopoulos and Papadakis (2008). They have reported this variation with respect to the period of exposure to salt spray. They measured a reduction of 14% in ultimate elongation with 20 days of exposure (approximately a mass loss of 10%).



Note: Group refers to the classification of specimens based on the degree of corrosion – specimens with a degree of corrosion less than 10% as group 1, 10-20% as group 2, 20-30% as group 3 and greater than 30% as group 4

Figure 2.8 Ultimate strain measured using nested extensometers -- 25 mm within 75 mm gauge length – [reproduced from Palsson and Mirza (2002)]



Note: RC16 and TC16 refer to plain and ribbed rebars, respectively, of 16 mm diameter embedded in concrete. R16 and T16 refer to corresponding bare rebars.

Figure 2.9 29% reduction in ductility (ultimate strain) due to 10% corrosion measured in [reproduced from Du et al. (2005)]

Youlin et al. (2012) and Francois et al. (2012) observed brittle fracture in corroded rebars without much necking. Figure 2.12 shows the reduction in ductility with reduction in effective diameter (computed using mass loss method). Zhang et al. (2012) expressed ductility of corroded rebars in terms of strength ratio (i.e., ultimate strength to yield strength). They observed a higher reduction in ultimate strength compared to yield strength and concluded that corrosion could lead to brittle failure of rebars. Kashani et al. (2013) reported that non-uniform pitting corrosion has a significant effect on plastic deformation. They reported a reduction of 50% in the plastic deformation due to a degree of corrosion of 10%.

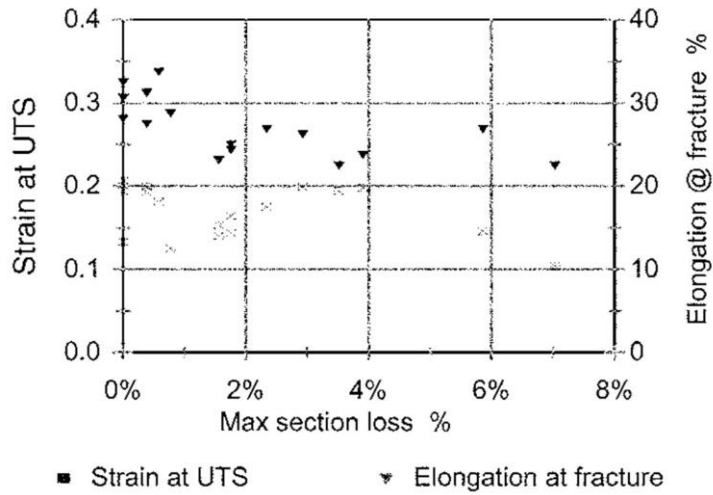


Figure 2.10 Decrease in ultimate strain with the reduction in the cross sectional area [reproduced from Cairns et al. (2005)]

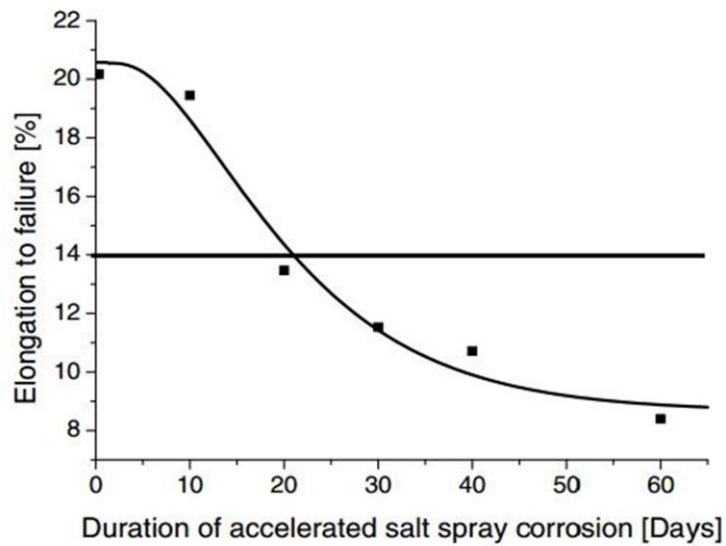
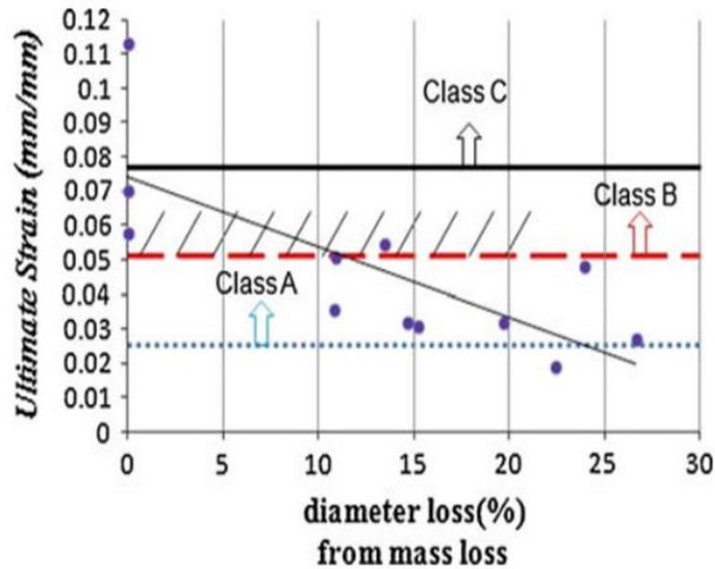


Figure 2.11 Exponential reduction in ductility with increasing degree of corrosion [reproduced from Apostolopoulos and Papadakis (2008)]



Note: Class A, B and C refers to categories of rebars based on minimum value of ultimate strain in Eurocode 2 (2002).

Figure 2.12 Reduction in ductility [reproduced from Francois et al. (2012)]

2.9.1 Effect of pattern of corrosion on ductility of rebars

Some of the previous studies have investigated further on the effect of corrosion on the ductility of the rebars. One of the major concerns regarding the ductility of the corroded rebars is the influence of the pattern of corrosion (discussed in Section 2.3). Palsson and Mirza (2002) have reported that the variation in the residual cross-sectional area along the length of the rebars, expressed in terms of the ratio of the smallest to the largest cross-sectional area along the gauge length, has a significant influence on the ultimate strain. This is shown in Figure 2.13. They reported that higher the non-uniformity in the cross-sectional area along the gauge length (lower ratio of the smallest to the largest cross-sectional area), lower is the ultimate strain exhibited by the rebars. Zhu and Francois (2013) concluded that the shape of the corrosion pit influences the ultimate strain of the rebar more than the depth of the pit and the loss in the cross-sectional area. Zhang et al. (2010) also concluded that the ultimate strain decreases exponentially with increase in 'k', which is a geometrical parameter of the hyperbolic pits on the rebars. Kashani et al. (2013) have concluded that the distribution of pits along the length is the most important parameter which influences the stress-strain behaviour of corroded rebars.

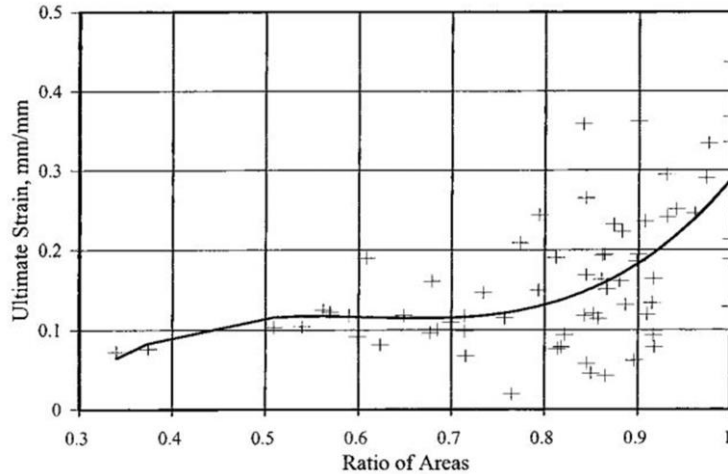


Figure 2.13 The influence of the variation in cross-sectional area on the ultimate strain [reproduced from Palsson and Mirza (2002)]

Although researchers have a similar opinion regarding the effect of corrosion on the ductility of the rebars, there are ambiguities in the measured strain values due to the selection of ‘suitable’ gauge lengths (as discussed before in Section 2.7). Also, the influence of the shape of the pit or the variation in cross-sectional area along the length on the strain in rebars gets neglected when strain is measured over the gauge length. Hence, there is a need for a better understanding of the effect of corrosion on the deformation of the corroded rebars.

2.10 EFFECT OF CORROSION ON ELASTIC MODULUS OF REBARS

Only a few of the previous studies have investigated the influence of corrosion on the elastic modulus of the rebars. Francois et al. (2013) reported that corrosion has no significant influence on the elastic modulus of rebars. Taha and Morsy (2013) also observed no considerable change in elastic modulus due to corrosion. However, Andisheh et al. (2014) observed a decrease in elastic modulus with increasing degree of corrosion. Lee and Cho (2007) reported a decrease in the elastic modulus computed using the nominal cross-sectional area.

2.11 CURRENT RESEARCH NEEDS

The review of the previous studies on the effect of corrosion on the stress-strain behaviour of the rebars highlights many issues associated with the testing and evaluation method. There are limited guidelines to test and assess the stress-strain behaviour of corroded rebars with uneven cross-sectional area along the length. This has led to the differences in adopted experimental techniques in the previous studies

(as shown in Table 2.1). The major drawbacks of the conventional methods of evaluation include the measurement of average reduction in the cross-sectional area along the length of the rebars and measurements of strain over 'suitable' or arbitrary gauge length. Also, the measurement of strain over the gauge length using extensometers does not capture the strain heterogeneity along the length of corroded rebars associated with the uneven residual cross-sectional area profile. Also, the review has exhibited the influence of the adopted experimental techniques on the measured mechanical properties. This has led to the differences in opinion among researchers regarding the effect of corrosion on the mechanical properties of the rebars (as shown in Table 2.2). This indicates the inadequacy of the conventional methods in testing and evaluating the effect of corrosion on the stress-strain behaviour of corroded rebars.

Table 2.1 Comparison of the experimental technique adopted in some of the previous studies

Method of inducing corrosion	a) Method of measuring residual CSA b) Length over which average CSA is measured	a) Stressed/Unstressed specimens b) Pattern of corrosion	a) Type/Grade of rebar b) Diameter of the specimen	Selected gauge length	Reference
Impressed current technique	a) Mass loss method b) NR	a) Unstressed b) NR	a) Grade 60 (ASTM A 615) b) 6 and 12 mm	NR	Almusallam (2001)
Naturally corroded specimen	a) Vernier calipers and average CSA loss b) 25 mm	a) Stressed b) Pitting	c) NR d) 16 mm	25 mm within 75 mm	Palsson and Mirza (2002)
Impressed current technique	a) Liquid displacement technique b) 10 mm	a) Unstressed b) NR	a) CEB Model 90 specimens b) 8, 16, and 32 mm	50 mm	Du et al. (2005 April)
Machined notches & anodic polarization	a) Weight loss and liquid displacement method b) NR	a) Unstressed b) Uniform and localized	a) NR b) 12, 16, 20 and 24 mm	Five times the diameter	Cairns et al. (2005)
Salt spray technique	a) Mass loss b) 250 mm	a) Unstressed b) NR	a) BSt 420 grade rebar (DIN 488-1) b) 10 mm	150 mm	Apostolopoulos and Papadakis (2007)
Impressed direct current and accelerated curing by cyclic wetting and drying in high temperature	a) Reduction in CSA not measured b) NA	a) Unstressed b) Uniform and pitting	a) SD 295 A (D10 and D13) and SD 345 D13 b) NR	NR	Lee and Cho (2007)
Naturally corroded and impressed current technique	a) Mass loss method b) 300 to 500 mm	a) Unstressed b) Pitting as well as uniform corrosion	a) NR b) 12 mm	50 mm	Zhang et al. (2012)
Long-term exposure to chlorides mixed with concrete	a) Mass loss after tension testing b) Varying lengths	a) Stressed b) Pitting	a) Rebars of 500 MPa b) 16 mm	200 mm	Francois et al. (2013)
Impressed current technique	a) Mass loss technique b) Over entire length of the specimen	a) Unstressed b) Pitting and uneven	a) B500B British standard rebars b) 8 and 12 mm	100 mm	Kashani et al. (2013)

CSA – Cross-sectional area; NR – Not Reported; NA – Not Applicable

Table 2.2 A comparison of the effect of corrosion on the mechanical properties of rebars reported in the literature

Yield Strength		Ultimate Strength		Ultimate strain	Elastic Modulus	Reference
Nominal	Actual	Nominal	Actual			
NR	Marginal decrease	NR	Marginal decrease	Decreases	NR	Almusallam (2001)
NR	No change, slight increase for pitted specimens	NR	No change	Decreases	NR	Palsson and Mirza (2002)
NR	Decreases	NR	Decreases	Decreases	NR	Du et al. (2005 April)
NR	No change	NR	Increases	Decreases	NR	Cairns et al. (2005)
Decreases	No change	Decreases	Decreases	Decreased	NR	Apostolopoulos and Papadakis (2007)
Decreases	NR	Decreases	NR	Decreases	Decreases (Nominal elastic modulus)	Lee and Cho (2007)
Yield load decreases	Decreases	Maximum load decreases	Decreases more than yield strength	Elongation decreases	NR	Zhang et al. (2012)
Decreases	No change	Decreases	Increases	Decreases	No change	Francois et al. (2013)
Decreases	Decreases	Decreases	Decreases	Decreases	NR	Kashani et al. (2013)

NR - Not Reported

Hence, there is a need for a more refined testing and evaluation method to assess the stress-strain behaviour of corroded rebars which can meet the following utilities.

- A more accurate method to estimate the profile of the residual cross-sectional area of the corroded rebars, which will, in turn, facilitate an accurate prediction of the probable fracture location(s)
- An utility to perform posterior analysis to compute the local deformation and the stress-strain behaviour close to the fracture location.
- Technique to capture the strain heterogeneity along the rebars due to the uneven cross-sectional area profile

Considering these requirements, this study proposes an improved method of evaluating mechanical properties of corroded rebars using Two-Dimensional Digital Image Correlation (2D DIC) technique. 2D DIC technique can estimate the full-field deformations over a predefined region on the surface of the deforming specimen. Full-field deformation measurement using 2D DIC gives the displacement of defined points on the predefined region along x - and y - axis of the specimen. The

measurement of full-field deformation can overcome the limitations of the conventional method of measuring the effective strain over the gauge length using extensometers. The full-field deformation gives the displacement of defined points spaced at regular intervals and thus, can capture the strain heterogeneity in the corroded rebars. Full-field deformation also aids in estimating the strain at the fracture location, which gives a better estimate of the stress-strain behaviour of the corroded rebars. The proposed method also incorporates 3D laser scanning to estimate the residual cross-sectional area profile along the rebars, which can facilitate an accurate identification of the fracture location (prior to the test).

2.12 DIGITAL IMAGE CORRELATION (DIC) TECHNIQUE

Digital Image Correlation (2D DIC) is a non-contact, optical technique of estimating the full-field deformations over a predefined region on the surface of the deforming specimen. The pre-defined region on the specimen over which displacements are measured is referred as the Area of Interest (AOI). DIC technique involves tracking the changes in position of the points on the AOI across a set of images captured during the deformation of the object. The movement of the point of interest is estimated by firstly locating the point in the reference configuration (i.e., the image of the specimen taken at the start of the test, which corresponds to the undeformed state); and then the tracking the corresponding locations of this point in the subsequent images containing the deformed state of the specimen.

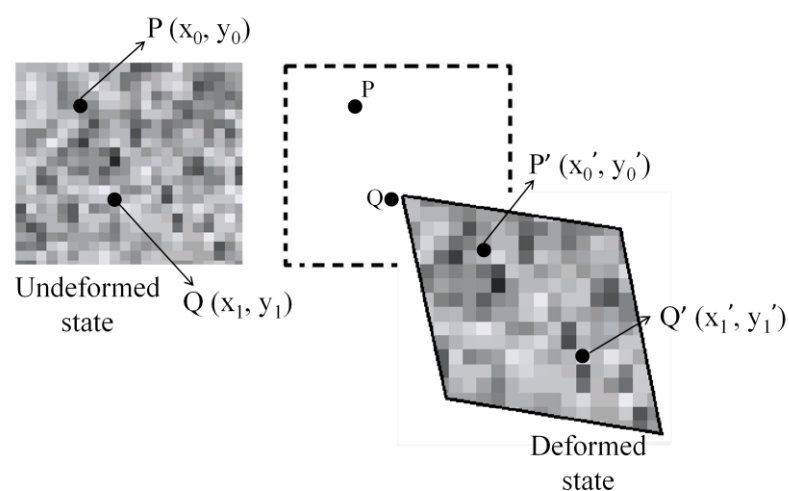


Figure 2.14 Schematic diagram illustrating the principles of DIC (adapted from Pan et al. 2009)

The process of tracking the movement of the points in the AOI is illustrated in Figure 2.14. Two points of interest, 'P' and 'Q' occupying the spatial coordinates (x_0, y_0) and (x_1, y_1) , are identified in the image of the undeformed state of the object (called the reference image). The change in position of these points is tracked in the subsequent images containing the deformed state of the specimen. 'P' and 'Q' occupying spatial coordinates (x_0', y_0') and (x_1', y_1') , respectively (Pan et al. 2009). Once the point correspondence is known between the two frames (the undeformed and the deformed state), the full-field displacements are estimated using Lukas-Kannade algorithm by comparing the position of every point in the current configuration with the respective position in the reference configuration (Sutton et al. 2009). To distinctly locate each point of interest on the AOI across the images by the DIC software program, the AOI of the specimens are speckled with a random distribution of dark and light blobs of paint (defined as speckles).

There are two variants of DIC technique – (a) Two Dimensional DIC technique (2D DIC), in which deformations are measured over a plane region on the object using one camera placed perpendicular to the 2D (plane) AOI, and (b) Three Dimensional DIC (3D DIC) technique, in which deformations are measured over a curved region on the object using two cameras focusing on the curved AOI. 2D DIC is adopted in this study, even though the testing of rebars typically required 3D DIC technique, considering its ease of application for users (especially from civil engineering community) who may not be familiar with the DIC technique. 3D DIC is a more sophisticated compared to 2D DIC and requires expertise in this technique.

2.12.1 Applications of DIC in civil engineering

Recently, DIC technique has been gaining wide acceptance in the field of civil engineering. The application of DIC technique in this discipline ranges from laboratory testing of materials to monitoring of the performance and the deflections in the real structures. The newly developed construction materials are being evaluated using DIC technique to characterize their mechanical behaviour. Boulekbache et al. (2013) have used DIC to study the failure mechanism of fibre reinforced concrete. They reported that DIC technique could provide accurate and detailed information regarding fracture mechanism in the splitting. Gencturk et al. 2014 have used DIC technique to study the brittle failure of prestressed concrete structures. Li et al. 2015 have studied the shear capacity of I-shaped prestressed concrete beams using 2D DIC

technique. Malesaet al. 2010 have employed DIC sensors to monitor the displacements in a longitudinal truss girder of a steel railway bridge in Poland when the locomotive passes over the bridge.

2.12.2 Vic-2DTM software program

The computation of full-field displacement (or strain) using DIC technique essentially requires an appropriate digital camera and a DIC software. There are several software available commercially that can compute full-field displacement from images of the deforming object using DIC technique. Vic-2DTM is one of the widely used commercial DIC software that computes the full-field displacements as well as the strains. This software provides an accuracy of one-hundredth of a pixel for the computed displacements.

The computation of full-field displacement (or strain) using Vic-2DTM requires a few parameter inputs. These parameters are *step size*, *subset size*, and *filter size*. The *step size* controls the spacing of the points in the AOI (in terms of pixels) whose movements are tracked across the images. For instance, a step size of 5 correlates every 5th pixel in both horizontal and vertical directions in the image. The deforming object is speckled before capturing the images to facilitate a point-to-point correlation across the images (as discussed before in Section 2.12). To uniquely identify the points across the images, a set of points, called the subset, in the neighbourhood of the point of interest is also identified. The *subset size* defines the size of the square grid of points selected around the point of interest (with the point of interest in the geometrical centre of the subset). For instance, a *subset size* of 25 selects a square grid of 25 × 25 pixels around the point of interest. The full-field displacement data is smoothed prior to strain computation to eliminate the noise in the data. *Filter size* defines the size of the smoothing window in terms of data points. For instance, a *filter size* of 5 selects a smoothing window over 5 × 5 data points in horizontal and vertical direction. The image analysis using DIC technique computes displacement (referred to as ‘*u*’ and ‘*v*’ in Vic-2DTM) and strain (referred to as ‘*exx*’ and ‘*eyy*’ in the software), both in longitudinal (*y*-axis) and lateral (*x*-axis) directions of the specimen (Vic-2D reference manual).

2.13 SUMMARY

A comprehensive review of the previous studies on the effect of corrosion on the stress-strain behaviour of corroded rebars was performed. The review revealed the differences in opinion among researchers regarding the effect of corrosion on strength properties. The possible reasons for the differences in opinion are also stated in this chapter. The results from previous studies also suggest the inadequacy of the conventional method of measuring strain using extensometer over a gauge length. Based on this review, the current research need are identified and discussed in this chapter. A review of the DIC technique and Vic-2DTM software is also provided in this chapter. The following chapter provides a detailed description of the experimental program formulated for meeting the objectives of this study.

CHAPTER 3

EXPERIMENTAL PROGRAM

3.1 INTRODUCTION

A detailed review of the literature brings into light the need for more information on the stress-strain behaviour of corroded rebars and the inadequacy of the conventional method of testing and evaluation for the assessment of the same. The current research needs are identified and discussed in Section 2.11. This chapter provides a detailed description of the experimental program formulated to meet the research objectives (stated in Section 1.3).

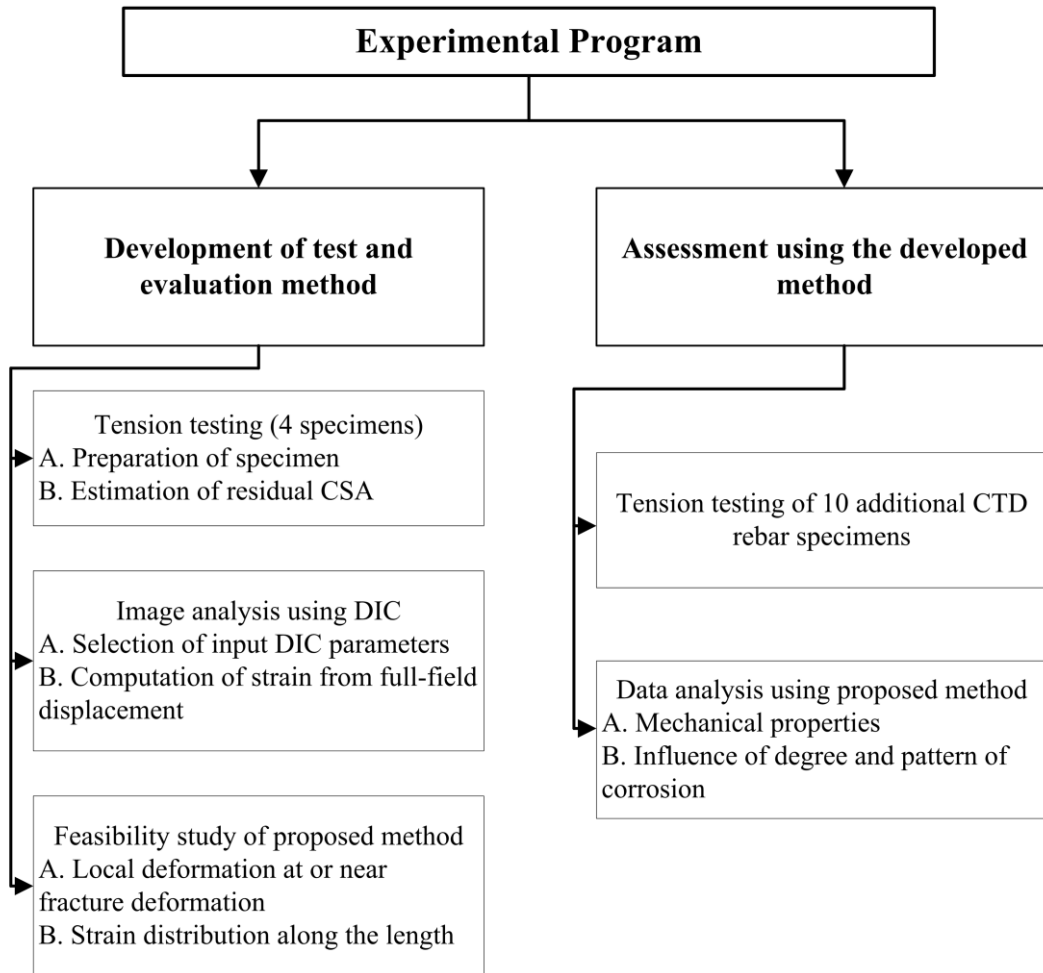


Figure 3.1 Flowchart providing an outline of the experimental program

An outline of the experimental program formulated for this study is presented in Figure 3.1. This study consists of two phases – (a) Development of the testing and evaluation method using 2D DIC technique; and (b) Evaluation of the effect of corrosion on the stress-strain behaviour of the Cold-Twisted Deformed (CTD) steel rebars using the developed method. This chapter provides a detailed description of the experimental techniques involved in the various elements in the two phases of the study. Before that, the details of the steel rebar specimens tested in this study are discussed in Section 3.2. The results obtained from the experiments are provided later in Chapter 4. A to-do procedure to assess the stress-strain behaviour of corroded rebars using the developed method is given in the Appendix of this thesis.

3.2 SPECIMEN DETAILS

Figure 3.2 shows these two types of steel rebars used in this study – a) Plain Mild (PM) steel rebars (without ribs) of 16 mm nominal diameter and b) Cold-Twisted Deformed (CTD) steel rebars, with helical ribs, of 12 mm nominal diameter (Refer Table 3.1 for the typical chemical composition of these steel types). Table 3.2 provides the details of the rebar specimens made from these two types of steel rebars. The specimens are named in increasing order of the degree of corrosion. The PM steel rebar specimen with negligible corrosion is named ‘S0’. The CTD steel specimens with the least degree of corrosion (3%) as ‘S1’ and that with the highest degree of corrosion (40%) as ‘S13’. Figure 3.3 shows the images of the testing regions of these fourteen specimens. The white dotted lines indicate the fracture location. The residual cross-sectional area at the fracture location (at the beginning of the tension test) is shown above corresponding rebars.

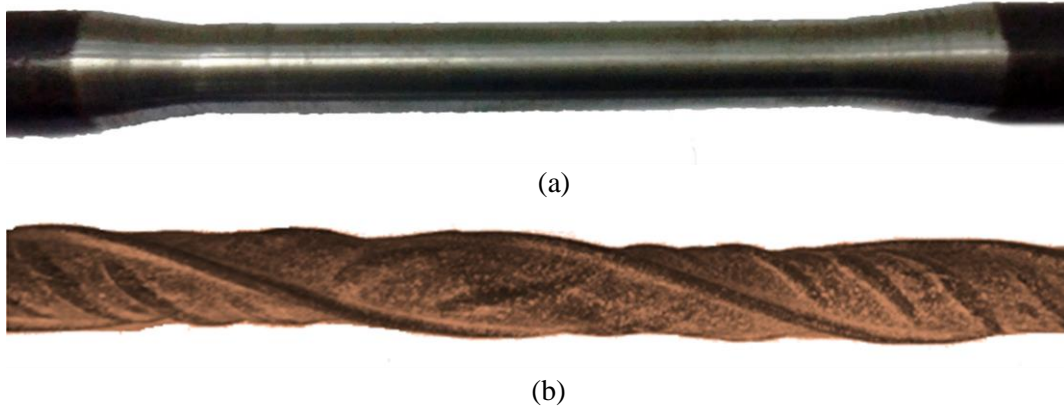


Figure 3.2 Two types of steel used in this study – (a) Plain Mild steel (PM) and (b) Cold-Twisted Deformed (CTD) steel rebars

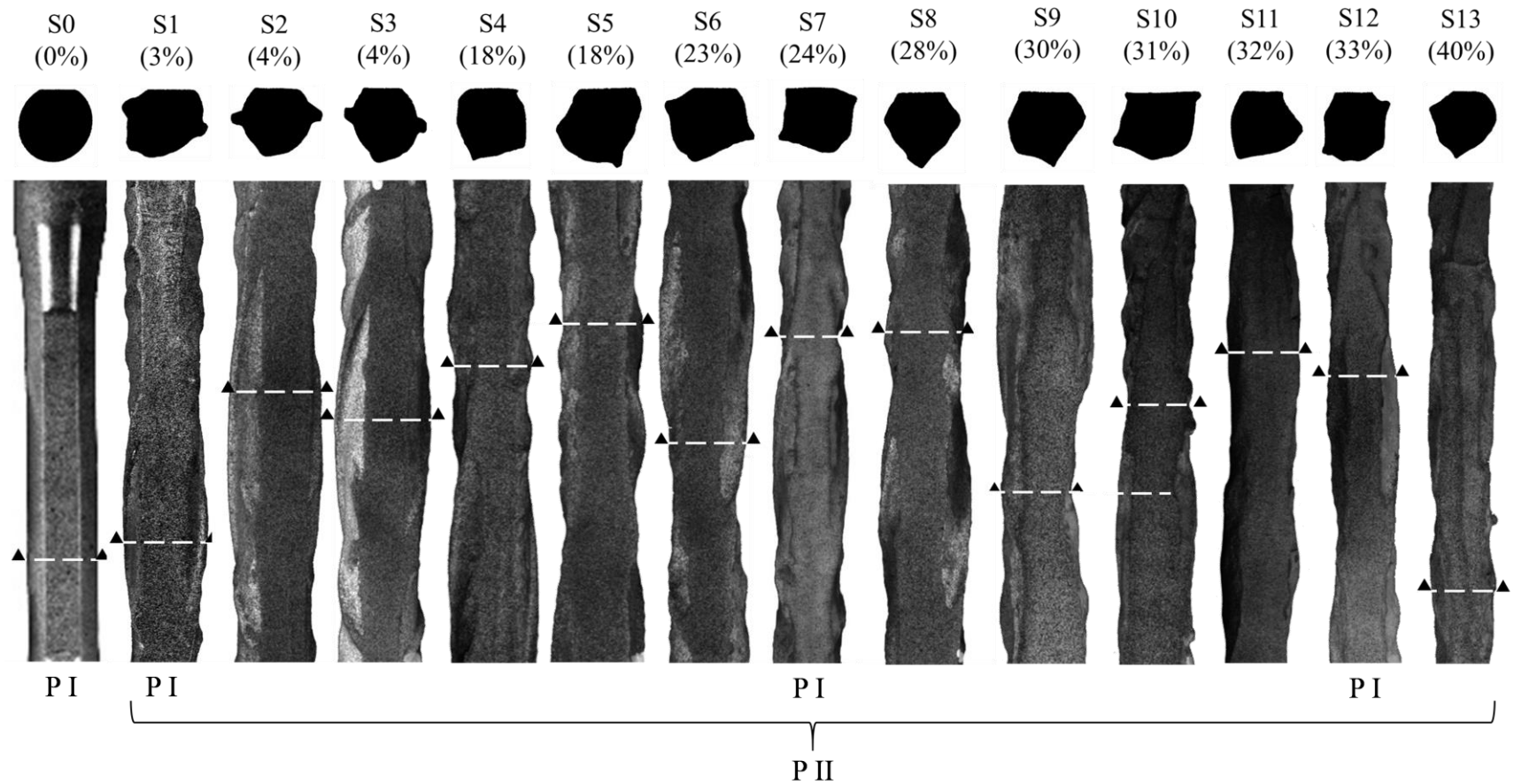
Table 3.1 Typical chemical composition of PM steel and CTD steel

Elements	Cu	Co	Al	Ni	Mo	Cr	S	P	Mn	Si	C	Fe
PM Steel	0.27	-	-	0.09	0.02	0.08	0.05	0.06	0.64	0.26	0.19	Re
CTD steel	0.09	0.01	0.01	0.07	0.01	0.07	0.27	0.09	0.45	0.23	0.13	Re

Re – Remaining

Table 3.2 Details of the specimens used in this study

Steel Type	Specimen ID	Degree of Corrosion (%)	Phase I (PI)	Phase II (PII)
Plain Mild (PM) steel	S0	0	✓	
Cold-Twisted Deformed (CTD) steel	S1	3	✓	✓
	S2	4		✓
	S3	4		✓
	S4	18		✓
	S5	18		✓
	S6	23		✓
	S7	24	✓	✓
	S8	28		✓
	S9	30		✓
	S10	31		✓
	S11	32		✓
	S12	33	✓	✓
	S13	40		✓



Note: The dotted lines indicate the fracture location on these specimens. The cross-sectional area at the fracture location (before the tension test) are shown above corresponding specimens. The specimen ID and the degree of corrosion (provided inside parenthesis) are marked on the top of each specimen. 'P I' and 'P II' represent Phase I and Phase II of this study.

Figure 3.3 Plain mild (PM) steel and corroded CTD rebar specimens with degree of corrosion varying from 3 to 40%.

The stress-strain behaviour of mild steel is well-characterized in literature and hence only one PM steel rebar with uniform cross-sectional area was used as the control specimen for this study. The CTD steel rebar specimens were extracted from the demolished part of a 15-year-old structure in the campus of Indian Institute of Technology Madras, Chennai, South India. These rebars were provided in the dummy column extension elements (on top of the roof slab) for the future extensions of the building (see Figure 3.4); and hence were not stressed under the load acting on the structure. The concrete used in this extension columns was highly porous and did not give sufficient protection from corrosion – in fact they functioned like a water sink and increased the probability of corrosion of the embedded CTD rebars.



Figure 3.4 The extender rebars (corroded CTD steel rebars) used in the dummy columns on top of the roof slab of the building

In Phase I, three rebars specimens of varying levels of corrosion, 3, 24, and 33%, were selected to assess the feasibility of this method to determine the stress-strain behaviour of corroded rebars with the uneven cross-sectional area. The quantification of the degree of corrosion is discussed later in Section 3.3.6. The second phase of the study involves the evaluation of the effect of corrosion on the stress-strain behaviour of corroded CTD rebars. CTD rebars, with a yield strength of ≈ 415 MPa, was introduced in India in 1967. CTD steel rebars were widely in use till the early 1990s

in the construction industry and later on discontinued from use due to their high vulnerability to corrosion (Basu et al. 2004). A significant number of the existing structures in India are constructed using these rebars, and several of them could be experiencing corrosion. Hence, the evaluation of the stress-strain behaviour of corroded CTD rebars would aid in estimating the performance of these structures experiencing corrosion. An additional ten corroded CTD rebar specimens, from the same lot of samples, are used for this assessment. The degree of corrosion on these specimens ranges from 4 to 40%. Since the CTD rebars were discontinued from use for more than two decades, no pristine rebars are available in the market. Hence, the mechanical properties of corroded CTD rebars are compared with those of the mildly corroded specimens (with less than 5% degree of corrosion) obtained from the same lot.

3.3 DEVELOPMENT OF TESTING AND EVALUATION METHOD

This section describes the process of development of a testing and evaluation method to assess the stress-strain behaviour of corroded rebars. Some of the experimental procedures involved in the testing and evaluation are conventionally practiced while some others are decided based on multiple trials. This section discusses the experimental procedures and the trials involved in the different steps of the method development in chronological order. The results from the comparison of the multiple trials involved (to estimate the residual cross-sectional area and to compute full-field strain) and the feasibility study of the proposed method are presented later in Section 4.2.

3.3.1 Specimen preparation

The details of the rebar specimens used for the method development are discussed earlier in Section 3.2. A typical tensile test specimen was made from the PM steel rebar of 16 mm diameter, by reducing the diameter to 12 mm for 60 mm length at the center of the rebar (as shown in Figure 3.2). The naturally corroded CTD rebars of 12 mm nominal diameter were cut into smaller specimens such that the corroded region lies to the middle of the specimens. This is done to avoid the fracture of these specimens inside or very close to the grips of the tensile testing machine if corroded regions lie to the end of these specimens. The least length of the specimens that could be cut in this fashion from the randomly corroded one metre long rebars (extracted

from the structure), was approximately 420 mm. Hence, the PM steel and all the CTD steel rebar specimens are cut to 420 mm long specimens.

The corroded CTD rebars were surrounded by corrosion products on the surface. To estimate the cross-sectional area of the remaining intact steel in the rebars, the corrosion products had to be removed. The corrosion products were removed from the surface of the rebars using the procedure recommended by ASTM G1-03. The cleaning solution was prepared by mixing 500 ml of Hydrochloric acid with 3.5 g of Hexamethylene Tetramine and diluted to 1000 ml using distilled water. Specimens were dipped in this solution for 10 minutes, and the corrosion products were mechanically removed using a wire brush. This process was repeated till the corrosion products were completely removed.

Because 2D DIC was selected for the evaluation, a plane surface was required for the measurement of full-field deformation. Hence, the specimens were milled for approximately 0.5 mm depth from the surface to obtain approximately a 6-7 mm wide plane surface as shown in Figure 3.5. The PM steel rebar was milled only for the 60 mm parallel length. The CTD steel rebars were milled for the entire jaw-to-jaw length (approximately 320 mm length). Figure 3.3 shows the milled CTD rebars of 3, 24 and 33% degree of corrosion used in this phase of the study. The white dotted line indicates the location of the fracture of these specimens under tension. It should be noted that the fracture surface may not be horizontal. However, these lines are drawn approximately along the center of the fracture line on the milled surface. The next step was to identify the probable fracture location on the specimen and to measure the residual cross-sectional area of the corroded rebars to estimate their strength properties after tension test. The estimation of the residual cross-sectional area of the corroded rebars is discussed next.

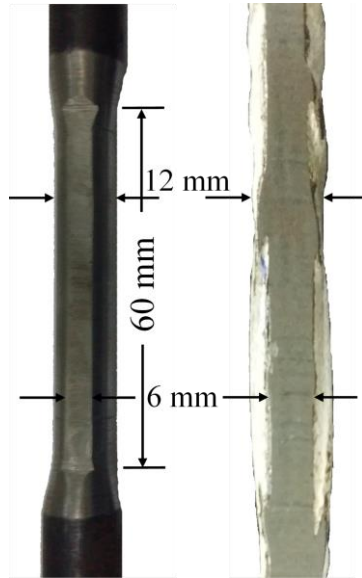


Figure 3.5 Milled surface on the PM steel and CTD steel rebars

3.3.2 Determination of residual cross-sectional area and identification of probable fracture location

One of the challenging tasks associated with the testing of corroded rebars is the prediction of the fracture location of the specimens prior to the tension test. The identification of the fracture location (before the tension test) requires an accurate estimation of the residual cross-sectional area along the length of the corroded rebar specimens (i.e., the ‘cross-sectional area profile’). The corroded rebars exhibit considerable variation in the cross-sectional area along the length. The commonly adopted techniques of estimating residual cross-sectional areas, the mass loss and the liquid displacement techniques (as discussed in Sections 2.6.1 and 2.6.2), can estimate only an average reduction in cross-sectional area over a certain length. In this study, an attempt was made to improve the estimation of the residual cross-sectional area. Three different techniques were attempted to estimate the residual cross-sectional area as close to the fracture location as possible. The following sections discuss these attempted techniques.

3.3.2.1 *Imprint technique*

The *imprint technique* involves creating a 3D impression of the surface of the rebars in some material and measuring the cross-sectional area of the fracture location of the specimen, after the tension test, from the imprint of the specimen. This technique required a material which can be molded according to the shape of the rebar and that

can hold the impression over time. Impression wax was found to be suitable for this technique, as wax can be used in the molten form to create the imprint and can store the impression well after cooling the solid form.

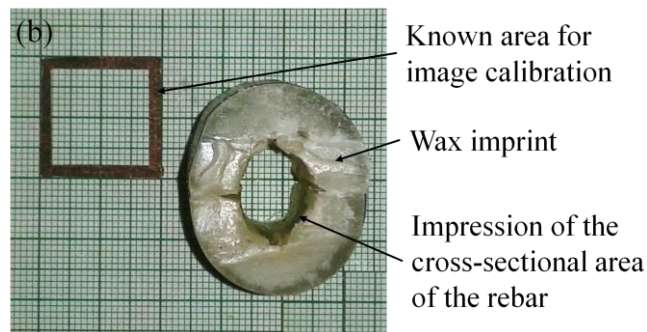
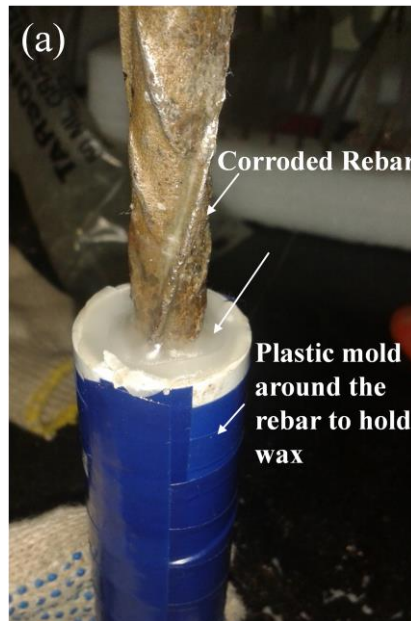


Figure 3.6 Wax imprinting technique to estimate the residual cross-sectional area at the fracture location of the corroded rebar specimen

Figure 3.6 illustrates the *imprint technique* using impression wax. A cylindrical plastic mold was made out of PVC pipe. The PVC pipe was cut into two halves longitudinally and held together using insulation tape as a cylindrical mold. The corroded rebar was held straight at the exact center of the mold. The molten wax was poured into the mold, filling the space between the rebar and the mold, as shown in Figure 3.6(a). The setup is left still till the wax hardened around the rebar. After the wax hardens around the rebar, the wax is separated from the rebar as two longitudinal halves along with the two halves of the mold. To separate out the hardened wax impression, a thin coat of oil is applied to both the plastic mold as well as on the rebar

before pouring the wax. Every 1 mm along the length was marked on the specimen as well as the imprint to identify the locations of the specimen on the wax imprint.

After the tension test of the specimen, the location of fracture was identified (with respect to the 1 mm marking on the specimen), and the corresponding location was identified on the wax imprint (using the 1 mm marking made on the wax imprint as well). The imprint was cut along the cross-section at this identified location. Figure 3.6(b) shows a cut surface of the wax imprint. The cross-sectional area of the rebar was measured from a digital image of the cut surface using an open access software, *ImageJ*. The images are taken such that image contains a known area to calibrate the distance in the images. The imprint of the cross-section of the corroded rebar is selected in the software to compute its area.

3.3.2.2 Volume measurement using micropipette

Another method attempted to measure the residual cross-sectional area along the length of the rebar was the volume measurement technique (which is similar to the liquid displacement technique). The corroded rebar was held vertically inside a graduated glass cylinder and water was poured into the cylinder using a micro-pipette till water level raises approximately 1 mm. The volume of the rebar over approximately 1 mm length is computed from the difference between the volumes of the graduated cylinder over 1 mm length (computed from the diameter of the cylinder) and the volume of the water poured in using micro-pipette. This process was repeated for the entire length of the specimen in intervals of approximately 1 mm and the volume of the water poured into the glass cylinder using the micropipette was recorded.

3.3.2.3 Three-Dimensional Laser Scanning

A more sophisticated, yet easier method was attempted next which was the 3D laser scanning technique. Figure 3.7 shows the 3D model of the PM steel and CTD steel rebar specimens obtained using the laser scanning technique. The corroded rebar specimens were laser scanned using a 3D laser scanner, Roland LPX 600 (with an accuracy of ± 0.05 mm), for the entire length of the rebar. This scanner provided an accuracy of 0.05 mm in the measurement. A longitudinal and circumferential scanning pitch of 1 and 0.32 mm, respectively, was selected based on the accuracy of estimation required for this study. It was assumed that the residual cross-sectional

area would be uniform over 1 mm length of the specimen. The laser could detect only white or light colored objects. Hence, the corroded rebar specimens were painted in a thin coat of white color before scanning. After the specimens had been scanned, the output file containing the spatial coordinates of each point on the specimen was exported by the supporting software, *Dr. Picza* (in *.txt format). The residual cross-sectional area at every 1 mm (equal to the selected longitudinal scanning pitch) was measured from the model using Matlab[®] from the output file.

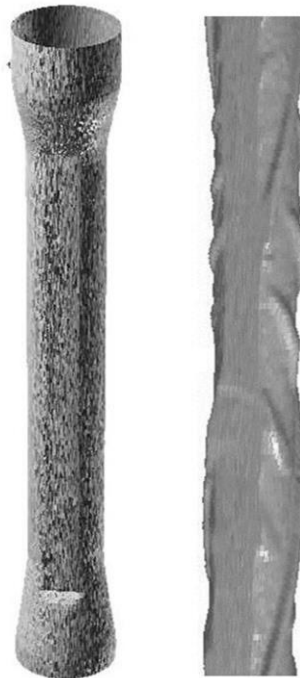


Figure 3.7. Virtual 3D model of the PM steel and CTD steel rebars obtained using laser scanning

Compared to the previously attempted techniques, the 3D laser scanning technique provided the most accurate estimate of the residual cross-sectional area along the rebar. Hence, the 3D laser scanning technique was adopted to measure the residual cross-sectional area of all the rebars in this study. The issues faced with the previously attempted techniques are discussed in Section 4.2.1.

Once the cross-sectional area profile was computed from the laser scan data, the location with the least cross-sectional area was located on the specimen. This location was considered as the most probable fracture location (assuming that fracture would depend upon the specimen geometry rather than any internal defects in the material). The possibility to have multiple locations on the specimen with numerically equal least cross-sectional area was very less, considering the accuracy of measurement

obtained from 3D laser scanning technique. However, the locations with nearly equal least cross-sectional areas were also identified, considering a possibility of failure at a location other than the one identified using laser scanning technique. The next step is to locate the region on the specimen where deformation has to be measured, which is discussed in the following section.

3.3.3 Selection of Area of Interest (AOI)

After identifying the probable fracture location(s) on the specimen, the region over which the (full-field) deformation has to be measured was identified. During the tension test, the images of the selected region will be captured by the camera for posterior DIC strain computations. The predefined region on the surface of the specimen where deformations are to be measured is referred to as the Area of Interest (AOI). Figure 3.8(a) shows the selected AOI for the corroded CTD rebars. In this study, a 60 mm long region along the length of the rebars was selected as the AOI such that the predicted fracture location lies to the center of this region. The length of the AOI was decided as 60 mm based on the recommended gauge length for specimens of 12 mm nominal diameter (five times the diameter) by ASTM E8-M (2013). Figure 3.8(b) shows another possibility of having more than one probable fracture location, less than 60 mm apart. In such cases, the AOI is selected including all the identified locations within the 60 mm. However, if there are multiple probable fracture locations identified on the specimens and lies more than 60 mm apart from each other, then AOI was defined with respect to the location with the absolute least cross-sectional area.

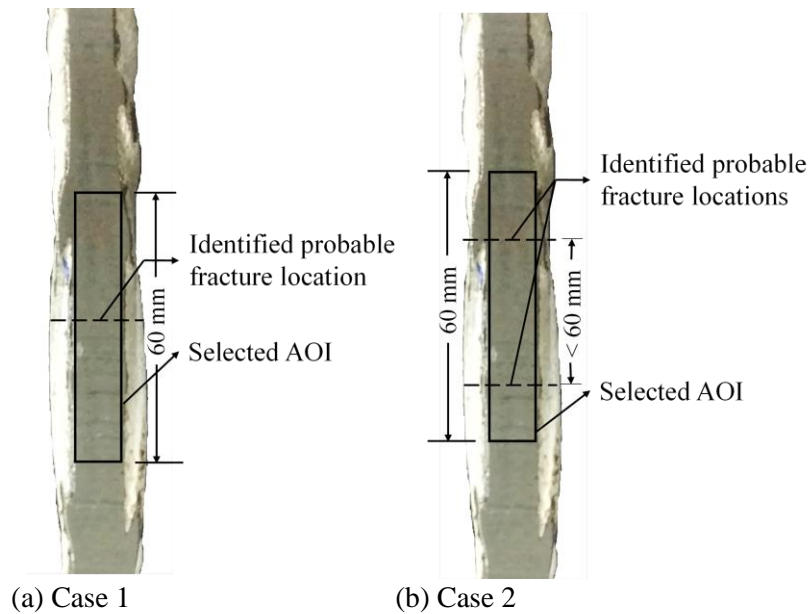


Figure 3.8 Illustration of the selection of AOI

3.3.4 Speckling

The measurement of full-field displacement using the DIC technique involves point-to-point correlation across a set of images taken while the specimen is deforming (under tension). The process involved in the computation of the full-field displacement using DIC technique is discussed in detailed later in Section 3.3.7. For point-to-point correlation, the DIC program should be able to identify each point on the AOI distinctly across the images. To facilitate this, the milled surface of the specimen was speckled with a random distribution of dark and light blobs using spray paint of contrasting colors (for example, black and white). Figure 3.9 shows the light and dark speckles on the surface of the specimen. In this study, speckling was done using two consecutive coats of jet black and plain white (non-reflective) *compact quick drying* 100% acrylic aerosol spray paint manufactured by Tavepaibul Company Limited. It was ensured that the blobs did not form a continuous layer on the steel surface. This is because a continuous layer of paint will not deform with the rebar and thus, will not help in the point-to-point correlation.

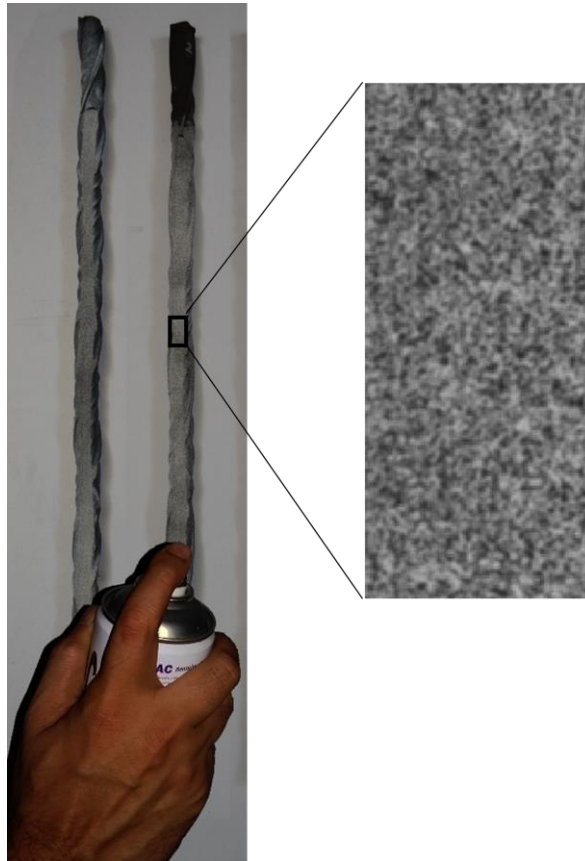


Figure 3.9 Speckling using black and white coloured spray paints and the speckles formed on the surface of the specimen

3.3.5 Tensile testing and image capture

Figure 3.10 shows the experimental setup for tension testing of the corroded rebar specimens and to capture the images for posterior DIC strain computations. The typical experimental test setup includes a tensile testing machine with a live upper jaw/end and a dead lower jaw/end, a charge-coupled device (CCD) camera to capture images (of resolution 1037×1391 pixels) at a uniform time intervals, and the lamps to provide appropriate adequate illumination. Computer systems were used for the image acquisition from the camera and the data acquisition from the tensile testing machine. In this study, two different tension testing machines were used due to logistic reasons. PM steel rebar was tested in Zwick Roell Z100 (of 100 kN load capacity) and corroded CTD rebars were tested in MTS model 311.11 (of 1000 kN load capacity). Both the experimental setups are shown as Figure 3.10 and Figure 3.11. EvolutionTM VF cooled monochrome model CCD camera from Media Cybernetics, Inc. is used in this study, which gives a resolution of 1.4 megapixels in a 12-bit digital output.

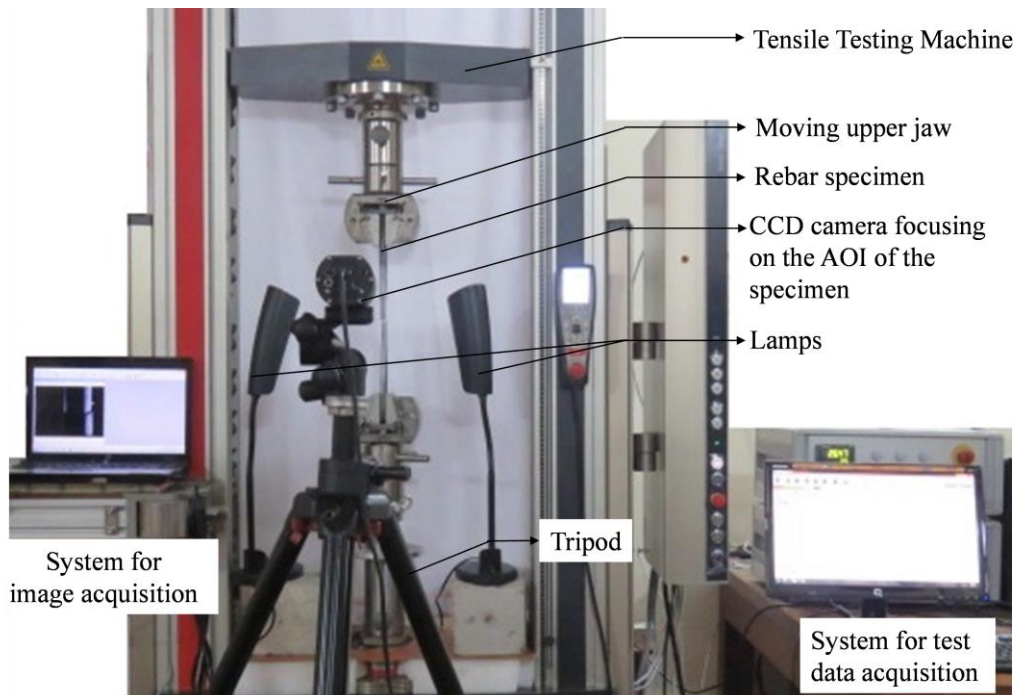


Figure 3.10. Experimental set up used for testing the plain mild steel specimens [Arrangement of camera, lights etc. and Zwick Roell (Model Z100) tension testing machine]

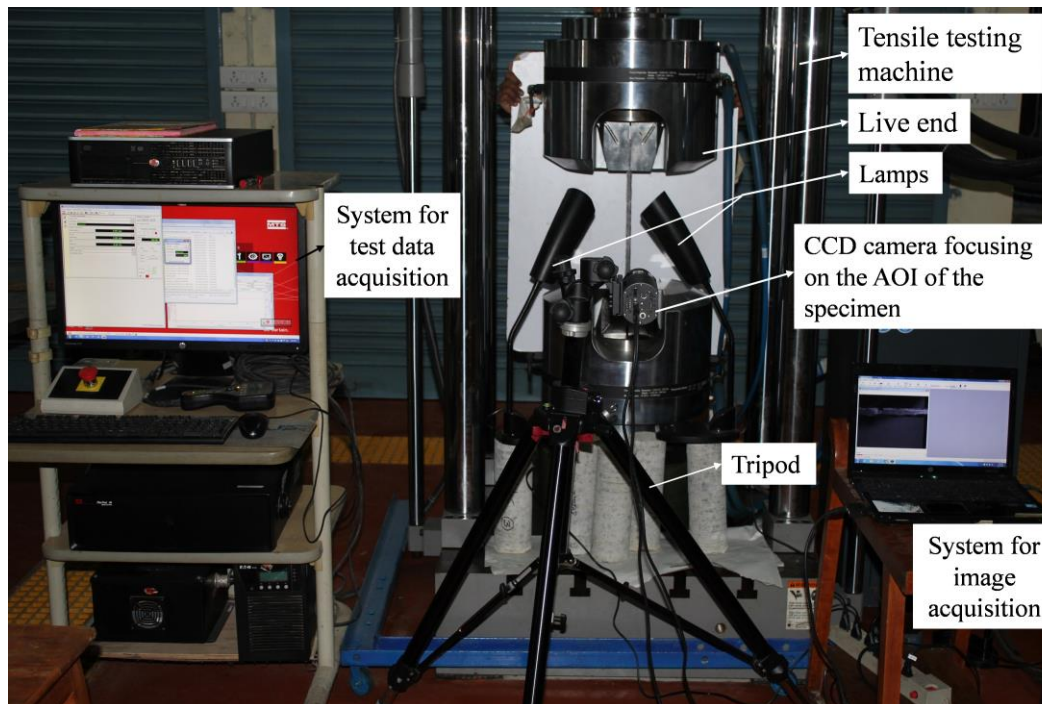


Figure 3.11. Experimental set up used for testing all the CTD steel specimens [Arrangement of camera, lights, etc. and the MTS (Model 311.11) tension testing machine]

Figure 3.12 shows the placement of the camera in the experimental setup. The camera was placed in front of the specimen such that focal plane of the camera is parallel to the AOI. While setting up the camera frame on the specimen, it was taken care that certain region of the specimen in the camera frame would move out during the deformation. Figure 3.13 shows two images of the specimen taken – one taken at the beginning of the test and another one just before fracture of the specimen. Points ‘A’ and ‘B’ mark the top and bottom of the viewing area of the camera (i.e., the image frame). As the specimen deformed under tension, a part of the specimen moved out of the viewing area of the camera (point ‘A’ is invisible in the second image in Figure 3.13). Hence, camera frame was positioned such that there was adequate margin towards the live jaw/end in the viewing area of the camera at the beginning of the test. The margin to be provided towards the live end was decided based on the anticipated total elongation of the PM and CTD steel rebars. As per the IS 432(Part-1):1982 and IS 1786:2008, the minimum ultimate elongation requirement for PM steel and high strength deformed steel rebars (CTD steel) is 23% and 14.5%, respectively, over a gauge length of $5.65\sqrt{A}$ (where A is the nominal cross-sectional area). An ultimate elongation of approximately 30% and 20% was anticipated for PM steel and CTD steel rebars in this study and consequently 80 mm (approx.) length of the rebar was included in the viewing area of the camera.

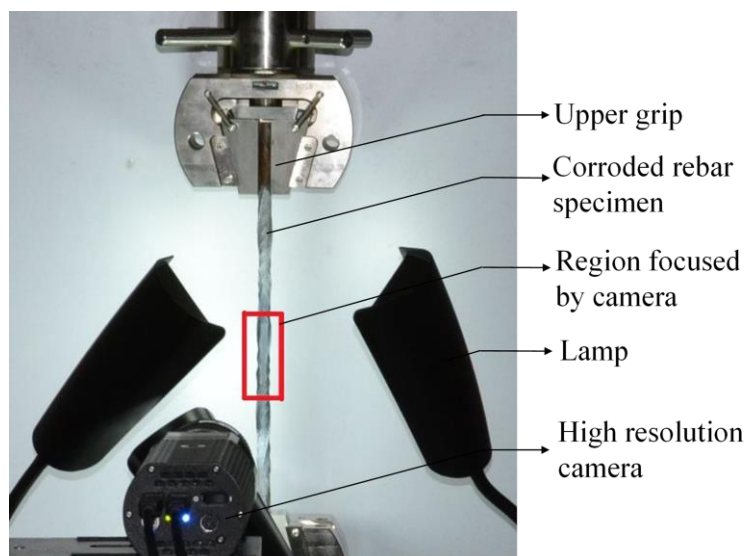


Figure 3.12 The placing of the camera with its focal plane parallel to the AOI

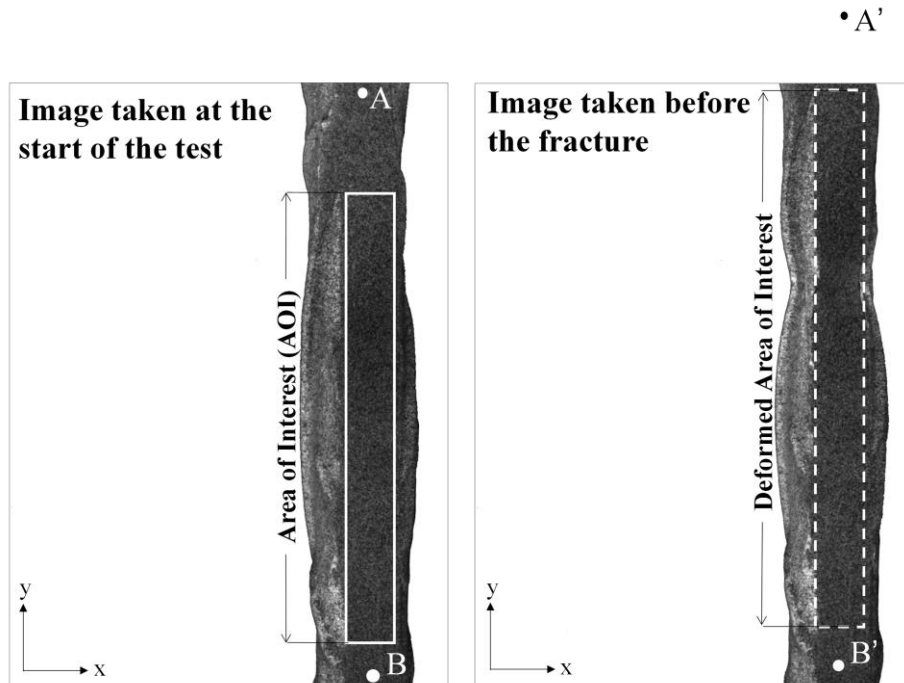


Figure 3.13 Initial and the final images of the AOI taken during the tension test of CTD rebar specimen

The distance between the points ‘A’ and ‘B’ (\overline{AB}) is recorded before the test to calibrate the images. The tensile test is conducted at a displacement rate of 2mm/minute (0.0013 inch/s), which complies with the strain rate recommendation as per IS 1608 (2005). The images of the AOI are captured at a rate of one image per second till the specimen fractures. For a relatively less corroded rebars, approximately 1000 images were captured during the tension test. The posteriori data analysis from the images and the tension test data acquired from the machine (after the tension test) are discussed in the following sections. After the tension testing of the corroded rebars, posteriori data analysis using DIC technique is performed to assess their stress-strain behaviour. Prior to that, the degree of corrosion on the each of the corroded rebars is quantified, which is discussed in the next section.

3.3.6 Quantification of degree of corrosion

Table 3.3 provides the computed degree of corrosion of the three CTD rebar specimens used for the method development. In this study, the degree of corrosion on each specimen was computed based on the loss (in percentage) in the cross-sectional area at the fractured location due to corrosion. The details of the computation are discussed in the following paragraph.

Figure 3.14 shows three different cross-sectional area of ribbed steel rebars before and after corrosion. A_o is the nominal cross-sectional area of a pristine 12 mm diameter rebar specimen. A_i indicates the cross-sectional area obtained after deducting the milled segment of the specimen from A_o . The area of the milled segment was computed from the chord length of the milled specimen (i.e., the width of the milled surface approximately). Due to the uneven surface of the corroded rebar, the depth of milling required to obtain a plane surface of minimum 6 mm width was different for each of the corroded rebar specimens. Consequently, the area of the milled segment varied from specimen to specimen. Hence, A_i was computed for each specimen separately, as shown in Table 3.3. For more details, refer to the appendix. A_{FL} (in Figure 3.14) is the computed residual cross-sectional area at the fractured location (at the beginning of the test) from the virtual 3D model of the specimen obtained using 3D laser scanning technique. The degree of corrosion is computed as given in equation (3.1).

$$\text{Degree of corrosion}(\%) = \frac{A_i - A_{FL}}{A_i} \times 100 \quad (3.1)$$

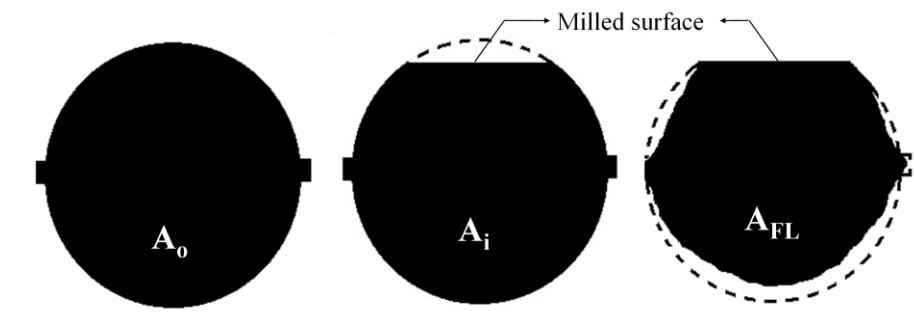


Figure 3.14 Schematic representation of the computation of degree of corrosion –
 (a) The original cross-sectional area of the pristine rebar, (b) The nominal cross-sectional area of the milled specimen (without considering the corrosion), and (c) The residual cross-sectional area at the fracture location of the specimen

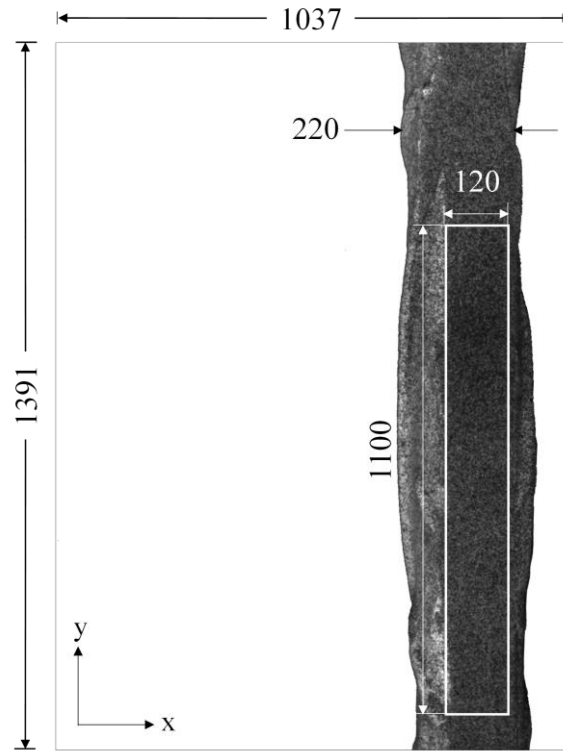
Table 3.3. Details of Computation of the degree of corrosion for the three CTD rebars

Sl. No.	Original cross-sectional area, A_o (mm^2)	Area of the milled off segment	Cross-sectional area of the milled specimen without corrosion, $A_i(\text{mm}^2)$	Cross-sectional area at the fracture location (after corrosion), A_{FL} (mm^2)	Degree of corrosion computed as per Eq. (1) (%)
1	116.2	5.11	111.06	107.24	3
2		3.07	113.13	85.36	25
3		4.51	111.69	75.05	33

3.3.7 Computation of full-field displacement using DIC technique

After the tension test of the corroded specimen, the images captured till the fracture of the specimen are analyzed using DIC technique to estimate the full-field displacement over the AOI. The DIC technique involves tracking the changes in the position of the points on the AOI across the images. This process is discussed in detail in Section 2.12). In this study, a commercially available DIC software, *Vic-2DTM*, is used to compute the full-field displacement and strains. The details of this software are discussed in detail in Section 2.12.2. This section discusses the procedure and criteria followed to decide the DIC parameters for computation of full-field displacement and strain over 60 mm long AOI of the corroded rebar specimens. It should be noted that the procedure followed in this study to select the DIC parameters and to compute the full-field strain is only due to certain challenges faced in this particular study involving a relatively long AOI of 60 mm length (which are discussed in detail in the following paragraphs). Testing of the rebar specimens with a smaller AOI may not encounter the issues faced in this study.

Figure 3.15 presents a typical image of the AOI taken in this study. x - and y - axis of the image is along the transverse and longitudinal axis of the specimen. Out of 1037×1391 pixels in the image, approximately 80 mm length of the specimen occupied 220×1391 pixels. The selected AOI occupied approximately 120×1100 pixels. The AOI on the specimen, thus, occupied only 10% (approx.) of the image. Hence, the computed displacement would have low resolution due to the relatively lower number of pixels occupied by the AOI.



Note: All the measurements are in pixels

Figure 3.15 Pixels occupied by the AOI in the image

The image analysis using Vic-2DTM involves the following procedure. Firstly, the images were calibrated based on a known length of the specimen (such as \overline{AB} , as shown in Figure 3.13). Then, the selected AOI of the specimen was defined in the software. The DIC parameters that are to be provided as an input to the software are discussed earlier in Section 2.12.2. In this study, an autocorrelation function is used to decide the *subset size*. This function computed the average speckle size (in pixels) on the specimen. Three times the average speckle size is taken as the *subset size*. The average speckle size in the corroded CTD specimens varied from 3-6 pixels. Hence, a *subset size* of 9, 13, 15, 17 and 19 are tries for the specimens. The *subset size* of 15 worked for all three specimens. Bornert et al. 2009 reported that the error in the computed displacement values is the least when a *step size* equal to or greater than the *subset size* is selected. For this study, both the *subset size* and *step size* were defined as 15. The image analysis using Vic-2DTM gave the displacement along X- (lateral direction of the specimen) and Y- directions (longitudinal direction of the specimen), abbreviated as '*u*' and '*v*', respectively, of the defined points of interest on the AOI (spaced 15 pixels apart, which is approximately 0.8-1 mm for the corroded CTD specimens). As per the measurements stated earlier in this section, the image analysis

using a *subset size* and *step size* of 15 would yield a displacement data matrix of size 8×73 (i.e., 8 data points along the X- axis and 73 data points along Y- axis).

The DIC technique only computes the full-field displacement. The full-field strain computation is only a mathematical operation which eliminates the noise in the displacement data and computes the strain by differentiation. The computation of strain using inbuilt function in Vic-2DTM software program and the associated issues are discussed in the next section.

3.3.8 Challenges associated with strain computation in Vic-2DTM

Vic-2DTM has an inbuilt feature to compute strain from the full-field displacement data. In general, the displacements resulting from full-field experimental techniques, such as DIC, are corrupted with noise and may lead to erroneous strains, if differentiated directly using any of the numerical differentiation schemes. Hence, conventionally, these displacements are smoothed, using 2D plane fitting, before the computing strain by differentiation (Sutton et al. 2009). The degree of smoothing involved in the strain computation using Vic-2DTM software depends on the input parameter, *filter size* (as discussed in 0). The least *filter size* value that can input into the software is 5. A filter size of 5 would average about 5 data points of the displacement matrix of size approximately 8×73 (as mentioned in the Section 3.3.7) along X- and Y- direction, i.e., the strain heterogeneity over approximately 4-5 mm length of the specimen. No prior database of the strain values at fracture location is available. Hence, the computed strains are questionable.

Hence, alternative methods to compute strains were also attempted to assess the reliability of full-field strain data using Vic-2DTM. The strain computation was attempted using two another methods – (a) Principal Component Analysis and (b) *Virtual extensometer method*'. The strain computations using these methods are discussed in detail in the following sections. A comparison of the results obtained using these strain computation method is presented in Section 4.2.2.

3.3.9 Strain computation using Principal Component Analysis (PCA)

Principal Component Analysis (PCA) is a multivariate tool for data dimension reduction and noise elimination. PCA is a statistical procedure that uses an orthogonal transformation to convert a set of observations of possibly correlated variables into a

set of values of linearly uncorrelated variables called principal components. This transformation is defined in such a way that the first principal component has the largest possible variance, i.e., it accounts for as much of the variability in the data as possible.

Recently, Grama and Subramanian (2014) proposed a new strain computation method using Principal Component Analysis (PCA). In this method, the prime variations in the displacements are captured using a few 1D (\ll rank of the displacement matrices) singular vectors, often called *dominant singular vectors*, which are systematically smoothed and differentiated for computing the strains. In the process of reconstructing the displacement using a few singular vectors, the dimensional reduction (the conventional 2D plane or 3D surface is converted to a simpler 1D curve fitting of series of the dominant singular vectors) and data denoising are achieved as additional benefits.

The number of dominant singular vectors are identified by inspecting the logarithmic singular values (Grاما and Subramanian 2014), which are smoothed using Legendre polynomials for computing displacement gradients ($\delta u/\delta x$, $\delta v/\delta x$, $\delta u/\delta y$ and $\delta v/\delta y$). The displacement gradient matrix, $[H]$, is assembled as given in Equation (3.2).

$$[H] = \begin{bmatrix} \frac{\delta u}{\delta x} & \frac{\delta v}{\delta x} \\ \frac{\delta u}{\delta y} & \frac{\delta v}{\delta y} \end{bmatrix} \quad (3.2)$$

The two-dimensional Lagrangian strain tensor, ε , is defined as given in Equation (3.3).

$$\varepsilon = \frac{1}{2} ([H] + [H]^T + [H]^T \times [H]) \quad (3.3)$$

The principal values of the strain tensor, ε , gives the measure of the principal strains. The algorithm for strain computation using PCA for the test specimens used in this study is modified by Sameer Sharma (from the algorithm in Grama and Subramanian 2009). The full-field strain matrix so computed is of the same size as that of displacement matrix.

3.3.10 Strain computation using ‘Virtual extensometer method (VEM)’

The strain computation using PCA is may not be very easy to use for users of DIC who are not familiar with the technique. Hence, an easier method of strain computation was sought for, referred in this study as *Virtual-Extensometer Method (VEM)*. The *VEM* involves no smoothing of the data. The strain was computed from 2 adjacent data points along the y-axis of the specimen in the full-field displacement matrix assuming the *step size* (15 pixels) as the gauge length. The strain, ε_{VEM} , is computed as given in the Equation (3.4).

$$\varepsilon_{VEM} = \frac{(v_p - v_q)}{15} \quad (3.4)$$

where v_p and v_q are the displacement along y- axis (longitudinal displacement) of points ‘p’ and ‘q’, spaced 15 pixels apart in the image. This computation yields a full-field strain matrix of size [m-1×n] when computed for a displacement matrix of size [m×n].

3.3.11 Computation of effective strain over the gauge length

The conventionally measured strain over a gauge length (of 60 mm for 12 mm nominal diameter specimens) using extensometers is computed using full-field displacement data obtained using DIC to compare the strain at fracture location to the conventionally known ranges of strain. The strain over the gauge length is denoted as ε_{gauge} is measured as given in Equation (3.5).

$$\varepsilon_{gauge} = \frac{(v_m - v_n)}{N} \quad (3.5)$$

where v_m and v_n are the average displacements over the cross-sectional area at points, ‘m’ at the top of the AOI and ‘n’ is the point at the bottom of the AOI, 60 mm apart in the specimen. N is the distance in pixels between the two points, ‘m’ and ‘n’.

3.3.12 Computation of stress

The stress experienced by the specimen is computed from the load data obtained from the tensile testing machine. Approximately 100 load values are recorded by the tensile testing machine in a second while one image is captured per second. Hence, every image is correlated to the mid-value of the load data recorded in a second. In this

study, two different values of stress are computed– (a) engineering stress, computed using the residual cross-sectional area at the fracture location, obtained from 3D laser scanning, which is abbreviated as σ_{engg} and (b) true stress, computed using the actual cross-sectional area at the fracture location at that particular instant of time (taking into account the reduction in cross-sectional area as the specimen deforms under load) abbreviated as σ_{true} .

The reduction in cross-sectional area with time is calculated assuming that volume of the specimen remains unchanged during plastic deformation and the volume change due to elastic deformation is negligibly small compared to plastic deformation at the fracture location. Roesler et al. (2007) have stated that this assumption is true in the case of metals and can be used to compute true stress. However, σ_{true} is computed only beyond yielding as the volume is not conserved during the elastic deformation of the specimen. It is to be noted that this assumption of volume conservation is true only at the fracture location of the specimen. As per this assumption, Equation (3.6) can be formulated.

$$A_1 \times h_1 = A_n \times h_n \quad (3.6)$$

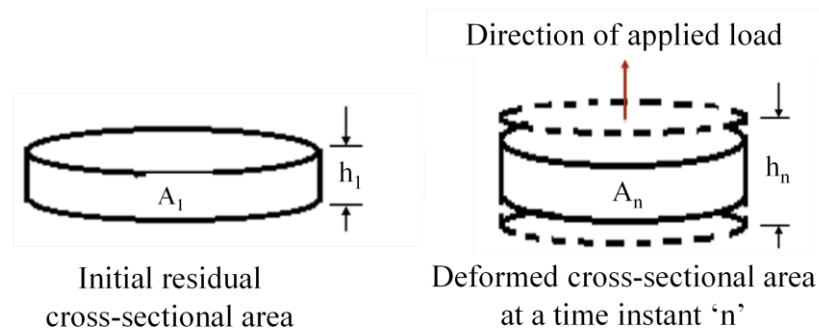


Figure 3.16. Schematic representation of the computation of instantaneous area

A_1 is the initial cross-sectional area at the beginning of the test, h_0 is a length of a segment including the fracture location (as shown in Figure 3.16) which is taken as 3 mm in this study, A_n is the actual cross-sectional area at any instant of time 'n', and h_n is the deformed length of the segment of initial thickness h_1 at any instant of time 'n'. A_n can be computed using the above equation as the other three variables are known. A_1 is the cross-sectional area at the fracture location measured from the 3D

model of the specimen. h_1 is taken as 1 mm, which includes the fracture location. The deformed length of the segment, h_n , is computed using Equation (3.7).

$$h_n = h_1 (1 + \varepsilon_{FL}) \quad (3.7)$$

where, ε_{FL} is the strain at fracture location at instant n . True stress (σ_{true}) at any instant of time, n , is calculated as given in Equation (3.8).

$$\sigma_{true,n} = \frac{P_n}{A_n} \quad (3.8)$$

Another alternative method of computing σ_{true} is by computing the lateral strain at fracture location (at every second) from the lateral displacement data obtained using DIC technique. However, due to the significant rotation in the specimen, especially due to the helical ribs around the rebar, the plane cross-sections do not remain plain during the tension test. The lateral displacement values (u) are affected by the rotation of the specimens, making lateral strain computation difficult.

After computation of stress and strain (using DIC technique), two different stress-strain curves are plotted for the specimens – (a) engineering stress-strain curve from σ_{engg} and the strain at fracture location (ε_{FL}), denoted as $\sigma_{engg}-\varepsilon_{FL}$, and (b) true stress-strain curve from σ_{true} and the strain at fracture location (ε_{FL}), denoted as $\sigma_{true}-\varepsilon_{FL}$. It should be noted that all the plotted stress-strain curves and the evaluated mechanical properties in this study correspond to the fracture location of the specimen unless specified otherwise.

3.3.13 Assessment of the feasibility of the proposed technique

The proposed testing and evaluation method using DIC technique was formulated to meet certain specific needs (which are stated in Section 2.11). These requirements include the estimation of mechanical properties close to the fracture location of the corroded rebars and the strain distribution along the rebars. The results obtained using the proposed method is evaluated for assessing the feasibility in meeting the intended purpose and the accuracy of estimation. This was done using the four specimens, one PM steel rebar and three corroded CTD rebar specimens, using in this part of the

study. The results of the feasibility study are presented later in Sections 4.2.3 and 4.2.4.

3.4 EVALUATION OF THE MECHANICAL PROPERTIES OF CORRODED REBARS USING THE DEVELOPED METHOD

The second phase of this study involves the assessment of the stress-strain behaviour of the naturally corroded unstressed CTD rebars using the developed method (as discussed in the previous section). A brief overview of the experimental procedure is presented in this section. The results obtained from the evaluation are presented in Section 4.3.

The details of the specimen used in this part of the study are discussed in Section 3.2. Figure 3.3 shows the thirteen corroded CTD rebar specimens (including the three specimens selected for the phase I) tested in the second phase of this study. Table 3.2 provides the details of the specimens. The corroded CTD rebar specimens were prepared as per the procedure discussed in Section 3.3.1. The residual cross-sectional area profile was estimated using 3D laser scanning technique and probable fracture location(s) was/were identified (as discussed in Section 3.3.2.3). The selection of AOI, speckling, and tension testing were carried out as per the procedure discussed in Sections 3.3.3 to 3.3.5. The degree of corrosion on these specimens was quantified after the tension test as per Equation (3.1). After the degree of corrosion on these specimens is quantified, the specimens are named in the increasing order of degree of corrosion, i.e., S1 with least degree of corrosion and S13 with the highest degree of corrosion. Out of these thirteen specimens, S1, S7, and S12 were used for development of the testing and evaluation method (first part of the study). The evaluation of the mechanical properties of these three specimens is included in this part of the study.

Table 3.4 presents the computation details of the degree of corrosion on each of the thirteen specimens. It should be noted that the details provided in Table 3.3 are repeated in Table 3.4 (details of S1, S7, and S12). After the tension test, the full-field displacement of the defined points on the AOI is computed using Vic-2DTM from the images captured during the tension test. The DIC parameters are similar to that mentioned in Section 3.3.7. The strain is computed using the PCA-based algorithm (as discussed in Section 3.3.9). Using the computed stress and strain values,

$\sigma_{engg}-\epsilon_{FL}$ curves and $\sigma_{true}-\epsilon_{FL}$ curves are plotted for all the thirteen CTD rebar specimens.

From the stress-strain curves plotted for the specimens, the effect of corrosion on their mechanical properties, namely, the yield strength, ultimate strength, ultimate strain and the elastic modulus, are evaluated at the fracture location. The major focus of the study is on the ductility of the corroded rebars. The ultimate strain measured over the gauge length and at the fracture location were compared. The strain distribution in the vicinity of the fracture location was compared among the corroded CTD specimens for a better understanding of the deformation in the corroded rebars. The influence of the pattern of corrosion on the ultimate strain is also studied. The evaluated effect of corrosion on the stress-strain behaviour and the mechanical properties are provided in Section 4.3.

Table 3.4. Computed degree of corrosion for the thirteen CTD specimens evaluated using the developed method

Specimen ID	Original cross-sectional area, A_o (mm ²)	Area of the milled off segment	Cross-sectional area of the milled specimen without corrosion (mm ²)	Cross-sectional area at the fracture location (after corrosion) (mm ²)	Degree of corrosion computed as per Eq. (1) (%)
S1	116.2	5.11	111.09	107.24	3
S2		4.40	111.8	107.63	4
S3		2.67	113.53	109.16	4
S4		2.56	113.64	92.76	18
S5		3.10	113.1	92.31	18
S6		3.52	112.68	87.06	23
S7		3.07	113.13	85.36	24
S8		2.37	113.83	81.62	28
S9		4.98	111.22	77.38	30
S10		3.45	112.75	77.99	31
S11		3.93	112.27	75.91	32
S12		4.51	111.69	75.05	33
S13		3.67	112.53	67.32	40

3.5 SUMMARY

This chapter first presented an overview of the experimental program and details of the specimens selected for this study. The experimental procedure involved in the two phases of this study – the method development and the assessment using the developed method – is discussed in detail in Sections 3.3 and 3.4. The various

techniques to estimate the residual cross-sectional area of the corroded rebars with the uneven cross-sectional area and alternative methods of strain computation attempted in this study are discussed in this chapter. A brief overview of the evaluation involved in the feasibility study of the proposed technique and assessment of the effect of corrosion on the stress-strain behaviour of corroded CTD rebars are also discussed.

CHAPTER 4

RESULTS AND DISCUSSION

4.1 INTRODUCTION

This chapter presents the results from the experimental program discussed in Chapter 3. The results from the two main phases of this study – development of the testing and evaluation method and evaluation using the developed method – are provided in this chapter. After this, the results from the evaluation of the effect of corrosion on the stress-strain behaviour of CTD rebars using the developed method are presented. The possible reasons for the observed results are also discussed in this chapter.

4.2 DEVELOPMENT OF TESTING AND EVALUATION METHOD

Section 3.3 presented the experimental procedure involved in the development of the testing and evaluation method. This involved multiple trials to arrive at a suitable technique to estimate the residual cross-sectional area and to predict the fracture location accurately prior to the test. Also, alternative methods of strain computation from the full-field displacement data were attempted. The following sections provide a comparison of the different techniques attempted for the estimation of residual cross-sectional area and the different methods of strain computation are presented. This is followed by a section providing the results from the study conducted for the assessment of the feasibility of the proposed method to evaluate the local mechanical properties and the strain distribution over the AOI.

4.2.1 Estimation of residual cross-sectional area

The techniques attempted to estimate the residual cross-sectional area and predict the fracture location prior to the test are discussed in Section 3.3.2. The first method attempted was the wax imprinting technique. However, this method did not provide an accurate solution. Figure 4.1 shows the cut surface of the wax imprint at a location. One of the issues faced with this technique was that it tends to break unevenly when cut at a location. It was difficult to obtain a perfectly horizontal cut in the wax imprint, thus making the measurement of the residual cross-sectional area difficult.

Also, the cut wax imprint revealed imperfections in the imprint as molten wax did not flow well around the ribs and the locally corroded regions on the corroded specimens, as shown in Figure 4.1. Another drawback of this technique is that it could not facilitate the prediction of the fracture location prior to the test. Therefore, this technique was eliminated.



Figure 4.1 Cut surface of a wax imprint of corroded specimen revealing imperfections in the imprint

The volume measurement technique using the micropipette also did not give an accurate estimate of the residual cross-sectional area over small length of specimen, approximately 1 mm. The meniscus formed by water inside the graduated cylinder led to error in the measurement. Also, it was difficult to keep track of the volume of the water poured in using the micropipette. The relative size of the graduated cylinder with respect to the size of the rebar also influenced the accuracy of the reading.

The 3D laser scanning gave very accurate estimate of the cross-sectional area profile of the corroded rebars. The residual cross-sectional area at one mm interval was obtained using this method. In this study, fracture location of all the specimens, except the two rebars with 3% (S1) and 4% (S2) degree of corrosion, coincided exactly with the identified probable fracture location estimated using 3D laser scanning technique. The failure in predicting the fracture location of these two rebars could be because there was no significant variation in the residual cross-sectional area and the fracture could have been initiated due to some internal defect or crack. This study proposes 3D laser scanning as an accurate method for assessing the residual cross-sectional area of the rebars. The approximation of uniform cross-sectional area

of 1 mm was sufficient to identify the fracture location accurately. Hence, 1 mm would be a suitable longitudinal pitch for laser scanning.

4.2.2 Selection of strain computation method

The three methods of strain computation, discussed earlier in Sections 3.3.8 to 3.3.10, are compared using the stress-strain curves plotted for the four specimens (one PM steel rebar and three corroded CTD rebars). Figure 4.3 shows the engineering stress-strain plots corresponding to the fracture location ($\sigma_{\text{engg}}-\epsilon_{\text{FL}}$ curve) plotted for all the four specimens using all the three attempted methods of strain computation. The blue dashed line indicates the strain computed using in-built function in Vic-2DTM software (using a filter size of 5), the red dash-dot line indicates strain computed using VEM and green solid line indicates strain computed using PCA based algorithm. The figure reveals considerable variations in the strain computed using the three methods. These differences are due to the variations in the degree of smoothing of the displacement data involved in each of these methods.

The stress-strain curve plotted for the control specimen (PMS steel rebar) as well as the corroded CTD rebars using VEM method showed considerable noise. This is because, VEM involves strain computation directly from the full-field displacement data containing noise (without any smoothing), which leads to error in the computed strain. It can also be seen that the plots using VEM method showed higher ultimate strain than the other two methods. However, this may not be a reliable estimate because the noises are not eliminated in this method. Hence, this method is not recommended for computing strain from the full-field deformation data.

The stress-strain curves plotted using Vic-2DTM and PCA based algorithm are similar for control specimen and CTD rebar with 24% corrosion. However, it is significantly different for CTD rebars with 3% and 33% corrosion. Figure 4.2 presents a comparison of the ultimate strain computed using PCA based algorithm and Vic-2DTM software. The plot exhibits considerable difference between the ultimate strain values obtained using the two methods. There are no database of evaluated values of ultimate strain exhibited at the fracture location of PM steel or CTD steel rebar to check the reliability of the obtained data. However, using logical reasoning, PCA based algorithm is a more reliable method than Vic-2DTM. This is because even the least *filter size* value of 5 may smooth considerable strain heterogeneity in the

full-field displacement data of specimens with AOI occupying less than 10% of the images. However, PCA based method eliminates the noise in the displacement data based on a mathematically reliable method of identifying the dominant eigen vectors of the data, rather than a fixed *filter size*. It should be noted that for specimens with AOI occupying larger part of the image may yield similar values of strain using Vic-2DTM as well as PCA based algorithm. In this study, the strain in all the rebar specimens are computed using PCA based algorithm.

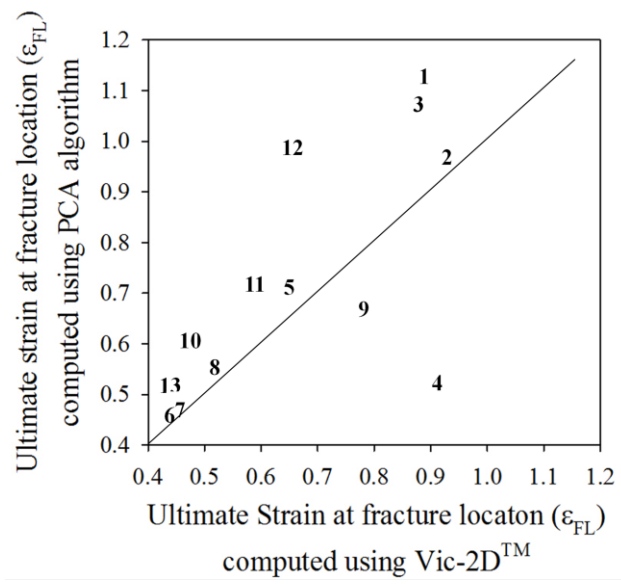


Figure 4.2 Comparison of the ultimate strain computed using PCA based algorithm and in-built function in Vic-2DTM software

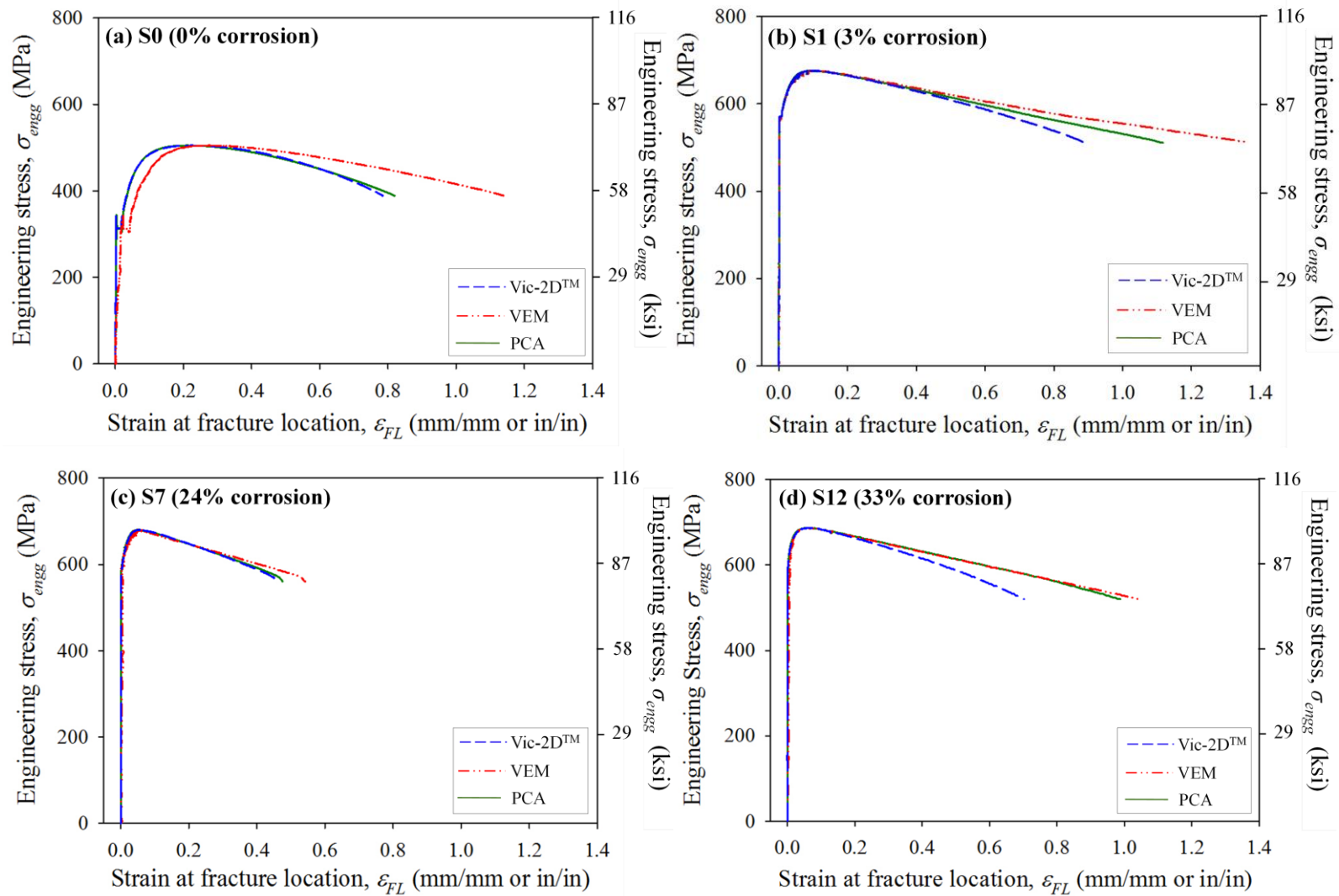


Figure 4.3 Comparison of the stress-strain curves plotted using all three methods of strain computation – Vic-2D™, VEM, and PCA based algorithm: (a) S0 (0% corrosion), (b) S1 (3% corrosion), (c) S7 (24% corrosion) and (d) S12 (33% corrosion)

4.2.3 True and engineering stress-strain curve plotted using the proposed method

One of the intended purpose of the proposed evaluation method using DIC technique is to evaluate the mechanical properties close to the fracture location of corroded rebars. The feasibility of the proposed method in assessing the local stress-strain properties nears the fracture location is assessed using four specimens, one PM steel and three corroded CTD steel rebars. Figure 4.4 shows the engineering and true stress-strain graphs plotted for specimens corresponding to the fracture location. The engineering stress-strain curve is denoted as $\sigma_{engg}-\epsilon_{FL}$ and the true stress-strain curve is denoted as $\sigma_{true}-\epsilon_{FL}$. The image analysis using a step size of 15 provides a strain at a location less than 0.5 mm from the fracture surface. Thus, the proposed method provides a sufficiently accurate estimate of the local mechanical properties at the fracture location.

The engineering stress-strain curve obtained using the conventional method of computing strain over the gauge length, is also plotted for all the specimens (denoted as $\sigma_{engg}-\epsilon_{gauge}$ in Figure 4.4). Evidently, the strain measured over 60 mm gauge length is significantly lower than that at the fracture location. It is observed that ϵ_{gauge} shows a systematic decrease from 0.16 to 0.08 (i.e., 16% to 8%) with increase in degree of corrosion from 3% to 33%. However, ϵ_{FL} does not show a similar decrease with increase in degree of corrosion. The ϵ_{FL} values are 1.11, 0.48 and 0.98 for CTD rebar specimens with 3%, 24% and 33% corrosion, respectively.

The computed true stress-strain curves showed a slight drop close to the fracture of the specimen, which differs from the theoretical concept of true stress-strain curve. Such a drop in the measured stress-strain curve is also specified by Roesler et al. (2007). This is reported to be due to the underestimation of the reduction in cross-sectional area at the fracture location by the assumption of volume conservation. Other possible reasons could be – (a) the error in the displacement measured using 2D DIC technique close to the fracture of the specimen due to significant out-of-plane displacement; or (b) the initiation of cracking at the rear side of the specimen due to which load carried by the specimen drops, while an increase in strain is measured at the milled surface of the specimen.

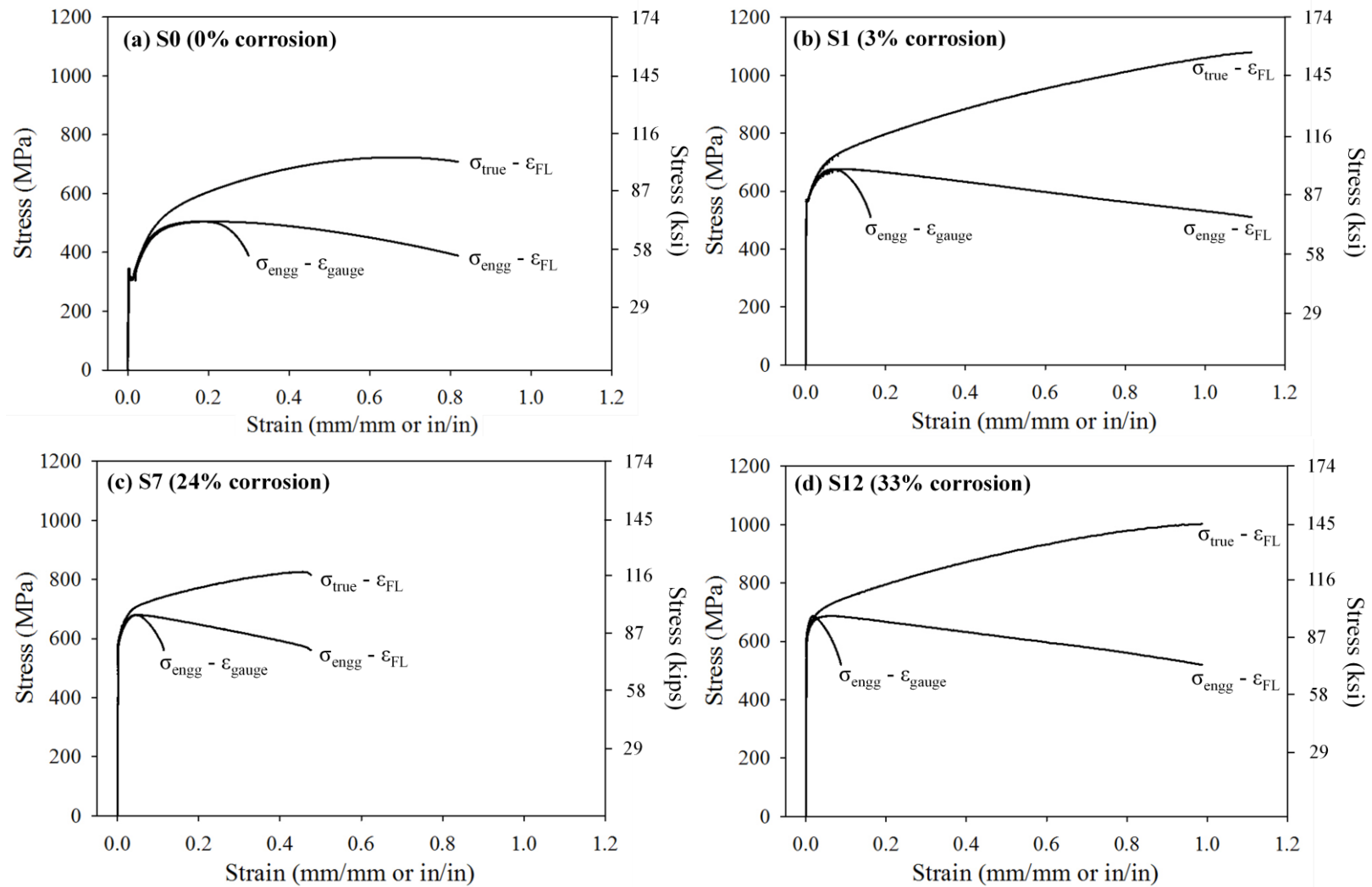


Figure 4.4 Comparison of the engineering and true stress-strain curves corresponding to the fracture location and engineering stress-strain curve obtained using the conventional method – (a) S0 (0% corrosion), (b) S1 (3% corrosion), (c) S7 (24% corrosion) and (d) S12 (33% corrosion)

4.2.4 Study of the strain distribution along the AOI

Another intended purpose of developing a refined testing and evaluation method was to capture the strain distribution along the length of the specimen. This would help to better understand the effect of corrosion (and the uneven cross-sectional area along the length) on the deformation (or ductility) of the rebars. The author would like to reinstate that a region of 60 mm length was selected as the AOI to understand the strain heterogeneity due to corrosion along the conventional gauge length (which is 60 mm for 12 mm nominal diameter rebars). The image analysis using a step size of 15 facilitated the study of strain distribution with sufficient accuracy. Depending on the calibration scale (which varies slightly from specimen to specimen), the image analysis provided the strain of the points on the AOI spaced at an interval of 0.8 to 1 mm along the length of the rebars for all the three corroded CTD rebars specimens.

The strain distribution along the length of the rebars is represented using the stress-strain curves plotted corresponding to fracture location and different points in the vicinity of the fracture location. Figure 4.5 shows the stress-strain curves plotted at the fracture location (location marked 'FL') and six different points, marked 'A' to 'F', each 5 mm apart from each other. The longest curve correspond to the fracture location, where the strain is the highest, and the subsequent curves from right to left corresponds to points 'A' to 'F' respectively. Evidently, the maximum strain decreases with the distance from the fracture location, i.e., from point 'A' to 'F'.

Figure 4.6 shows a comparison of the strain distribution in the CTD rebar specimens with 3%, 24% and 33% corrosion. The relative positions of the stress-strain curves corresponding to points 'FL', 'A', 'B' and so on is significantly different for each of these specimens. This indicates that the deformation along the gauge length (or AOI) is significantly different for each of the corroded specimen depending on the cross-sectional area profile. To understand the ductility of the corroded rebars, it is essential to understand how the strain distribution varies from specimen to specimen. Hence, full-field deformation techniques are essential to understand the strain distribution along the length of the specimen.

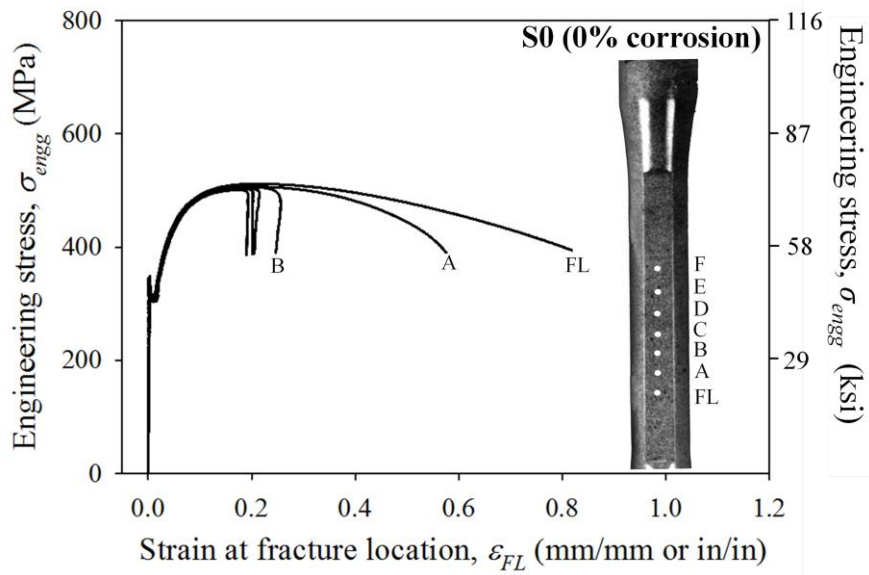


Figure 4.5 Stress-strain curves at different points along the control specimen indicating the strain distribution

The developed method of testing and evaluating corroded rebars using 3D laser scanning and DIC techniques can thus capture the strain distribution along the AOI of the corroded rebars with uneven cross-sectional area and the local mechanical properties at (or very close to) the fracture location with sufficient accuracy.

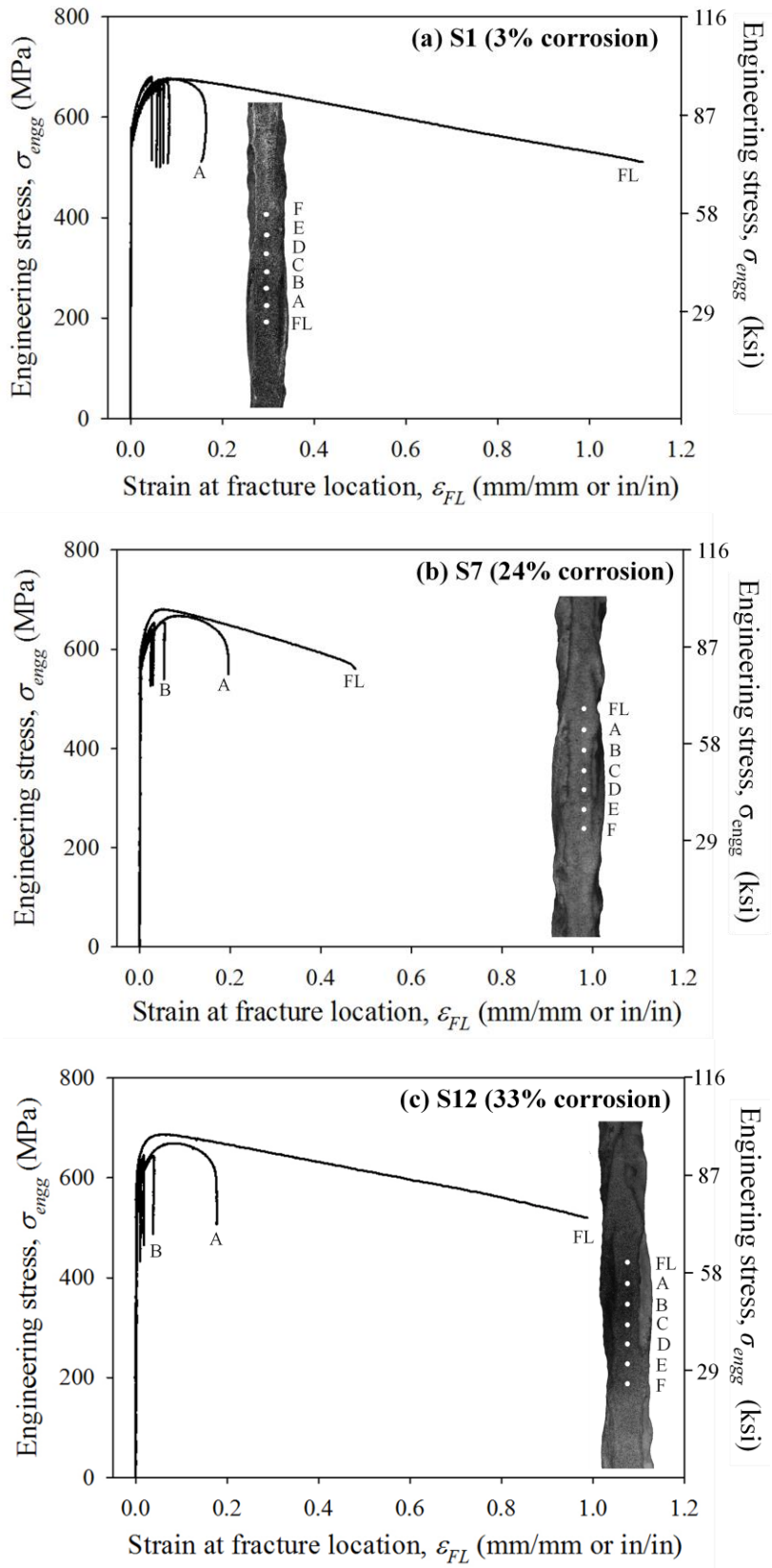


Figure 4.6 Strain distribution along the length of CTD rebars with 3, 24 and 33% corrosion

4.3 STRESS-STRAIN BEHAVIOUR OF CORRODED CTD REBARS

This section presents the results obtained from the evaluation of the effect of corrosion on the stress-strain behaviour of CTD rebars using the developed method. In this section, the term ‘strength’ refers to the ability of the residual steel to withstand the load, computed using the residual cross-sectional area at the fracture location. The plots in this section provides the results obtained from the evaluation of thirteen CTD rebar specimens, 3 of them selected for the first phase of the study, and ten additional specimens selected for the second phase of this study (named S1 to S13, in increasing order of the degree of corrosion on them, as discussed in Section 3.4). The data points in the graphs provided in this section have been replaced by the specimen IDs for more clarity. It should be noted that the data points might appear as two clusters in the plots as there are no specimens with the degree of corrosion in between 4 to 18%. Table 4.1 presents the computed mechanical properties of the thirteen corroded CTD rebar specimens. The details on the data provided in the table will be provided appropriately at multiple locations in the following sections.

Table 4.1 Computed mechanical properties at the fracture location of corroded unstressed CTD steel rebars

Specimen ID	Degree of corrosion (%)	Proof stress, σ_p (MPa)	Ultimate Strength, σ_u(MPa)	Ultimate strain at fracture location, $\epsilon_{FL,ult}$(%)
S1	3	569	676	112
S2	4	602	725	97
S3	4	592	688	109
S4	18	538	640	52
S5	18	577	674	71
S6	23	665	780	46
S7	24	587	680	48
S8	28	658	762	55
S9	30	542	667	67
S10	31	588	669	72
S11	32	600	733	99
S12	33	642	687	51
S13	40	682	784	61

4.3.1 Stress-strain curves obtained using the developed method

After testing the corroded CTD rebars under tension and the posterior evaluation using DIC technique, the engineering and true stress-strain curves corresponding to the fracture location of the corroded CTD specimens were plotted. Figure 4.7 shows the engineering and true stress-strain curves plotted for the thirteen specimens. The solid lines labelled in black indicate the engineering stress-strain curves and the dotted lines labelled in blue indicate the true stress-strain curves. For clarity, the stress-strain curves of the thirteen specimens are provided in two separate plots. Figure 4.7(a) and Figure 4.7(b) provides the stress-strain plots of specimens S1 to S7 and S8 to S13, respectively.

The engineering and true stress strain curves for S5, S6, and S8 exhibits a sudden drop towards the end of the curve. This could be due to initiation of fracture at the rear side of the specimen (the side of the specimen not in the camera vision), which leads to sudden reduction in the load carried by the specimen. This is one of the limitation of the 2D DIC technique. However, the measured strain shows a decrease till the fracture line appears on the surface of the specimen viewed by the camera (i.e., the milled surface).

A slight drop is noticed in the true stress-strain curves plotted for most of the specimens very close to the fracture. The possible reasons for this observed drop in the computed true stress-strain plot is discussed in Section 4.2.3. The mechanical properties, the yield strength, ultimate strength, ultimate strain and elastic modulus, are estimated from the engineering stress-strain curves and the effect of corrosion on each of these properties is evaluated. The results from these evaluations are provided in the following sections. It should be noted that this study includes the evaluation of only engineering mechanical properties.

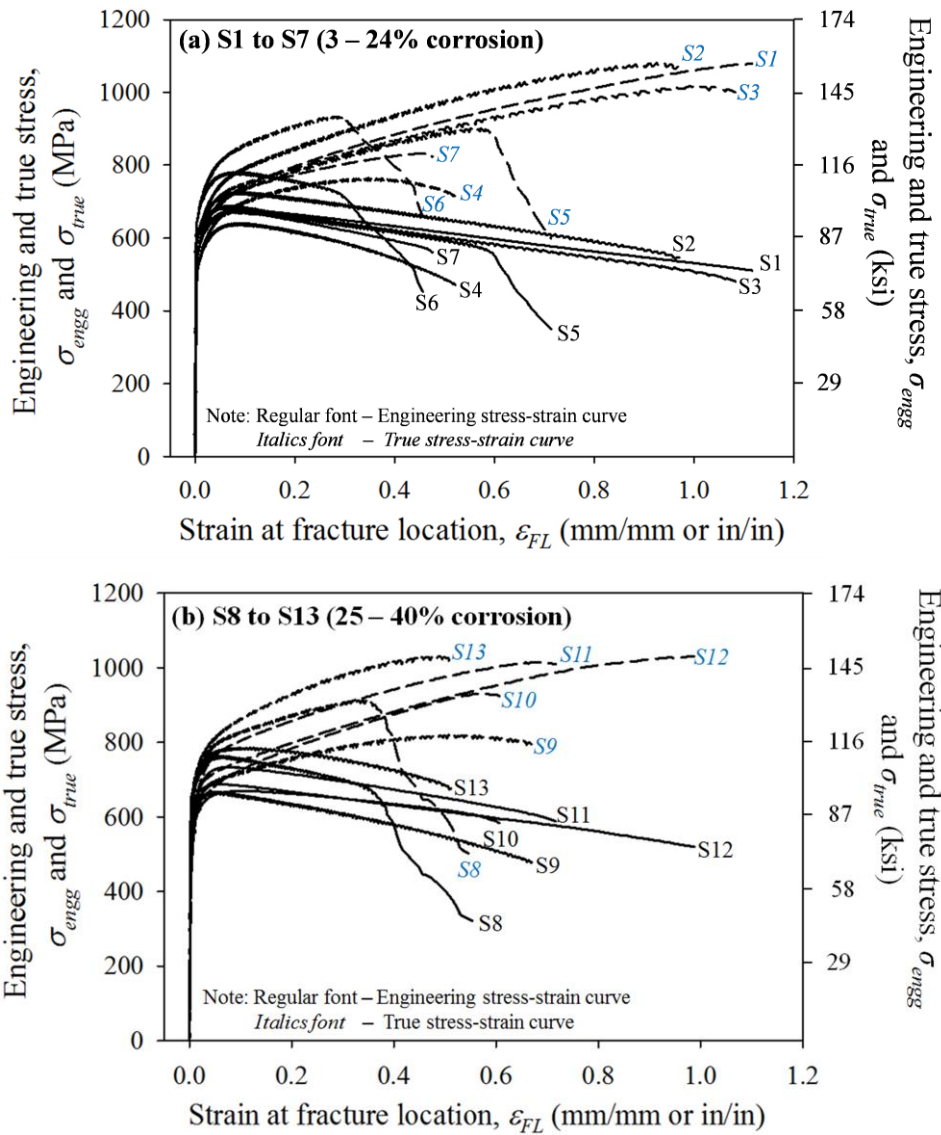


Figure 4.7 Engineering and true stress-strain curves of the thirteen corroded CTD specimens- (a) S1 to S7 (3 – 24% corrosion) and (b) S8 to S13 (25 – 40% corrosion)

4.3.2 Strain distribution along the length of rebars

The strain distribution in the vicinity (30 mm) of the fracture location, along the CTD rebar specimens, were compared. Figure 4.8 to Figure 4.12 presents the stress-strain curves plotted at different locations along the length of the specimen, 5 mm apart, in the vicinity of the fracture location (similar to those presented in Section 4.2.4). The figures corresponding to S2 and S3, with 4% corrosion (as shown in Figure 4.8), exhibits very similar strain distribution (in terms of the relative positions of the stress-strain curves) along the length. While the other specimens with degree of

corrosion ranging from 18 to 40% (S4 to S13), as shown in Figure 4.9 to Figure 4.12, exhibits significant difference in the strain distribution in the vicinity of fracture location.

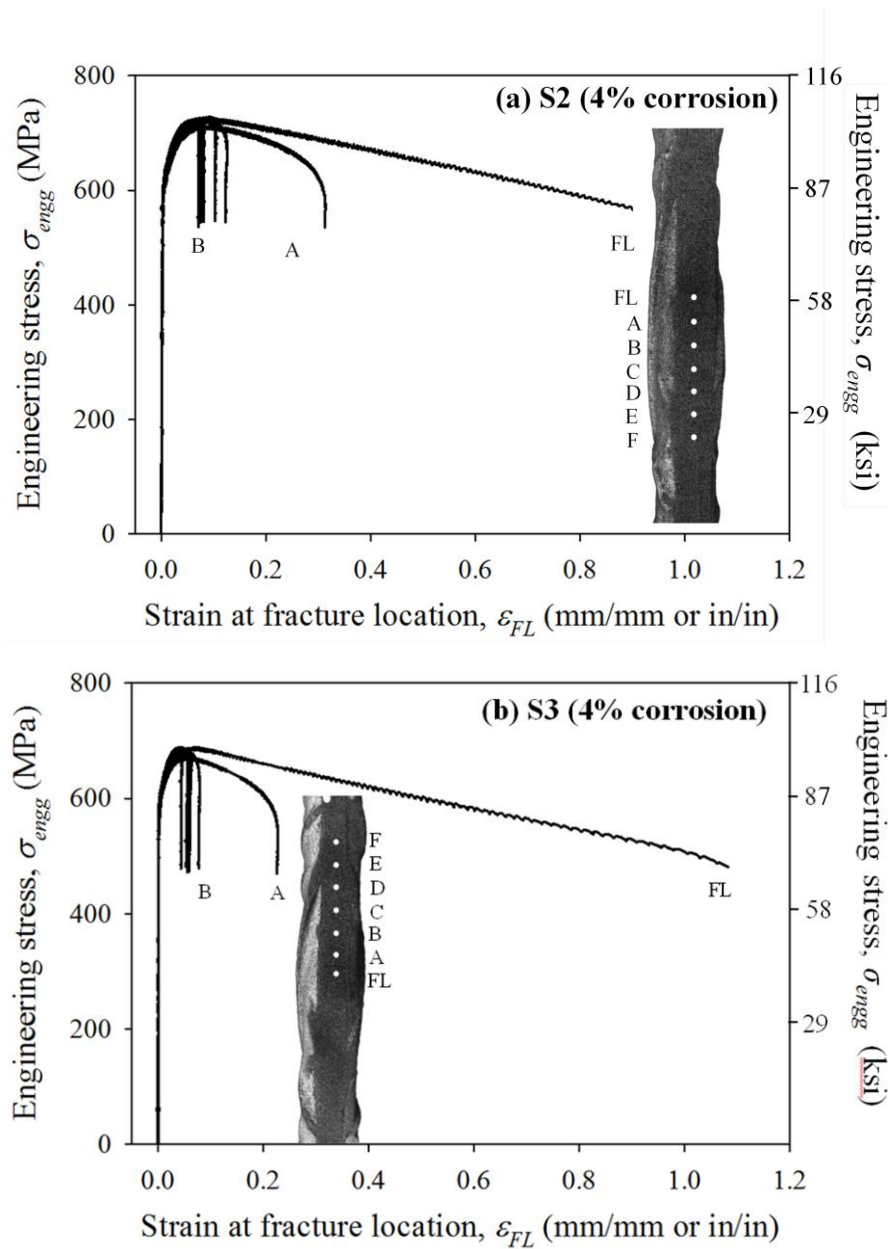


Figure 4.8 Effect of corrosion on the strain distribution along the length of the CTD rebar specimens – (a) S2 (4% corrosion) and (b) S3 (4% corrosion)

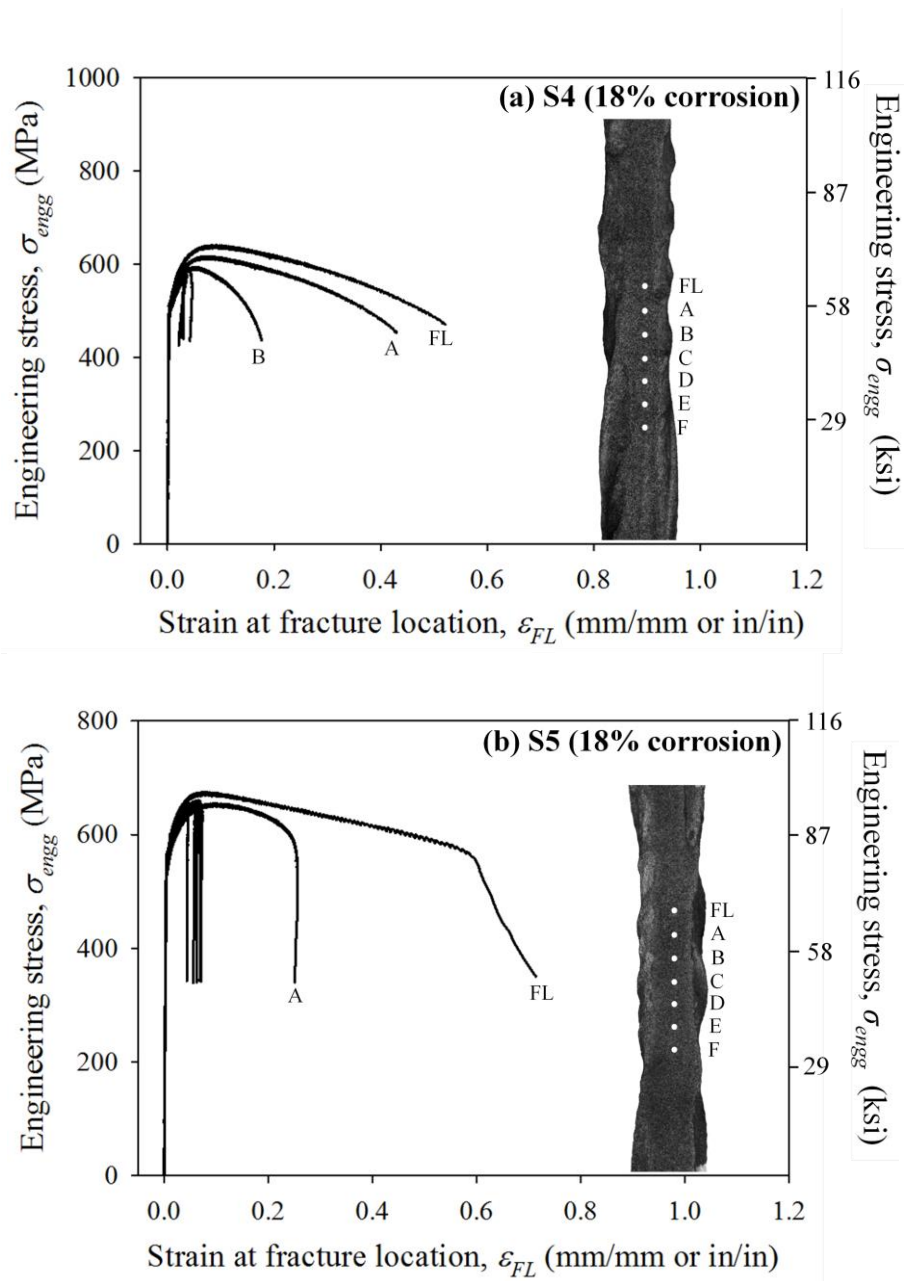


Figure 4.9 Effect of corrosion on the strain distribution along the length of the CTD rebar specimens – (a) S4 (18% corrosion) and (b) S5 (18% corrosion)

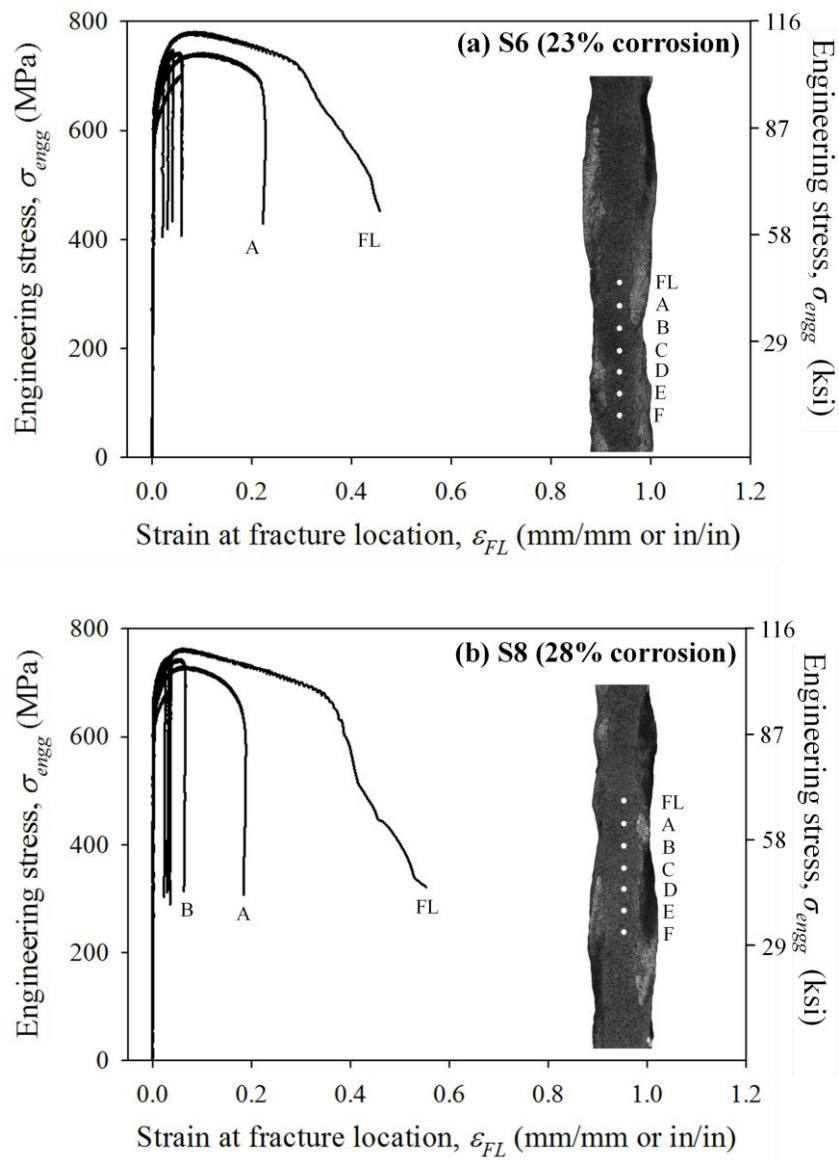


Figure 4.10 Effect of corrosion on the strain distribution along the length of the CTD rebar specimens – (a) S6 (23% corrosion) and (b) S8 (28% corrosion)

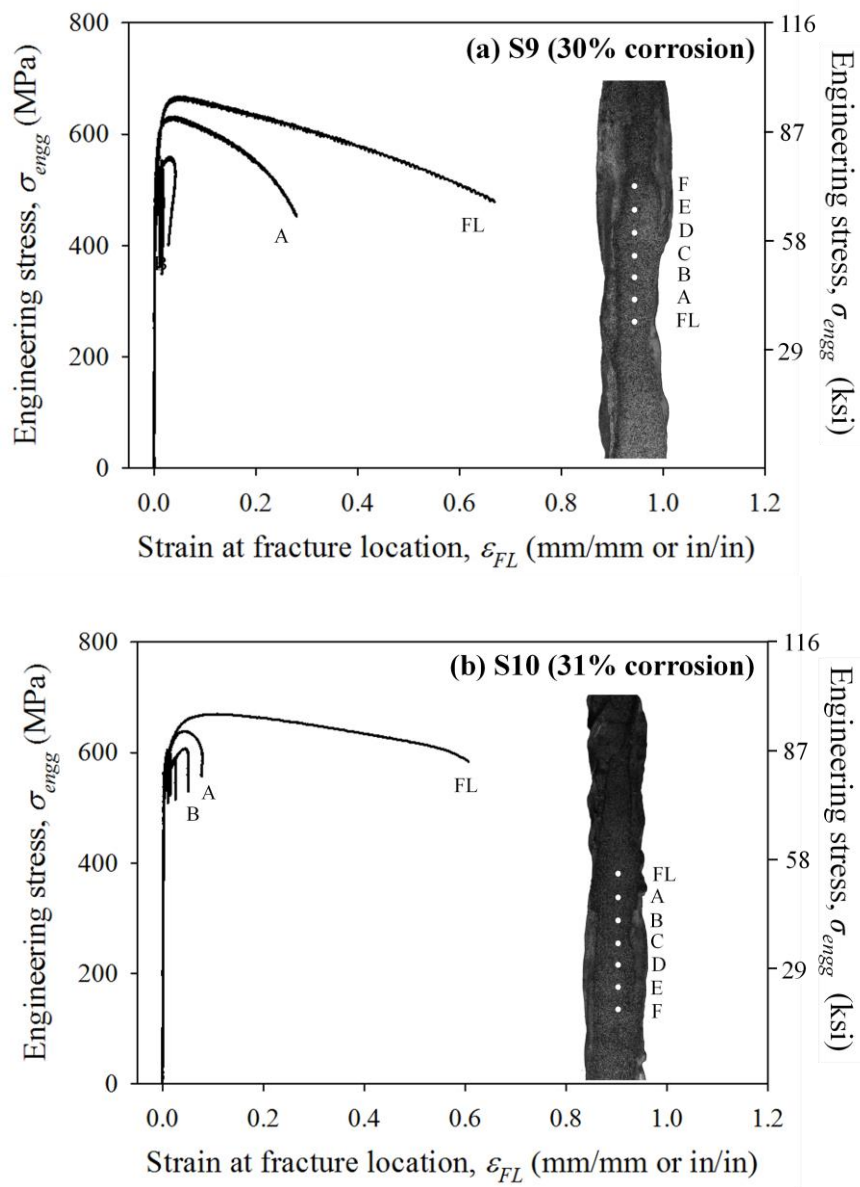


Figure 4.11 Effect of corrosion on the strain distribution along the length of the CTD rebar specimens – (a) S9 (30% corrosion) and (b) S10 (31% corrosion)

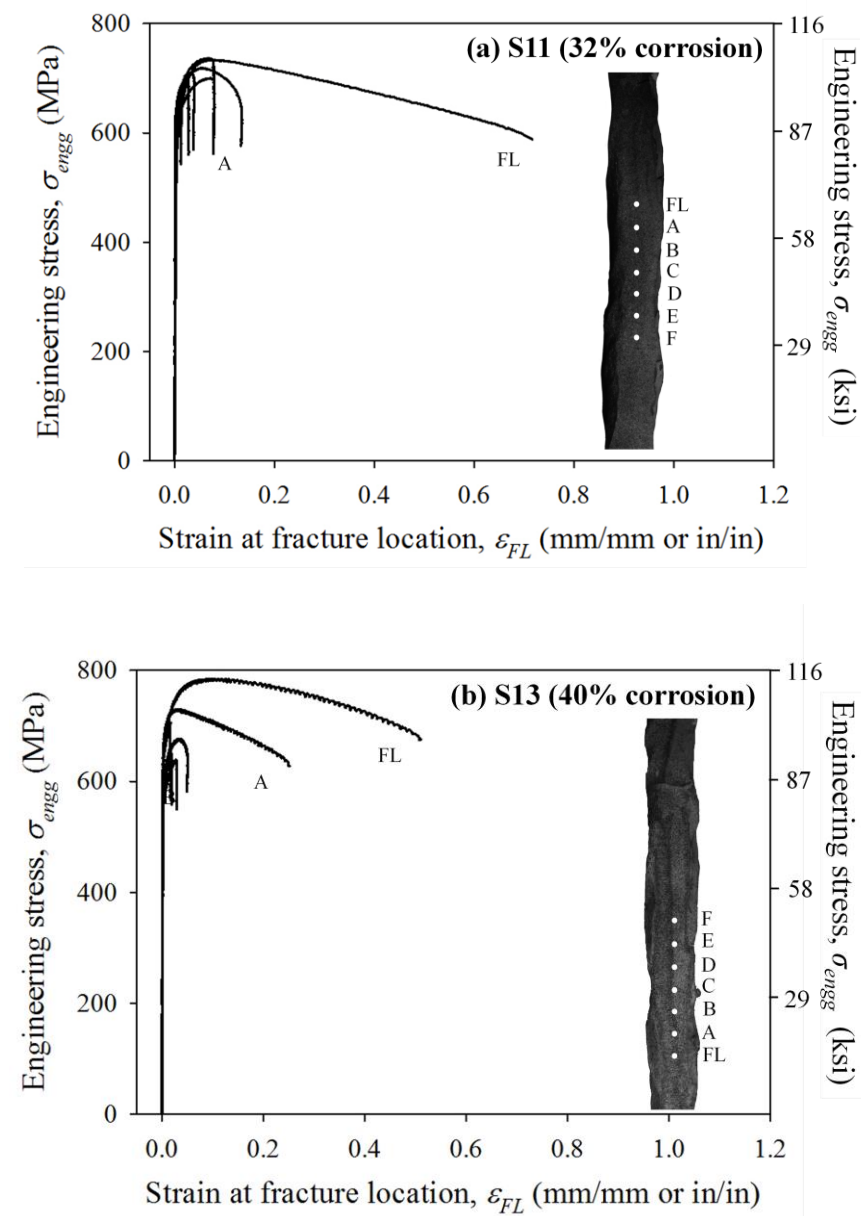


Figure 4.12 Effect of corrosion on the strain distribution along the length of the CTD rebar specimens – (a) S11 (32% corrosion) and (b) S13 (40% corrosion)

4.3.3 Effect of corrosion on proof stress

In this study, the yield strength of the CTD rebar specimens is defined as the offset yield point (proof stress denoted as σ_p) corresponding to 0.2% plastic strain because, unlike PM steel, CTD steel does not exhibit a definite yield point in the stress-strain curve. Figure 4.13 shows the variation in σ_p with increasing degree of corrosion (3 to 40%). The values of σ_p of the thirteen specimens ranges from approximately 540 to

680 MPa, however, no significant trend is visible from the plot, indicating that corrosion may not have a significant effect of the proof stress of the material.

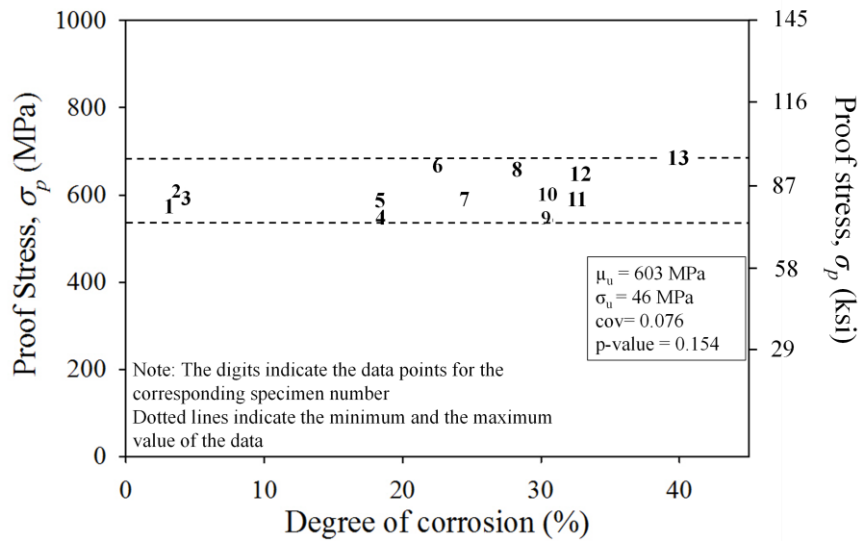


Figure 4.13 Variation in the proof stress of CTD rebar specimens with increasing degree of corrosion

The statistical significance of the data on proof stress of the specimens was determined using the Student's t-test. The specimens were grouped into two groups for this purpose – (a) one group with degree of corrosion < 5% (negligible corrosion), i.e., S1, S2, and S3 and (b) the other group with degree of corrosion > 5%, i.e., specimens S4 to S13. The null hypothesis of this test is that corrosion has no effect of the proof stress of the CTD rebars. A one tailed t-test was selected, because the only expected variation in the proof stress due to corrosion is a decrease. The selected sets of data have unequal sample size and unequal variance. Considering the inherent scatter in most corrosion tests data, a suitable confidence interval of 90% is selected for this test ($\alpha=0.1$). The t-test gave a p-value of 0.154, which indicates that the null hypothesis can be accepted. Also, the coefficient of variation of the proof stress data is 0.076 which is acceptable. Hence, it can be concluded that corrosion does not have a significant effect on the proof stress of the unstressed CTD steel rebars.

4.3.4 Effect of corrosion on ultimate strength

The ultimate strength is computed as the stress experienced by the specimen at the peak load and is denoted as σ_u . Figure 4.14 shows the variation of σ_u of the rebars with increasing degree of corrosion. σ_u values of the thirteen CTD rebar specimens ranges from approximately 640 to 780 MPa (refer Table 4.1 for more details). The plot do not exhibit any visible trend in the variation of σ_u with increasing degree of corrosion.

The statistical significance of the ultimate strength data is also determined using Student's t -test on the same two group of specimens as discussed in Section 4.3.2. A one-tailed t -test using a 90% confidence interval yielded a p -value of 0.32 ($> \alpha = 0.10$). The coefficient of variation of the data is 0.066, which is acceptable. This suggests that corrosion does a have a significant effect on the ultimate strength of unstressed CTD rebars.

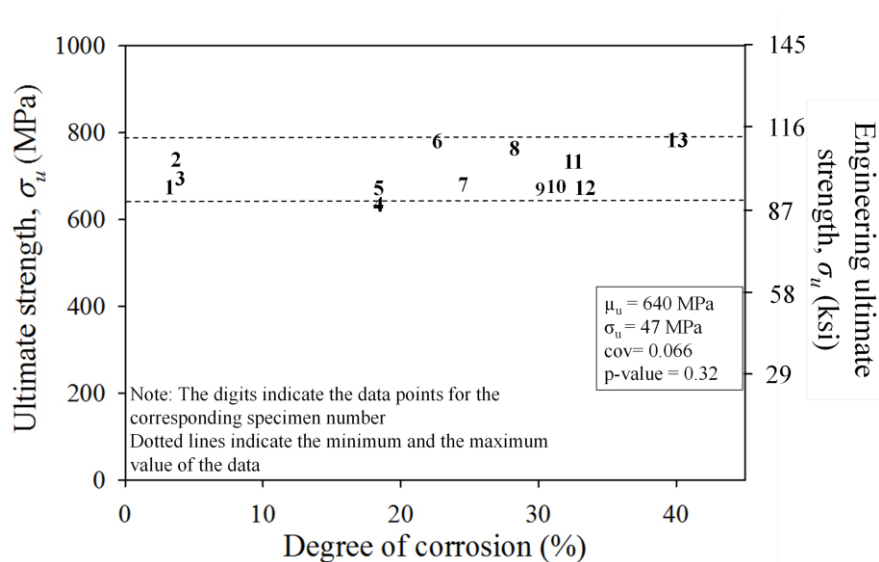


Figure 4.14 Variation in ultimate strength of rebars with increasing degree of corrosion

However, the load capacity of the rebars might reduce due to the reduction in the cross-sectional area due to corrosion. However, this study shows that the strength properties of the residual intact steel are not significantly affected for unstressed CTD rebar specimens due to corrosion. This aspect should be kept in mind while computing the current structural performance of the reinforced concrete structures.

The residual cross-sectional area of the corroded rebars should be considered to assess the actual strength properties of the rebars.

4.3.5 Effect of corrosion on ultimate strain

The ductility of rebars expressed in terms of the strain in the specimen at fracture. In this study, ultimate strain is measured over 60 mm gauge length as well as at the fracture location. The ultimate strain measured over 60 mm gauge length is denoted as $\epsilon_{gauge,ult}$ and ultimate strain at fracture location is denoted as $\epsilon_{FL,ult}$. Figure 4.15(a) shows the variation in $\epsilon_{gauge,ult}$ with increasing degree of corrosion. The plot shows a significant reduction in $\epsilon_{gauge,ult}$ due to corrosion. This observed reduction could be due to the stress-concentration at the fracture location, which leads to strain localization at this point. Consequently, only a smaller fraction of the gauge length would undergo plastic deformation (i.e., exhibit higher strain).

Figure 4.15(b) shows the variation in $\epsilon_{FL,ult}$ with increasing degree of corrosion. The plot displays no significant trend in the variation of $\epsilon_{FL,ult}$ with increasing degree of corrosion. However, the plots exhibits huge scatter in $\epsilon_{FL,ult}$ ranging between 0.457 to 1.117 (i.e., approximately 46 to 112%). This observation suggests that $\epsilon_{gauge,ult}$ does not represent the $\epsilon_{FL,ult}$, as both these values displays different trend with respect to degree of corrosion. One of the reasons for this scatter could be the cross-sectional area profile of the specimens at the fracture location, or in other words, the pattern of corrosion. The influence of pattern of corrosion on $\epsilon_{FL,ult}$ values was investigated to gain a better understanding.

4.3.6 Effect of pattern of corrosion on the ultimate strain measured at fracture location

The different topographies of the corroded specimens are discussed in Section 2.3. The pattern of corrosion is claimed to influence the ultimate strain in specimens by researchers. In this study, the pattern of corrosion is quantified in terms of the rate of change of cross-sectional area over 1 mm. This is illustrated in Figure 4.16. The plot shows the cross-sectional area profile along 4 mm length to either side of the fracture location (denoted as FL in x-axis) of three specimens S2, S6 and S12. The slope of the change in cross-sectional area over 1 mm at the fracture location is measured. The highest of the slopes to either end is considered and is denoted as dA/dy , i.e., change

in cross-sectional area with respect to length of the specimen. Greater the value of dA/dy , more localized is the pattern of corrosion at the fracture location. A smaller value of dA/dy indicate relatively uniform pattern of corrosion. The values of dA/dy of the thirteen specimens are presented in Table 4.2. It should be noted that the dA/dy values are very low for the difference among them to be distinctly visible from Figure 4.16.

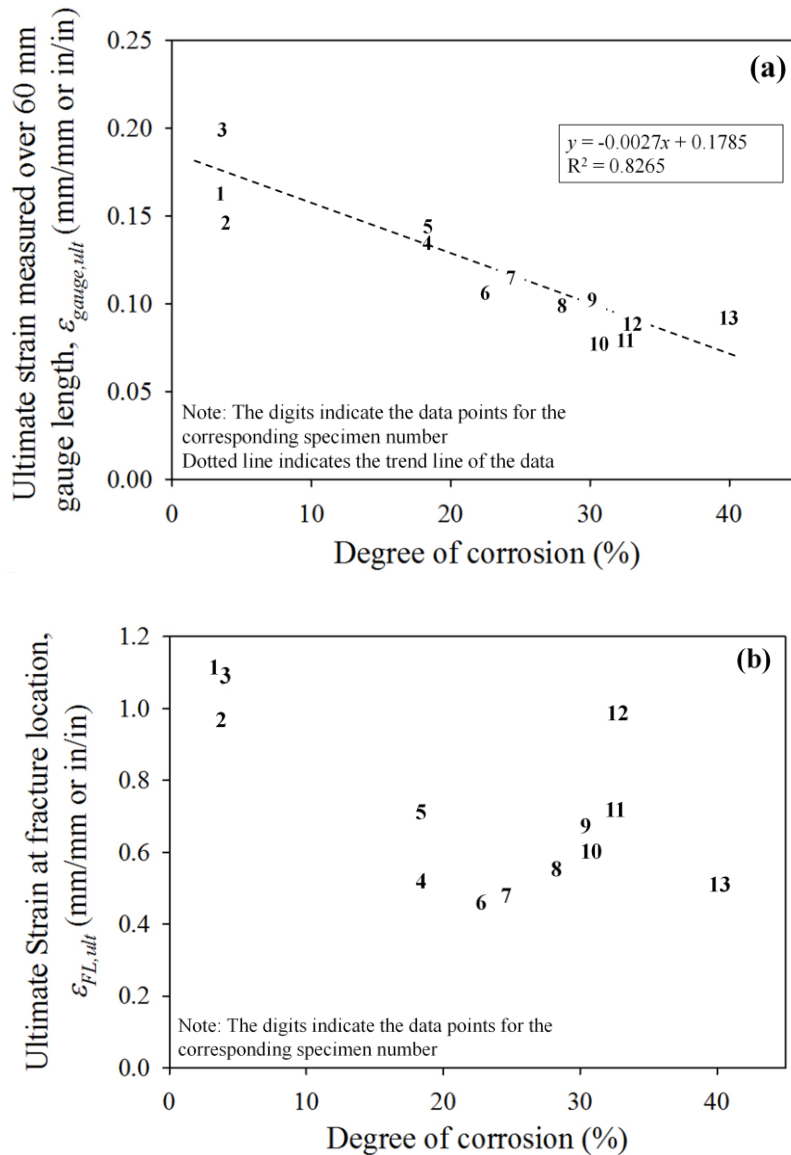


Figure 4.15 Variation in (a) effective ultimate strain measured over 60 mm gauge length and (b) ultimate strain measured at the fracture location, with increasing degree of corrosion

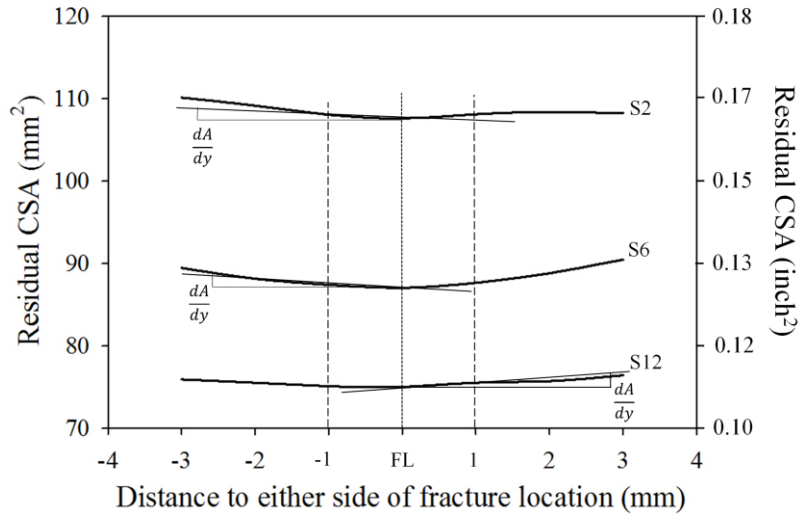


Figure 4.16 Rate of change of cross-sectional area at the fracture location (over 1 mm) for specimens S2, S6 and S12

Table 4.2 The rate of change of cross-sectional area (dA/dy) at the fracture location quantifying the localization of corrosion

ID	S1	S2	S3	S4	S5	S6	S7	S8	S9	S10	S11	S12	S13
dA/dy	0.54	0.76	0.37	0.83	0.69	0.86	0.93	0.80	0.62	2.76	0.59	0.50	0.81

Figure 4.17 shows the variation in $\epsilon_{FL,ult}$ with increasing dA/dy . The plots shows that $\epsilon_{FL,ult}$ decreases with increase in dA/dy . This indicates that the pattern of corrosion has a significant influence on the ductility of the unstressed rebars measured in terms of $\epsilon_{FL,ult}$. The rebar with a localized corrosion would exhibit very low ultimate strain. The degree of corrosion may not represent the pattern of corrosion. It is to be noted that ultimate strain of Specimen 10 is not shown Figure 4.16, as it was an outlier; it showed a coordinate of (0.606, 2.764) in this plot.

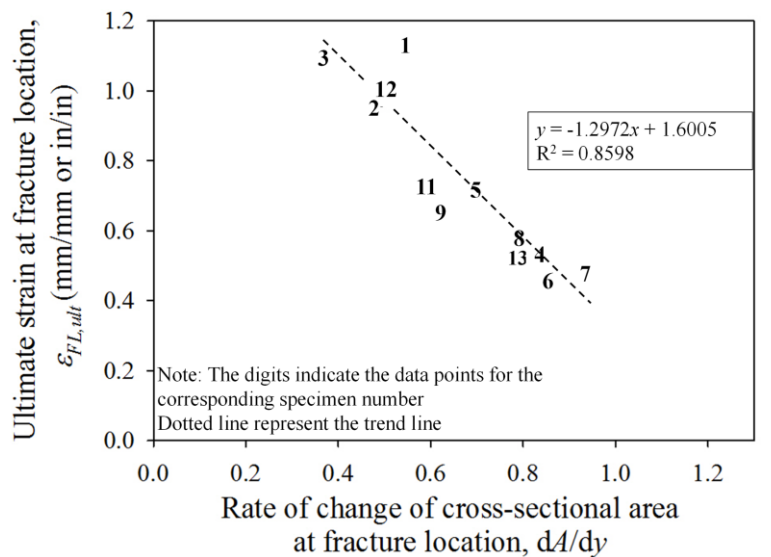


Figure 4.17 Variation in ultimate strain at fracture location with the rate of change of cross-sectional area at the fracture location

The influence of the pattern of corrosion on the ductility of the rebars highlights the need for full-field deformation technique to assess the stress-strain behaviour of corroded rebars. The measurement of strain over the gauge length does not take into account the pattern of corrosion and the associated variations in the strain distribution along the length. Hence the measurement of strain over a gauge length for corroded rebars with highly uneven cross-sectional area could be ambiguous. Also, it is a point to be highlighted that only a very accurate estimation of the residual cross-sectional area profile can bring out the influence of the pattern of corrosion on $\epsilon_{FL,ult}$.

4.3.7 Effect of corrosion on elastic modulus

Figure 4.18 shows the variation in elastic modulus of rebars with increasing degree of corrosion. Specimens 3, 9, 10, 11, and 13 exhibit an elastic modulus of $\approx 2 \times 10^5$ MPa. However, there are considerable scatter among the determined elastic modulus of the other specimens. The reasoning for this is as follows. The tension testing machine used for these tests had a capacity of 1000 kN. Typically, the precision/control of most tension testing machines are poor at a load less than 2% of its capacity (i.e., 20 kN). The elastic limits of the test specimens correspond to low load levels (between 20 and 30 kN). At this range of load, the precision/control of the tension testing machine might have been insufficient – resulting in a huge scatter in elastic

modulus values. In short, the data on elastic modulus presented in this section may be erroneous. Hence, further discussion on this is avoided.

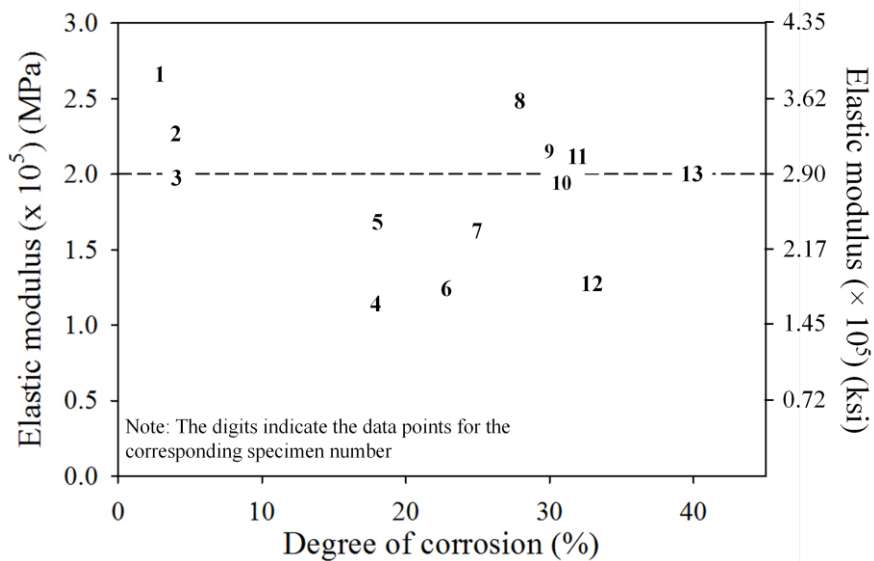


Figure 4.18 Variation in elastic modulus with increasing degree of corrosion

4.4 SUMMARY

This chapter presented the results obtained from the two phases of this study – (a) development of the testing and evaluation method, and (b) determination of the mechanical properties of corroded CTD rebars using the developed method. Section 4.2 include comparison of the different experimental methods attempted to estimate the residual cross-sectional area of corroded CTD rebars, comparison of the different strain computation method, and the feasibility study for the proposed method. The second phase of this study, presented in Section 4.3, includes evaluation of the effect of corrosion on the stress-strain behaviour of corroded CTD steel rebars. This section focusses on the stress-strain behaviour, strain distribution along the length of the rebars, the effect of corrosion on the mechanical properties, the yield strength, ultimate strength, and ultimate strain of the corroded rebars.

CHAPTER 5

CONCLUSIONS AND RECOMMENDATIONS

5.1 INTRODUCTION

This chapter presents the conclusions drawn from this research project on the assessment of the stress-strain behaviour of corroded steel rebars using DIC technique. This study was conducted in two phases. First, a refined testing and evaluation method using DIC technique was developed. This phase tried multiple alternatives to develop a holistic procedure to assess the stress-strain behaviour of corroded rebars. A feasibility of the proposed method to meet the intended requirements was assessed using a set of rebar specimens. In the next phase of the study, the effect of corrosion on the stress-strain behaviour of naturally corroded unstressed CTD rebars was evaluated using the developed test method.

5.2 LIMITATIONS AND ASSUMPTIONS

The proposed testing and evaluation method for assessing the stress-strain behaviour of corroded rebars using DIC technique has the following limitations:

- The steel rebars are a typical case where 3D DIC is to be utilized. However, 3D DIC is very sophisticated procedure and also demands expertise in this technique from the user. For the ease of testing and evaluation, 2D DIC technique was used in this study. The evaluation of the stress-strain behaviour of corroded rebars using 2D DIC was facilitated in this study by milling the specimen for approximately 0.5 mm longitudinally to obtain a plane surface on the rebar. The displacements and strain are computed on the milled surface of the specimen assuming that this would give a good representation of the strain across the cross-section of the rebar. Also, it is assumed that milling would not generate any changes in the microstructure of the steel. The study shows that the pattern of corrosion significantly influences the ultimate strain in the rebars. It is assumed that milling does not alter the existing pattern of corrosion significantly.
- One of the major limitations associated with the use of 2D DIC is that it cannot capture the out-of-plane bending in the specimen. There would be considerable

out-of-plane deformation associated with necking of the specimen. Hence, the strain beyond the peak of the stress-strain curve may not be very reliable.

- Capturing the strain in images using a single camera focussed on the milled surface does not capture the deformation on other side of the specimen. Sometimes, the fracture initiates on the other side, which would lead to the measurement of a higher strain at the milled surface. Hence, 2D DIC may not give an accurate strain measurement close to fracture of the specimen. This is evident in Figure 4.7 as a sudden drop in the stress-strain curves for a few specimens.
- This study involves the study of only unstressed corroded rebars. The corrosion in combination with the stress in the specimen may lead to different conclusions from the study.
- Sufficient number of specimens was not obtained from the corroded CTD rebar sample collected from the demolished structure. Also, the data lacks a proper control specimen due to non-availability of CTD rebars in the market. Hence, the results from the assessment of the effect of corrosion on the stress-strain behaviour of rebars are compared to that of specimens with less than 5% corrosion. It is assumed that a degree of corrosion less than 5% does not change the stress-strain behaviour significantly.

5.3 USE OF DIC TECHNIQUE TO ASSESS THE STRESS-STRAIN BEHAVIOUR OF CORRODED REBARS

This method was proposed to meet certain requirements that can improve the evaluation of mechanical properties of corroded rebars. The following conclusions were drawn from the first phase of the study which includes development of the testing and evaluation method and the assessment of the feasibility of the developed method to meet the intended requirements.

- PCA based algorithm is a more reliable method of strain computation from the full-field displacement data to estimate the strain distribution along the length of the specimen.
- Out of the attempted methods, 3D laser scanning gave the most accurate estimation of residual cross-sectional area profile of the specimen and an accurate prediction of the fracture location prior to the testing.
- The proposed test method can compute the local mechanical properties very close to the fracture location. The proposed method could compute the mechanical

properties of the specimen not more than 0.5 mm away from fracture location on the specimen.

- The proposed method was successful in capturing strain at intervals of approximately 0.8-1 mm length along the rebars (over 60 mm long AOI). This gives an accurate estimate of the strain distribution along the AOI, which provides a better understanding of the deformation of corroded rebars and the strain heterogeneity associated with the uneven cross-sectional area.
- The proposed method also facilitates the computation of a close approximate of the true stress-strain curve assuming the conservation of volume over the fracture location.

5.4 EFFECT OF CORROSION ON MECHANICAL PROPERTIES OF CORRODED CTD REBARS EVALUATED USING THE DEVELOPED METHOD

The testing and evaluation method developed in the first phase of this study is used to evaluate the effect of mechanical properties of the local mechanical properties close to the fracture location of the naturally corroded unstressed CTD rebar specimens. The conclusions drawn from the assessment of stress-strain behaviour of the CTD rebars are as follows.

- Corrosion does not have a significant effect on the strength properties, the yield strength and the ultimate strength, of corroded rebars. The residual intact steel in the unstressed rebars with degree of corrosion as high as 40% exhibit similar strength properties as the specimens with less than 5% corrosion.
- The ultimate strain measured over 60 mm gauge length shows a decreasing trend with increasing degree of corrosion.
- The ultimate strain measured at the fracture location does not show a significant trend with increasing degree of corrosion. Thus, the measurement of strain over the gauge length does not represent the ductility of the rebars at the fracture location.
- The pattern of corrosion has a significant influence in the ultimate strain exhibited by the specimens at the fracture location. The ultimate strain at fracture location decreases with increasing degree of localization of corrosion.

- This study emphasizes the need for full-field deformation technique to accurately estimate the mechanical properties of corroded rebars with uneven cross-sectional area.

5.5 FUTURE RECOMMENDATIONS

The recommendations for the future work include the following:

- Corroded rebars should be evaluated using 3D DIC, which can facilitate a better and a more accurate assessment of the effect of corrosion on their stress-strain behaviour.
- The naturally corroded rebars collected from the parts of the structure stressed under the load should be assessed using the developed method to better understand the performance of corroded rebars inside the existing structures experiencing in-service stress and corrosion.
- A more extensive study should be conducted using a larger sample size to develop numerical relationship between degree of corrosion and the variation in the ultimate strain.

REFERENCES

1. **Ahmad, S.** (2009). Techniques for inducing accelerated corrosion of steel in concret,*Arabian Journal for Science and Engineering*, **34**(2), 95-104.
2. **Almusallam, A. A.** (2001). Effect of degree of corrosion on the properties of reinforcing steel bars,*Construction Building MAterials.*, **15**(8), 361-368.
3. **Apostolopoulos, C. A., and Papadakis, V. G.** (2008). Consequences of steel corrosion on the ductility properties of reinforcement bar,*Construction Building Materials*,**22**(12), 2316-2324.
4. **Apostolopoulos, C. A., & Kappatos, V.** (2013). Tensile properties of corroded embedded steel bars B500c in concrete, *International Journal of Structural Integrity*, **4**(2), 275-294.
5. **ASTM A615 / A615M-16**, Standard Specification for Deformed and Plain Carbon-Steel Bars for Concrete Reinforcement, ASTM International, West Conshohocken, PA, 2016, DOI: 10.1520/A0615_A0615M-16, www.astm.org
6. **ASTM G1-03**, Standard Practice for Preparing, Cleaning, and Evaluating Corrosion Test Specimens, ASTM International, West Conshohocken, PA, 2011, DOI: 10.1520/G0001-03R11, www.astm.org
7. **Basu, P. C., Shylamoni, P., Roshan, A. D., and Roshan, A. D.** (2004). Characterisation of steel reinforcement for RC structures: An overview and related issues,*Indian Concrete Journal*, **78**(1), 19-30.
8. **Bornert, M., Brémand, F., Doumalin, P., Dupré, J. C., Fazzini, M., Grédiac, M., Hild, F., Mistou, S., Molimard, J., Orteu, J. J., Robert, L., Surrel, Y., Vacher, P., and Wattrisse, B.** (2009). Assessment of Digital Image Correlation Measurement Errors: Methodology and Results,*Experimental Mechanics*,**49**, 353–370.

9. **Boulekbache, B., Hamrat, M., Chemrouk, M., and Amziane, S.** (2015). Failure mechanism of fibre reinforced concrete under splitting test using digital image correlation, *Materials and Structures*, **48**, 2713-2726.
10. **Cairns, J., Plizzari, G. A., Yingang, D., Law, D. W., and Franzoni, C.** (2005). Mechanical properties of corrosion-damaged reinforcement, *ACI Materials Journal*, **102**(4), 256-264.
11. **De Wilder, K., Lava, P., Debruyne, D., Wang, Y., De Roeck, G., and Vandewalle, L.** (2015). Experimental investigation on the shear capacity of prestressed concrete beam using Digital Image Correlation, *Engineering Structures*, **82**, 82-92.
12. **Du, Y. G., Clark, L. A., and Chan, A. H. C.** (2005a). Residual capacity of corroded reinforcing bars, *Magazine of Concrete Research*, **57** (3), 135-147.
13. **Du, Y. G., Clark L. A., and Chan A. H. C.** (2005b). Effect of corrosion on ductility of reinforcing bars, *Magazine of Concrete Research*, **7**, 407-419.
14. **Dutton, M.** (2012). Digital image correlation for evaluating structural engineering materials, Department of Civil Engineering, Queen's University Kingston, Ontario, Canada.
https://qspace.library.queensu.ca/bitstream/1974/7552/1/Dutton_Michael_G_201209_MASC.pdf(Mar. 27, 2016)
15. **Francois, R., Khan, I., and Dang, V. H.** (2013). Impact of corrosion on mechanical properties of steel embedded in 27-year-old corroded reinforced concrete beams, *Materials and Structures*, **46**(6), 899-910.
16. **Gencturk, B., Hossain, K., Kapadia, A., Labib, E., and Mo, Y. L.** (2014). Use of digital image correlation technique in full-scale testing of prestressed concrete structures, *Measurement*, **47**, 505-515.
17. **Glass, G. K., and Buenfeld, N. R.** (2001). Chloride-induced corrosion of steel in concrete, *Progress in Structural Engineering and Materials*, **2**(4), 448-458.

18. **Grama, S. N., and Subramanian, S. J.** (2014). Computation of full-field strains using principal component analysis, *Experimental Mechanics*, **54**(6), 913-933.
19. **IS 1608:2005**, Mechanical Testing of Metals – Tensile Testing, Bureau of Indian Standards, Manak Bhavan, 9 Bahadur Zafar Marg, New Delhi 110002, 2005.
20. **IS 1786:2008**, High Strength Deformed Steel Bars and Wires for Concrete Reinforcement – Specifications, Bureau of Indian Standards, Manak Bhavan, 9 Bahadur Zafar Marg, New Delhi 110002, 2008.
21. **IS 432 (Part 1): 1982**, Mild Steel and Medium Tensile Steel Bars and Hard-Drawn Steel for Concrete Reinforcement, Bureau of Indian Standards, Manak Bhavan, 9 Bahadur Zafar Marg, New Delhi 110002, 1982.
22. **Kashani , M. M., Crewe, A. J., and Alexander, N. A.** (2013). Nonlinear stress–strain behaviour of corrosion-damaged reinforcing bars including inelastic buckling, *Engineering Structures*, **48**, 417-429.
23. **Koch, G., Varney, J., Thmpson, N., Moghissi, O., Gould, M., and Payer, J.** (2016), International measures of prevention, application, and Economics of corrosion technologies study, *Impact*, NACE International.
24. **Lee, H. S., and Cho, Y. S.** (2009). Evaluation of the mechanical properties of steel reinforcement embedded in concrete specimen as a function of the degree of reinforcement corrosion, *International Journal of Fracture*, **157**(1), 81-88.
25. **Malesa, M., Szczepanek, D., Kujawińska, M., Świercz, A., & Kołakowski, P.** (2010). Monitoring of civil engineering structures using Digital Image Correlation technique. *EPJ Web of Conferences*, **6**, 31014.
26. **McCormick, N., and Lord, J.** (2010). Digital Image Correlation, *Materials Today*, **13**(12), 52-54.
27. **Palsson, R., and Mirza, M. S.** (2002). Mechanical response of corroded steel reinforcement of abandoned concrete bridge, *ACI Materials Journal*, **99**(2), 157-162.

28. **Pan, B., Qian, K., Xie, H., and Asundi, A.** (2009). Two-dimensional digital image correlation for in-plane displacement and strain measurement: a review, *Measurement science and Technology*, **20**(6), 062001.
29. **Rösler, J., Harders, H., & Baeker, M.** (2007). Mechanical behaviour of engineering materials: metals, ceramics, polymers, and composites. *Springer Science & Business Media*.
30. **Singh, B. K., Basak, M., West, M., and Guha, I.** (2010). Estimating the cost of corrosion in Indian industry, *Proceeding of Petrotech 2010*, New Delhi, India, Paper ID : 20100815, 1-7.
31. **Taha, A. N., and Morsy, M.** (2015). Study of the behaviour of corroded steel bar and convenient method of repairing, *HBRC Journal*, in press. <http://dx.doi.org/10.1016/j.hbrej.2014.11.004> (April 10, 2016)
32. The Freepress Journal, 2012. India loses \$40 billion a year due to corrosion in infra.
33. **Wang, X., Zhang, W., Gu, X., and Dai, H.** (2013). Determination of residual cross-sectional areas of corroded bars in reinforced concrete structures using easy-to-measure variables, *Construction Building Materials*, **38**, 846-853.
34. **Li, X. Y. and Zhang, Z. G.** (2011). The Impact of Corrosion on the Mechanical Properties of Smooth Steel Rebar HPB235, *Advanced Materials Research*, **179**, 28-31.
35. **Xu Youlin, Cheng Zhijun, Wang Xiaofeng, Liu Lixin, Guan Pinwu, Yang Shuhui.** (2003). Experimental Research on Mechanical Properties of Corroded Steel Bars. International Symposium on Research and Applications of High Strength Reinforcing Bar.
36. **Yuan, Y., Ji, Y., and Shah, S. P.** (2007). Comparison of two accelerated corrosion techniques for concrete structures, *ACI Structural Journal*, **104**(3) 344-347.
37. **Zhang, W., Song, X., Gu, X., and Li, S.** (2012). Tensile and fatigue behaviour of corroded rebars, *Construction Building Materials*, **34**, 409-417.

38. **Zhu, W. and Francois, R.** (2013). Effect of corrosion pattern on the ductility of tensile reinforcement extracted from a 26-year-old corroded beam, *Advances in Concrete Constructon*, **1**(2), 121-13.

APPENDIX

Prenormative Test Method for

ASSESSMENT OF STRESS-STRAIN BEHAVIOUR OF CORRODED REBARS USING DEVELOPED TESTING AND EVALUATION METHOD

1. Scope

- 1.1. This test and evaluation method gives the stress-strain curve and mechanical properties corresponding to the fracture location of the corroded rebars.
- 1.2. This document does not purport to address the safety concerns associated with the use of the proposed method. The use of hazardous materials and heavy machinery may be involved in the test procedure. It is the user's responsibility to establish appropriate safety measures and health practices prior to use.
- 1.3. SI units are used throughout this document.

2. Referred Documents

- 2.1. American Society of Testing and Materials, 2011, G1-03, "Standard Practice for Preparing, Cleaning and Evaluating Corrosion Test Specimens", ASTM, Conshohocken, PA
- 2.2. American Society of Testing and Materials, 2012, A370-12, "Standard Test Methods and Definitions for Mechanical Testing of Steel Products", ASTM, Conshohocken, PA
- 2.3. American Society of Testing and Materials, 2008, E 8/E 8M-08, "Standard Test Methods of Tension Testing of Metallic Materials", ASTM, Conshohocken, PA
- 2.4. Indian Standard, 2004, IS:432(Part I), "Specification for Mild Steel and Medium Tensile Steel Bars and Hard-Drawn Steel Wire for Concrete Reinforcement – Part I Mild Steel and Medium Tensile Steel Bars", BIS, NewDelhi
- 2.5. Indian Standard, 1995, IS 1608, "Mechanical Testing of Metals – Tensile Testing", BIS, NewDelhi

2.6. Indian Standard, 2008, IS 1786, “High Strength Deformed Steel Bars and Wires for Concrete Reinforcement – Specification”, BIS, NewDelhi

3. Summary of Test and Evaluation Method

3.1. This test method assesses the stress-strain behaviour and estimates the mechanical properties of corroded rebars. The full-field deformation technique, Two-Dimensional Digital Image Correlation (2D DIC), is utilized for the assessment. The corroded steel rebars with curved surface is milled to facilitate the use of 2D DIC technique. The corroded rebar specimens are scanned using Three Dimensional Laser Scanning technique to estimate the profile of the residual cross-sectional area of the rebars and to predict the probable fracture location prior to the test. The Area of interest (AOI) is defined on the specimen based on the identified probable fracture location and this region is speckled. The tension test is conducted based on the guidelines laid down by ASTM E 8/E 8M-08. During the deformation of the specimen under tension, images are captured at regular time intervals. After the fracture of the specimen under tension, the full-field deformation and strains of the defined points on the AOI is computed using the DIC software, Vic-2DTM. The DIC parameters, step size, subset size and filter size, are selected based on the average speckle size and the pixel resolution of the AOI. The stress-strain curve is plotted using the stress and strain values computed at or very close (not greater than 0.5 mm away) to the fracture location. The mechanical properties of the specimen, the elastic modulus, yield strength, ultimate strength and ultimate strain at the fracture, are evaluated using the stress-strain curve plotted. Figure A.1 shows a flowchart of the testing and evaluation procedure.

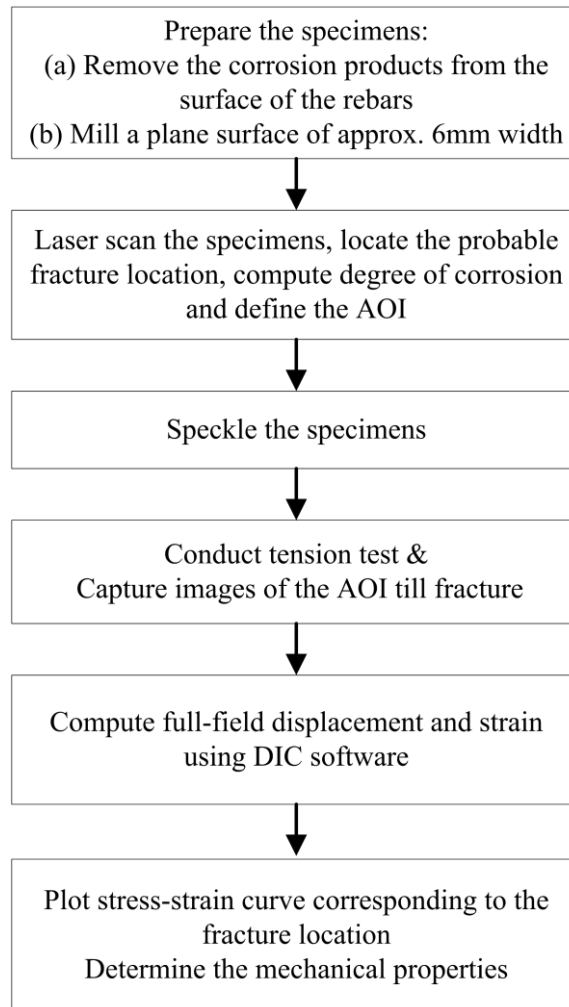


Figure A.1 Flowchart of the testing and evaluation procedure using the developed method

4. Significance and use

4.1. The assessment of the stress-strain behaviour of corroded rebars will help to understand the performance of reinforced concrete structures experiencing corrosion. This would help to estimate the service life of the structure and to formulate effective repair or maintenance strategies, thereby helping to ensure adequate performance and safety of the corroding structures.

4.2. The use of DIC technique for the assessment of the stress-strain behaviour of corroded rebars can overcome the drawbacks of the conventional methods of evaluation. The full-field deformation measurement can capture the strain heterogeneity due to the uneven cross-sectional area of the

corroded rebars, which would facilitate a better understanding of the effect of corrosion on the ductility of rebars.

5. Disadvantages

- 5.1. Rebar specimens typically require 3D DIC technique to estimate the full-field deformation. For the ease of use, 2D DIC technique is adopted. The rebars, thus, need to be milled to facilitate the assessment using the 2D DIC technique.
- 5.2. The strain computed beyond necking of the specimens using the developed method may not be very accurate due to the significant out-of-plane deformations in the specimen which 2D DIC technique cannot capture.

6. Equipment

The testing and evaluation using this method requires the following equipment:

- 6.1. Wire Brush – Wire brushes with steel spikes can be used to remove the corrosion products from the surface of the rebars.
- 6.2. Lathe Machine: A machine that can remove the steel from the surface of the rebar to create a smooth plane surface. The equipment should be able to remove the steel surface without heating the steel.
- 6.3. 3D LaserScanner: Laser Scanner which gives sufficient accuracy (approximately ± 0.05 mm) can be used for the estimation of the residual cross-sectional area at intervals less than or equal to 1 mm length.
- 6.4. Tensile testing machine: A displacement control tensile testing machine of minimum load capacity of 100 kN can be used to test corroded rebars till fracture.
- 6.5. CCD Camera: A digital camera that can capture a minimum of 2 images per second of image resolution at least 1.4 megapixel resolution (i.e., 1037×1391 pixels) can be used for capturing the images during the deformation of the specimen. The camera sensor should not get heated up during the test.

- 6.6. Tripod: CCD camera can be placed on a tripod with leveling options to position the camera with its focal plane exactly parallel to the AOI on the milled surface.
- 6.7. Lamps – Light lamps of sufficient numbers can be used to provide sufficient illumination (depending on the natural lighting of the room) for clarity of the captured images.
- 6.8. Computer systems: The computer system that can support Vic-2D™ software can be used to estimate the full-field deformation on a predefined region of the specimens.
- 6.9. Vic-snap™ software – this software can be used to capture the images of the specimen during the tension test at a desired regular time interval and to save the images to the system, simultaneously.
- 6.10. Vic-2D™ – this DIC software can be used to compute the full-field deformation over the AOI of the specimen.

7. Materials and Reagents

The specimen preparation and testing using the proposed method requires the following materials and reagents:

- 7.1. Steel rebars – Smooth or ribbed steel rebars, having varying degree of corrosion, induced in the rebars naturally or artificially, can be tested using the proposed method
- 7.2. Cleaning solution – Add 3.5 g of Hexamethylene Tetramine to 500 ml of Hydrochloric acid (specific gravity 1.19) and dilute it to 1000 ml using reagent water.
- 7.3. Spray Paints – Acrylic aerosol spray paints of non-reflective contrasting colors can be used to speckle the surface of the specimen.

8. Procedure for preparation of the specimen

- 8.1. Cut the corroded rebars to specimens such that the corroded region of the rebar (regions with relatively smaller cross-sectional area) lies at the middle of the specimen.
- 8.2. Prepare the cleaning solution for removing the corrosion products (rust, mill scales etc.) as mentioned in Clause 7.2. Dip the corroded rebars

specimen in the solution for 10 minutes and remove the corrosion products mechanically using a wire brush. Repeat this process till the corrosion products are removed completely using the same prepared solution. Ensure that specimens are not kept immersed in the cleaning solution for more than 10 minutes, which may lead to etching of the steel.

- 8.3. Mill the surface to appropriate depth using a Lathe machine such that milled surface has at least 6 mm width. Leave at least 50 mm (grip length) on either ends of the specimen unmilled. Ensure that the rebar is held straight while milling to obtain a smooth plane surface on the rebar.
 - 8.4. Scan the grip-to-grip length of the specimen using a suitable 3D laser scanner to create a digital 3D model of the surface of the specimen. Select a longitudinal and circumferential scanning pitch less than or equal to 1 mm. A 3D scanner that can provide an accuracy of approximately ± 0.05 mm is recommended.
 - 8.5. Extract the scan data (the spatial coordinates on the points on the surface of the specimen) from the laser scanner in .txt or .xls format. Compute the residual cross-sectional area at regular length intervals (least unit of length is the longitudinal scanning pitch), of the specimen from the scan data using a custom-made computer algorithm.
 - 8.6. Identify the location with the least residual cross-sectional area from the computed residual cross-sectional area profile of the specimen.
 - 8.7. Define the region on the surface of the specimen [Area of Interest (AOI)] where the full-field deformation are to be measured. The length of the AOI should be less than 60 mm (along the rebar) to obtain sufficient pixel resolution for an accurate estimation of full-field displacement.
 - 8.8. Speckle the rebars over the selected AOI with two consecutive coats of contrasting colors using spray paint (conforming to Clause 7.3). Ensure that the blobs do not form a thick continuous layer of paint.
9. Procedure for tension testing of corroded rebars and capturing the images
- 9.1. Place the specimen (prepared as per the guidelines provided in Clause 8) between the grips of the tension testing machine.
 - 9.2. Place a CCD camera on the tripod in front of the tension testing machine with the focal plane of the camera parallel to the milled surface.

- 9.3. Position the camera to focus on the AOI of the specimen. Leave sufficient margin towards the live end/jaw of the tension testing machine, to ensure that the AOI remains within the focus of the camera till the fracture of the specimen.
 - 9.4. Place the electric lamps near the specimen (without blocking the view of the camera) to provide sufficient illumination for the images captured.
 - 9.5. Do the fine adjustments with the camera lens till the speckles are distinctly visible through the camera vision.
 - 9.6. Mark the points on the top and bottom of the image frame in the camera on the specimen (say, 'A' and 'B'). The markings should be made to the side of the specimen such that it does not interfere with the speckles, but is visible in the image. Record the distance between these two points precisely.
 - 9.7. Conduct a displacement control tension test at a suitable displacement rate. Capture the images using the CCD camera at desired time intervals till the fracture of the specimen. A displacement rate not less than 2 mm/min and an imaging rate of at least 2 images per second is recommended.
 - 9.8. Save the images to the system using Vic-snapTM software.
 - 9.9. Export the load, displacement and the time data from the tension testing machine in a suitable format.
10. Procedure for computation of full-field displacement and strains using Vic-2DTM
- 10.1. Open the Vic-2DTM software interface. Click 'speckle images' to upload the set of images corresponding to the tested specimen
 - 10.2. Right click the first image on the list and click *Set as reference image* in the drop-down menu.
 - 10.3. Click *calibrate scale* from the *Calibration* menu and join the two point marked on the specimen, at the top and bottom of the image frame, before the test (points 'A' and 'B') using *line* option and enter the recorded distance measured between these two points. This generates a calibration scale (in mm/pixel). Record the calibration scale for further data analysis.
 - 10.4. Define the AOI (selected before the tension test) in the *Reference Image* using *Rectangle* selection tool. Restrict the selected AOI within the milled region of the specimen and exclude the projections on the sides of the specimen due to the ribs.

- 10.5. Enter suitable *step size* and *subset size* depending on the pixel resolution of the AOI (i.e., the number of pixels occupied by the AOI in the image of size 1037×1391 pixels) and the accuracy required by the user.
 - 10.6. Select the *Run correlation Entry* from the *Data* menu to run the image analysis.
 - 10.7. In the *File* tab in the pop-up window, specify the location in the system where the output files are to be saved by clicking the icon next to *Output directory*.
 - 10.8. In the Options tab, select Optimized 6-tap, Normalized squared differences, and uniform weights in the first three drop down menu. Check Incremental correlation.
 - 10.9. Choose the default values in the *Threshold* tab.
 - 10.10. In Post-processing tab, check *Strain Computation* and *Compute principal strain* and select *Filter size* as 5 (which is the minimum possible value), *Filter* as Decay Filter and *Strain tensor* as Lagrange.
 - 10.11. Click *Run*.
 - 10.12. Export the data as Mat files
 - 10.13. Save the *Project* file.
11. Steps involved in the data analysis

11.1. Computation of the degree of corrosion

11.1.1. Identify the location which fractured on the 3D virtual model and estimate the residual cross-sectional area at that location using the computed cross-sectional area profile (A_{FL}).

11.1.2. Compute the nominal cross-sectional area of the as-received milled specimen (A_i):

11.1.2.1. Compute the area of the milled segment. Figure A.2 shows the nominal cross-sectional area of the pristine rebar, with a segment milled off to obtain a plane surface. Consider the width (l_c) of the plane surface as the chord of the milled segment (the portion removed to obtain the plane surface). ‘ R ’ (shown in Figure A.2) is the nominal radius of the rebar (without considering the ribs). ‘ h ’ is the depth of milling and

' r ' is the distance between the chord and the centre of the base circle of the rebar. ' θ ' is the angle subtended by the chord at the centre. Compute the area of the milled segment using the equations 12 and 13.

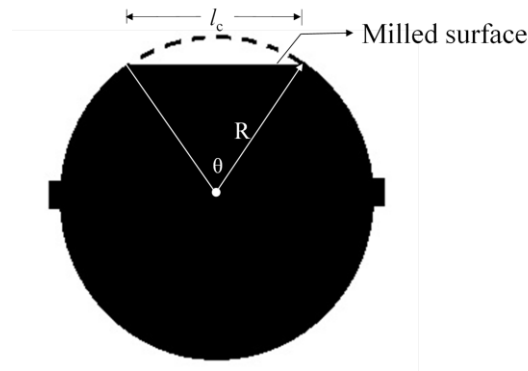


Figure A.2 The nominal cross-sectional area of a pristine rebar showing the radius (R) and chord length (l_c)

$$\theta = 2\sin^{-1}\left(\frac{l_c}{2R}\right) \quad (3)$$

$$\text{Area of the milled segment} = \frac{1}{2}(2R \times (\theta - \sin\theta)) \quad (4)$$

11.1.2.2. Compute nominal cross-sectional area of the milled specimen (A_i) by deducting the area of the milled segment from the nominal cross-sectional area of the milled segment A_o .

11.1.3. Compute the degree of corrosion as $\frac{A_i - A_{FL}}{A_i} \times 100$.

11.2. Computation of strain at fracture location

11.2.1. From the eyy variable in the mat -file corresponding to each specimen, select the row corresponding to the fracture location.

11.2.2. Using a custom-made computer algorithm, select this row (corresponding to the fracture location) from eyy variable from the mat -files corresponding to all specimens in chronological order

into a new excel sheet. Compute the average value across the row to reduce the strain matrix to an equivalent single value.

11.3. Correlation of load and strain data

11.3.1. Match the load values logged in one second to the images captured in one second (or lowest unit of time interval chosen for image capture, 'n').

11.3.2. Correlate the strain value corresponding to one image to the mid-value of the load data logged during that interval of time (equivalent load)

11.4. Compute the engineering stress (σ_{engg}) from the equivalent load value at every instant of time 'n' using A_{FL} .

11.5. Plot the stress-strain curve corresponding to the fracture location using the computed stress and strain values (as per Clause 11.4 and 11.2, respectively)

12. Results

12.1. Report the elastic modulus, yield strength (or proof stress), ultimate strength, and strain at fracture computed from the plotted stress-strain curve.

LIST OF PUBLICATIONS

1. **Rajagopal, R., Sharma, S., Pillai, R. G., and Subramanian, S. J.** (2015), Feasibility of Digital Image Correlation Technique to Determine Mechanical Properties of Corroded Rebars, *Concrete 2015 and Rilem Week*, Melbourne, Australia, Aug 30 – Sept 2, 2015.
2. **Rajagopal, R., Sharma, S., Pillai, R. G., and Subramanian, S. J.** (2016), Assessment of Stress-Strain Behavior of Corroded Steel Rebars Using Digital Image Correlation (DIC) Technique, *ASCE Journal of Engineering Mechanics* (Submitted)

CURRICULUM VITAE

Name: Ranjitha Rajagopal

Date of Birth: 09 November 1991

Ranjitha Rajagopal was born and brought up in Kerala, India. She received her bachelor's degree in civil engineering technology from Government Engineering College Trichur in 2009. Immediately she joined for the M.S. (research) program in Indian Institute of Technology Madras, Chennai, India. She specialized in Building Technology during her Master's program and also worked as research assistant in the Building Technology and Construction Management (BTCM) division of Civil Engineering department in IITM. This thesis, under the supervision of Dr. Radhakrishna G. Pillai (Assistant professor, IITM) focuses on the development of a pre-normative procedure for evaluation of mechanical properties of corroded rebars using Digital Image Correlation (DIC). This research work was carried out in collaboration with the research group under the supervision of Prof. Sankara J. Subramanian of Engineering Design department, IITM.

Ms. Ranjitha Rajagopal can be contacted at:

c/o Mr. P. Rajagopal,
Apartment 401 A, Iris Avenue,
Kalathilpady, Vadavathoor P.O.,
Kottayam, India – 686010.
Ph: 0481-2577220
Email: ranjitha.rajagopal9@gmail.com

GENERAL TEST COMMITTEE

CHAIR PERSON:

Prof. K. Ananthanarayan
Professor
Department of Civil Engineering

GUIDE:

Dr. Radhakrishna G. Pillai
Assistant Professor
Department of Civil Engineering

MEMBERS:

Prof. Amlan Kumar Senguptha
Professor
Department of Civil Engineering

Prof. M. S. Sivakumar
Professor
Department of Applied Mechanics